CENTRO DE INVESTIGACIÓN CIENTÍFICA Y DE EDUCACIÓN SUPERIOR
DE ENSENADA

PROGRAMA DE POSGRADO EN CIENCIAS
EN FÍSICA DE MATERIALES

KINETIC STUDIES OF THE DEMINERALIZATION AND DEPROTEINIZATION ON TRABECULAR AND CORTICAL BOVINE FEMUR BONE AND ANTLER BONE

THESIS

submitted in partial satisfaction of the requirements for the degree of
DOCTOR OF SCIENCE

Presents:

ANA BERTHA CASTRO CESEÑA

April, 2011, Ensenada, Baja California, México.

ABSTRACT of the thesis presented by **Ana Bertha Castro Ceseña** as a partial requirement to obtain the DOCTOR OF SCIENCE degree in PHYSICS OF MATERIALS. Ensenada, Baja California. April 2011.

KINETIC STUDIES OF THE DEMINERALIZATION AND DEPROTEINATION ON TRABECULAR AND CORTICAL BOVINE FEMUR BONE AND ANTLER BONE

Abstract approved by:

Dr. Joanna McKittrick Co-advisor	Dr. Gustavo Hirata Flores Co-advisor

Bones are composite materials hierarchically structured. They are mainly composed of a mineral and a protein phase. The study of bone demineralization and deproteinization is important from biological and materials science perspectives. However, there is scarce information about its kinetics. The goal of this work is to contribute to the interpretation of the kinetics of the *in vitro* demineralization and deproteinization processes of bone. For this, cortical and trabecular bovine femur bones were demineralized using different concentrations of HCl (0.1 N, 0.6 N and 1 N) at different temperatures (0°C, 20°C and 37°C). The results were compared to those obtained for deer antler bone wherever possible. Deproteinization was carried out using an aqueous 6% NaOCl solution at 37°C, 50°C and 60°C. The kinetic parameters (rate constant and activation energy) were calculated considering the surface area per bone volume corresponding to each type of bone. Three different stages are clearly identified during the demineralization reactions: a) in the first stage, the rate constant increase as HCl diffused from the periphery to the core of the sample; b) in the second stage, demineralization occur at steady state, and finally, c) in the third stage, the rate constant diminish as the mineral become depleted. A statistical analysis of the rate constants shows that cortical bones demineralize and deproteinize at a slower rate than trabecular bones. On the other hand, the activation energy for trabecular and cortical bones is different for both demineralization and deproteinization. These results are attributed to the chemical and structural differences that exist between cortical and trabecular bones. According to protein quantification experiments obtained in this work, the protein concentration values are almost the same for both types of bones. These results show that the individual inner matrix architecture of trabecular and cortical bones and characteristics such as the mineral concentration and its bonding with collagen fibers are the responsible

factors that control the extraordinary physicochemical properties found for cortical and trabecular bones, and not the protein concentration. The present work shows that although cortical and trabecular bones are constituted by the same main components: mineral, protein and water, differences such as their inner architecture directly influence their physicochemical characteristics. In addition, the obtained results indicate that mineral and protein depletion in trabecular and cortical bones are independently regulated.

Keywords: bone, trabecular, cortical, antler, kinetics, demineralization, deproteination, rate constant, activation energy.

RESUMEN de la tesis de Ana Bertha Castro Ceseña, presentada como requisito parcial para la obtención del grado de DOCTOR EN CIENCIAS EN FÍSICA DE MATERIALES. Ensenada, Baja California. Abril de 2011.

ESTUDIOS CINÉTICOS DE LA DESMINERALIZACIÓN Y DESPROTEINIZACIÓN DE FÉMUR BOVINO POROSO Y COMPACTO Y ASTA

Los huesos son materiales compositos estructurados jerárquicamente. Están compuestos principalmente por una fase mineral y una proteica. El estudio de la desmineralización y la desproteinización es importante desde un punto de vista biológico así como de ciencia de materiales. Sin embargo, la información acerca de su cinética es escasa. El objetivo de este trabajo es contribuir en la interpretación de la cinética *in vitro* de los procesos de desmineralización y desproteinización en hueso. Para esto, se desmineralizó fémur bovino poroso y compacto usando diferentes concentraciones de HCl (0.1 N, 0.6 N y 1 N)) a diferentes temperaturas (0°C, 20°C y 37°C), y los resultados se compararon, en la medida de lo posible, con los obtenidos para asta de venado. La desproteinización se llevó a cabo usando una solución acuosa de NaOCl al 6% a 37°C, 50°C y 60°C. Se calcularon los parámetros cinéticos (constante de velocidad y energía de activación) en función del área superficial por volumen de hueso correspondiente a cada tipo de hueso. Claramente se identificaron tres etapas diferentes durante las reacciones de desmineralización: a) en la primera etapa, la constante de rapidez incrementa conforme el HCl se difunde desde la periferia hacia el centro de la muestra; b) en la segunda etapa, la desmineralización sucede en un estado estable, y finalmente, c) in la tercera etapa, la constante de rapidez disminuye conforme la concentración de mineral disminuye. El análisis estadístico de las constantes de velocidad muestra que el hueso compacto se desmineraliza y desproteiniza a una menor rapidez que el hueso poroso. Por otro lado, la energía de activación es diferente tanto para hueso compacto como para hueso poroso, para ambos casos: desmineralización y desproteinización. Estos resultados se atribuyen a las diferencias químicas y estructurales existentes entre los huesos poroso y compacto. Según los resultados de cuantificación de proteína obtenidos en el presente trabajo, los valores de concentración de proteína son prácticamente iguales para los dos tipos de hueso. Estos resultados muestran que la arquitectura de la matriz interna de los huesos poroso y compacto, en conjunto con características como la concentración de mineral y su enlace con las fibras de colágeno son los factores responsables que controlan las extraordinarias propiedades fisicoquímicas encontradas en los huesos poroso y compacto, y no la concentración de proteína. El presente trabajo muestra que aunque los huesos poroso y compacto están constituidos por los mismos componentes principales: mineral, proteína y agua, diferencias tales como la arquitectura de su matriz interna afecta directamente sus características fisicoquímicas. Así mismo, los

resultados obtenidos indican que la pérdida de mineral y proteína son reguladas de manera independiente en los huesos poroso y compacto.

Palabras clave: hueso, asta, poroso, compacto, cinética, desmineralización, desproteinización, constante de velocidad, energía de activación.

TO

MY PARENTS,

ARTURO CASTRO AND BERTHA CESEÑA DE CASTRO

For their infinite love and unconditional support

ACKNOWLEDGEMENTS

I am completely grateful to my advisors, Professors Joanna McKittrick and Gustavo Hirata-Flores, for their advice, guidance, support and mentorship throughout the development of this thesis work. I am thankful to my committee members, Professors Pilar Sánchez-Saavedra, Leonel Cota-Araiza, and Mark Meyers, for their valuable insights, support and enthusiasm to this work. I would also like to acknowledge all the fellow students in Professors McKittrick, Hirata-Flores and Sánchez-Saavedra's group for their support and friendship. M.Sc. Ekaterina E. Novitscaya and Professor Po-Yu Chen are especially acknowledged for their guidance, support and inspiring to this work. The financial support by the Consejo Nacional de Ciencia y Tecnología (CONACyT) (#164429) and Centro de Investigación Científica y de Educación Superior de Ensenada (CICESE) (#14112) is gratefully aknowlegded. This research was funded by the National Science Foundation, Division of Materials Research, Biomaterials Program (Grant DMR 0510138) and by a UC-MEXUS project (2009–2010). Partial support from DGAPA-UNAM (Grant # 114010-3) is also acknowledged.

This multidisciplinary work would not been possible without the help and valuable comments from all the collaborators. Professor Pilar Sánchez-Saavedra offered guidance, insights and provided me a space at her laboratory to develop all the bone deproteinization experiments. Discussions with Professor Leonel Cota-Araiza were always insightful and inspiring. I also acknowledge Professor Elizabeth Ponce-Rivas for her valuable research discussions. I am grateful to Professor Beatriz Cordero-Esquivel, who generously allowed me to use her laboratory facilities. I acknowledge M.Sc. Arturo Susarrey-Arce for his valuable discussions, enthusiasm and support of this work. I thank Dr. Ever Arenas-Berumen for his assistance with IR spectrometry, who inspired me with his discipline to work. I also would like to thank Mario Vega-Aguilar, from Earth Sciences CICESE, for his assistance with ICP measurements. I thank Patricia Ascencio and Norberto Flores (Aquaculture, CICESE) for their help in the sample preparation. I acknowledge

Alejandro Tiznado from CNyN-UNAM for his valuable support in the use of laboratory facilities for sample cleaning. Eloisa Aparicio at CNyN-UNAM always offered me her valuable and kind help on the X-ray diffraction performing. I acknowledge Carlos Rodríguez his assistance on X-ray diffractograms interpretation. I also would like to thank Miriam Poumian-Tapia from Oceanology, CICESE, for her support on the freeze drying of samples. I am also grateful to Ekaterina Novitscaya and Sara G. Bodde for their warm hospitality during my stays in San Diego.

My family and my dear friends have provided tremendous support throughout my graduate studies which none of this accomplishment would have been possible. I especially acknowledge my parents, who always inspired and unconditionally supported me.

VITA

1999-2004 Instituto Tecnológico de Tijuana, Tijuana, Baja California
2004 B.S.in Biochemical Engineering

2004-2011 Centro de Investigación Científica y de Educación Superior de Ensenada (CICESE), Ensenada, Baja California
2006 M.Sc.in Marine Biotechnology
2011 D.Sc.in Physics of Materials

FIELD OF STUDY

Major: Biological materials with emphasis on physicochemical and biological properties.

LIST OF PUBLICATIONS

Journal publications

A. B. Castro-Ceseña, E. E. Novitskaya, P. Y. Chen, G. A. Hirata, J. McKittrick. Kinetic studies of the demineralization of bone. *Materials Science and Engineering C*. 2011. 31:523-530.

Ekaterina Novitskaya, Po-Yu Chen, Steve Lee, Ana Castro-Ceseña, Gustavo Hirata, Vlado A. Lubarda, and Joanna McKittrick. *"Anisotropy of the compressive mechanical properties of bovine cortical bone and the mineral and protein constituents".* ActaBiomaterialia (submitted).

Conference proceedings

Ana B. Castro-Ceseña, Ekaterina Novitskaya, Po-Yu Chen, M. del Pilar Sánchez-Saavedra, Gustavo Hirata, and Joanna McKittrick. *"Comparision of Demineralized and Deproteinized Bone"*. 2010 MRS Fall Meeting Proceedings, Cambridge Journals Online.

Ekaterina Novitskaya, Ana Castro-Ceseña, Po-Yu Chen, Joshua Vasquez, Robert Urbaniak, Steve Lee, Gustavo Hirata, and Joanna McKittrick. *"Investigations into Demineralized Cortical Bone"*. 2010 MRSFall Meeting Proceedings, Cambridge Journals Online.

Manuscripts in preparation

Ana B. Castro-Ceseña, Ekaterina E. Novitskaya, Po-Yu Chen, M. Pilar Sánchez-Saavedra, Gustavo A. Hirata, Joanna McKittrick. *"Kinetic studies of the deproteinization of bone at different temperatures*".

A.B. Castro-Ceseña, M. del Pilar Sánchez-Saavedra, and F. Márquez-Rocha. *"Partial purification and characterization of sardine byproduct proteolytic enzymes for its use in the production of sardine byproduct hydrolysates"*.

LIST OF PRESENTATIONS

Invited talks

Ana Bertha Castro Ceseña. *"Nanotechnology: Materials Science and Biotechnology convergence".* Tijuana Institute of Technology, Academic Week, Tijuana, Baja California, October 29th – November 1st 2007.

Ana Bertha Castro Ceseña. *"Biological materials: learning from nature".* Tijuana Institute of Technology, Academic Week, Tijuana, Baja California, October 25th – 29th 2010.

Oral presentations

A. B. Castro-Ceseña, E. E. Novitskaya, P. Y. Chen, G. A. Hirata, J. McKittrick. *"Structural Investigations on Demineralized and Deproteinated Bone"*. The Minerals, Metals and Materials Society, TMS 2010 Meting, Seattle, WA, February 14th – 17th 2010.

Ekaterina Evdokimenko, Ana Castro-Ceseña, Po-Yu Chen, Joshua Vasquez, Robert Urbaniak, Steve Lee and Joanna McKittrick. *"Mechanical and physical properties of demineralized bone"*. The Materials Research Society, MRS Fall 2010 Meeting, Boston MA, November 29th – December 3rd 2010.

A. B. Castro-Ceseña, E. E. Novitskaya, P. Y. Chen, M. del Pilar Sánchez-Saavedra, G. A. Hirata, J. McKittrick. *"Kinetic studies of the demineralization and deproteination of bone"*. The Materials Research Society, MRS Fall 2010 Meeting, Boston MA, November 29th – December 3rd 2010.

A.B. Castro-Ceseña, E. E. Novitskaya, P. Y. Chen, M. del Pilar Sánchez-Saavedra, G. A. Hirata, J. McKittrick. *"Bone demineralization and deproteination studies: A biochemical-kinetic focus"*. The Minerals, Metals and Materials Society, TMS 2010 Meting, San Diego, CA, February 27th – March 3rd 2011.

Poster presentations

R.M. Feliz-Navarro, S.W. Lin, A.B. Castro-Ceseña and J.A. Casco-Carrete. *"Cyanide destruction and simultaneous recovery of copper with an electrochemical reactor"*, Chemistry Research on the Frontier Symposium, October 23th – 25th 2002.

A.B. Castro-Ceseña, P.-Y. Chen, D. Toroian, P.A. Price, G.A. Hirata, and J. McKittrick. *"Nano- and microscopic investigations on demineralized and*

deproteinated bone." The 3rd International Conference on Mechanics of Biomaterials & Tissues, Clearwater Beach, FL. 2009.

A.B. Castro-Ceseña, E. Noviskaya, P.Y. Chen, J. McKittrick and G.A. Hirata. *"Decalcification kinetics and mechanical properties of cow femur and deer antler"*, XV Materials Science Symposium, Ensenada, Baja California, February 15th – 19th 2010.

Ekaterina Evdokimenko, Ana Castro-Ceseña, Po-Yu Chen, Joshua Vasquez, Robert Urbaniak and Joanna McKittrick. *"Mechanical and physical properties of demineralized and deproteinated compact bone"*. University of California, San Diego, UCSD Research Expo 2010, La Jolla, San Diego, April 15th 2010.

A.B. Castro-Ceseña, E. Novitskaya, P.Y. Chen, M. Pilar Sánchez-Saavedra, J. McKittrick and G.A. Hirata. *"Bovine femur bone demineralization and deproteinization kinetic studies"*, XVI Materials Science Symposium, Ensenada, Baja California, February 23th – 25th 2011.

Ekaterina Evdokimenko,Po-Yu Chen, Steve Lee, Ana Castro-Ceseña, Jun Li, Gustavo Hirata, Iwona Jasik, Vlado Lubarda, and Joanna McKittrick. *"Anisotropy in the compressive mechanical properties of bovine cortical bone"*. University of California, San Diego, UCSD Research Expo 2011, La Jolla, San Diego, April 14th 2011.

Imparted workshops

Ana Bertha Castro Ceseña. Workshop: *"DNA oligonucleotides purification by Poliacrylamide Gel Electrophoresis (PAGE)"*. Tijuana Institute of Technology, Academic Week, Tijuana, Baja California, October 27th – 31st 2008.

TABLE OF CONTENTS

TABLE OF CONTENTS (CONTINUATION)

TABLE OF CONTENTS (CONTINUATION)

Page

LIST OF FIGURES

LIST OF FIGURES (CONTINUATION)

LIST OF FIGURES (CONTINUATION)

LIST OF FIGURES (CONTINUATION)

LIST OF FIGURES (CONTINUATION)

LIST OF TABLES

LIST OF TABLES

Chapter I

Introduction

Mineralized biological materials have outstanding mechanical properties that are a result of millions of years of evolution. These biological materials are basically composed of interpenetrated organic (proteins) and inorganic (mineral) matrices, which interact with each other in a synergistic manner leading to an enhancement of their mechanical function.

Biological materials such as bones, antlers, teeth and mollusk shells consist of a limited number of chemical elements (C, O, N, H, P, S), minerals and proteins. Figure 1 shows the characteristic features that biological materials possess. For example, they comprise a hierarchical structure in which each step of the scaffold has a specific function, they are synthesized under mild conditions, they can have more than one function (they are multifunctional), they self-assemble, and are composed of minerals and proteins as their building blocks.

A distinguishing feature found in nature is the hierarchical arrangement of its structures. Nature organizes biological materials from the atomistic and molecular scales to macroscopic scales. An excellent example of materials with this type of arrangement is the bone.

The present work is focused on bones. Bones are hierarchically-structured composite materials, which are lightweight and perform several functions. They give mobility, structure and support to the body. Supply the organisms with the required minerals and possess extraordinary mechanical properties. Bones, such as antler bone, have also outstanding mechanical properties.

Bones, as the other mineralized biological materials, are composed of a protein phase, collagen in this case, and a mineral phase, which is hydroxyapatite. The

process of removing the mineral phase is called *demineralization*, and by analogy, the process of the protein removing is named *deproteinization*.

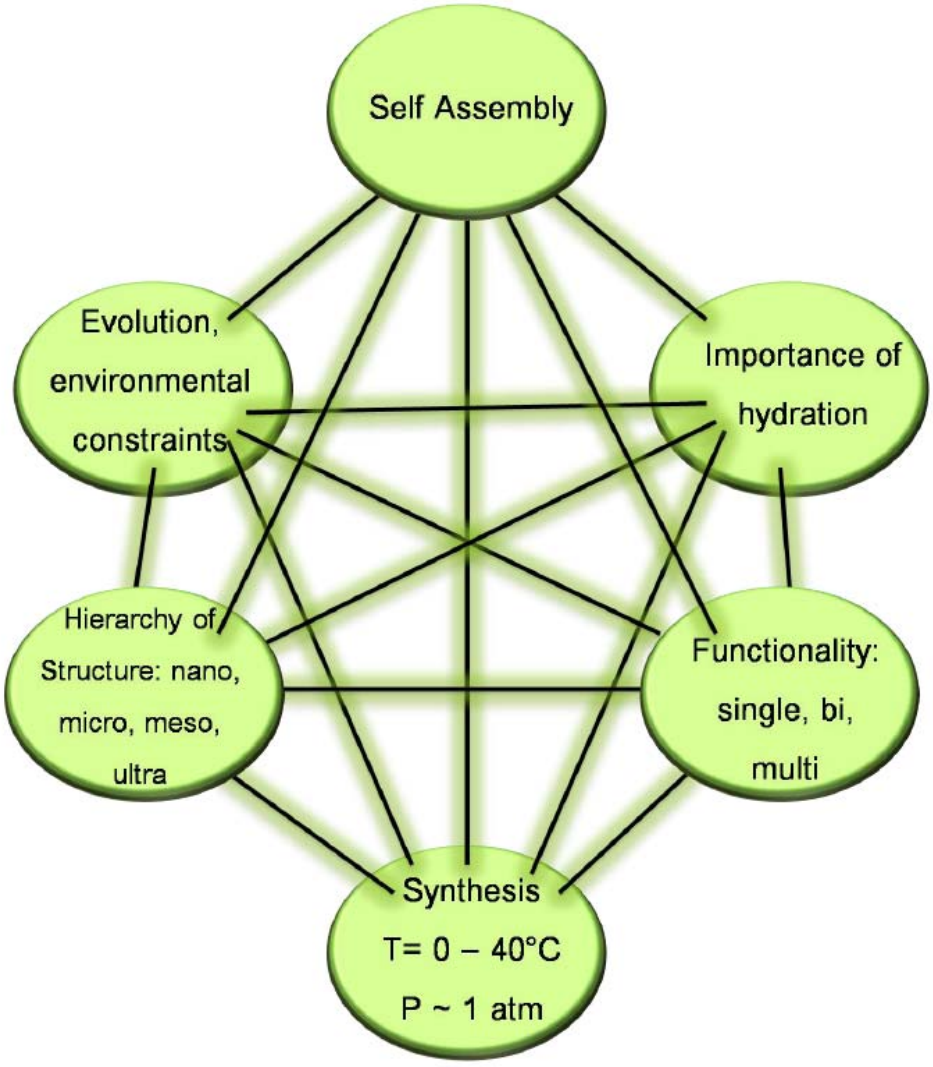

Figure 1. *Distinguishing features of biological materials (from Meyers et al., 2010).*

The study of bone demineralization is considered important from two perspectives. From a biological point of view, bones supply ~99% of the calcium and ~90% of the phosphorous in the human body. Bones simultaneously absorb

and release these minerals as required, keeping a constant concentration in the blood (Audersik and Audersik, 1996). When this balance is lost, osteoporosis can arise as a consequence (Kanis *et al*., 2000). Osteoporosis is a condition of micro-architectural loss of bone tissue leading to decreased density and bone fragility. It disproportionately affects women more than men and is estimated to affect 1 in 3 women beyond the age of 50 years. It has been projected that approximately 9.4 million women in the United States have lost more than 25% of their peak bone mass, and 1.3 million fractures occur annually secondary to osteoporosis (Downey and Siegal, 2006). As a consequence, synthetic and natural bone graft substitutes prepared from demineralized bone matrix have been used as scaffolds for bone repair (Chakkalakal *et al*., 2001; Mauney *et al*., 2005; Li *et al*., 2006; Dodds *et al*., 2010; Wang *et al.*, 2010). From the materials science perspective, the bone mineral phase has been studied due to its extremely important role in the mechanical properties of the bone. Currey performed studies about the relationship between the mineral content of the bone and the mechanical consequences of its variation (Currey, 1990). In Figure 2 (adapted from Currey, 1990), the relationship between the mineral content for various mineralized biological materials and the elastic modulus is shown. These results clearly indicate that the resistance of the bone material to stress is strongly related to the mineral content (Figure 2).

On the other hand, there is an increasing interest in the study of deproteinized bovine bone (DBB) due to its osteoinductive potential and applications in periodontology and oral implants (Benke *et al*., 2001; Carter *et al*., 2002; Stavropoulos and Karring, 2010). The uses of DBB as a bone substitute go so far that there is available a commercial brand of it. BioOss® (Geistlich, Wolhusen, Switzerland) is a deproteinized sterilized bovine bone constituted by a calcium-deficient carbonate apatite, which from a chemical and physical perspective, is identical to human bone (Sollazzo *et al*., 2010). This natural bone substitute has trabecular architecture and high porosity, which promotes the invasion of blood vessels and bone cells thereby, induces the ossification of the defect (Benke *et al*., 2001). Previous studies on DBB have been mainly focused on its uses and its

effects at long term as oral implants (You *et al.*, 2007; Mooren *et al*., 2010; Mordenfeld *et al*., 2010) however, there is a lack of information about the physicochemical characteristics of the *in vitro* demineralization and deproteinization processes in bone. Moreover, there is scarcity of information regarding parallel comparison of cortical and trabecular bones demineralization and deproteinization, which would give new insights on how the bone inner matrix structure differences on trabecular and cortical bones affect these processes, considering that the major bone components: mineral and protein, are the same in both types of bones. Therefore, a detail study of the chemistry, specifically of the kinetics of the *in vitro* mechanisms of bone demineralization and deproteinization have a great importance in the interpretation of these mechanisms.

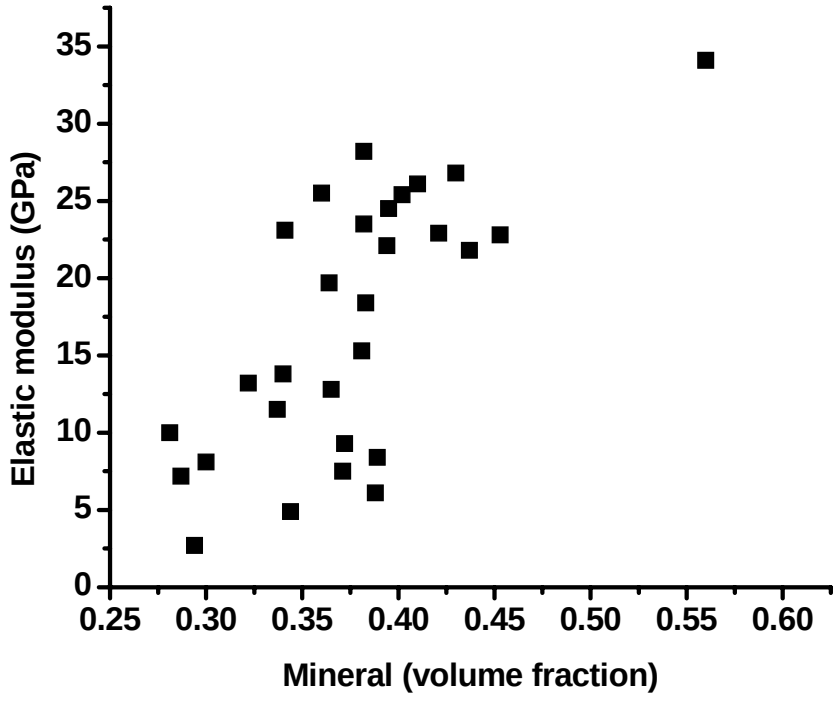

Figure 2. *Young's modulus as a function of mineral content for various mineralized biological materials. Data plotted from Currey, 1990.*

This thesis work presents a comprehensive kinetic analysis of the *in vitro* bone demineralization and deproteinization processes. The results obtained were

associated with the structural characteristics of both types of bone (cortical and trabecular). For this purpose, the present document has been constituted into five chapters and one appendix, which are briefly described below.

Chapter II presents an elemental background about bone structure, its major building blocks, and hierarchical assembly. As well as previous demineralization and deproteinization works performed by other authors. Next to Chapter II, the hypothesis and goals of this investigation are presented.

Chapter III describes in detail the methodology used in this thesis work for *in vitro* bovine bone (cortical and trabecular) and antler bone (cortical) demineralization and the calculation of its kinetics parameters (order of reaction, rate constant and activation energy). The results obtained are discussed and the conclusions presented.

Chapter IV is about the methodology used here for the determination of the kinetics (rate constant and activation energy) for the deproteinization of bovine femur bone (cortical and trabecular). The results are discussed and the obtained conclusions are presented.

Chapter V presents a summary of the results and conclusions obtained in this thesis work.

Chapter VI discusses the contributions of the present thesis and work for the future.

Finally, as an appendix, a basic glossary of some biochemical and physiological related terms used in this document has been included. This vocabulary can be identified along this document as underlined words. In addition, an article published from the present thesis work is included.

Chapter II

Background

The basic structure of bones, such as the mineral and the organic phases are presented in this chapter. The hierarchical levels of the bone are described, as well as the differences between cortical and trabecular bones. A brief description of the importance, growing and structure of elk antlers is showed. In addition, a concise review of the previous works and findings on bone demineralization and deproteinization processes are presented.

II.1 Bone structure

II.1.1 Major building blocks

Bone is a hierarchically-structured composite biological material. The organic matrix is mainly composed of collagen and the inorganic is composed of hydroxyapatite; water is also present. But minor constituents, such as non-collagenous proteins (NCPs), are also present and are thought to play an important role in bone mineralization. The composition of bone is around 65 wt% mineral phase, 25 wt% organic, and 10 wt% water (Weiner and Wagner, 1998; Olszta *et al*., 2007).

II.1.1.1 Mineral phase

The crystals of bone have varying sizes, which values range from a length of 30-50 nm; and a width of 15-30 nm. The crystals are plate-shaped and very thin (2-10 nm). The carbonated form of apatite has the mineral name of Dahllite, but the biological apatite is named hydroxyapatite. Bone hydroxyapatite consists of carbonated and phosphated apatite, $Ca_5(PO_4)_3(OH)$, with a Ca/P ratio less than 1.67. There is still scarce information about the atomic structures in the surface of

hydroxyapatite. But, by Atomic Force Microscopy (AFM) of synthetic apatite it is known that the surface is highly ordered and coincided to the bulk structure. Also, there are some proposed explanations about the plate-shaped of these crystals; one is that they grow via an octacalcium phosphate transition phase. Octacalcium phosphate crystals are plate-shaped and have a structure similar to apatite, except for the presence of a hydrated layer. Bone, as other living tissues, is continuously undergoing remodeling and repair. It is thought that the small size and/or non-stoichiometry of the hydroxyapatite crystals apparently confers to the mineral phase the solubility needed for resorption of the bone by osteoclasts (the bone resorbing cells) (Weiner and Wagner, 1998; Olszta *et al*., 2007).

The mineral phase of bone has been well characterized using Fourier Transform Infrared Microscopy (FT-IRM). As previously mentioned, bone hydroxyapatite is composed of carbonated and phosphated apatite. The carbonated apatite vibrates between 840 and 890 cm^{-1}, while the phosphated apatite has a frequency of vibration of 900-1200 cm^{-1} (Camacho *et al*., 1999). Figure 3 shows an FT-IRM spectrum obtained from trabecular human bone.

TEM analysis of the hydroxyapatite found in elk antler bone showed mineral crystallites with a thickness of 4 nm and platelets with a range in length and width from 20 to 70 nm, very similar to those found in skeletal bone (Figure 4) (Chen *et al*., 2009).

II.1.1.2 Organic phase

The organic matrix of bone consists of collagen, NCPs, and lipids. The collagen molecule has a repetitive nature of the aminoacids $–(Gly\text{-}X\text{-}Y\text{-})_n–$, where X and Y are frequently proline (Pro) and hydroxyproline (Hyp) residues which form the tropocollagen triple helix (Olszta *et al*., 2007). Figure 5 shows the triple-helical structure of the collagen molecule.

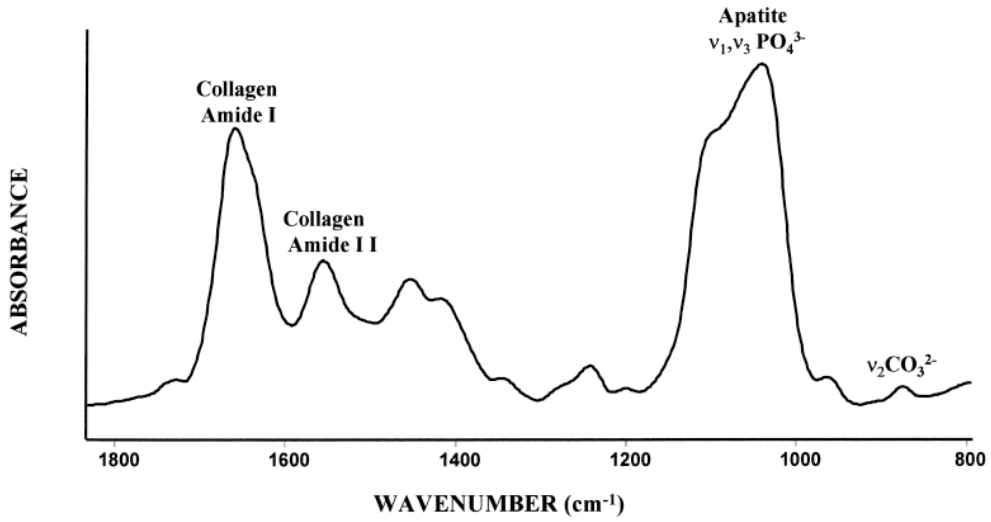

***Figure 3**. Typical FT-IRM spectrum of trabecular human bone showing the frequencies of vibration of carbonated apatite at 840-890 cm^{-1} and the phosphated apatite at 900-1200 cm^{-1}. The vibration frequency for the amide I at 1595 to 1720 cm^{-1} for the collagen is also showed (from Camacho et al., 1999).*

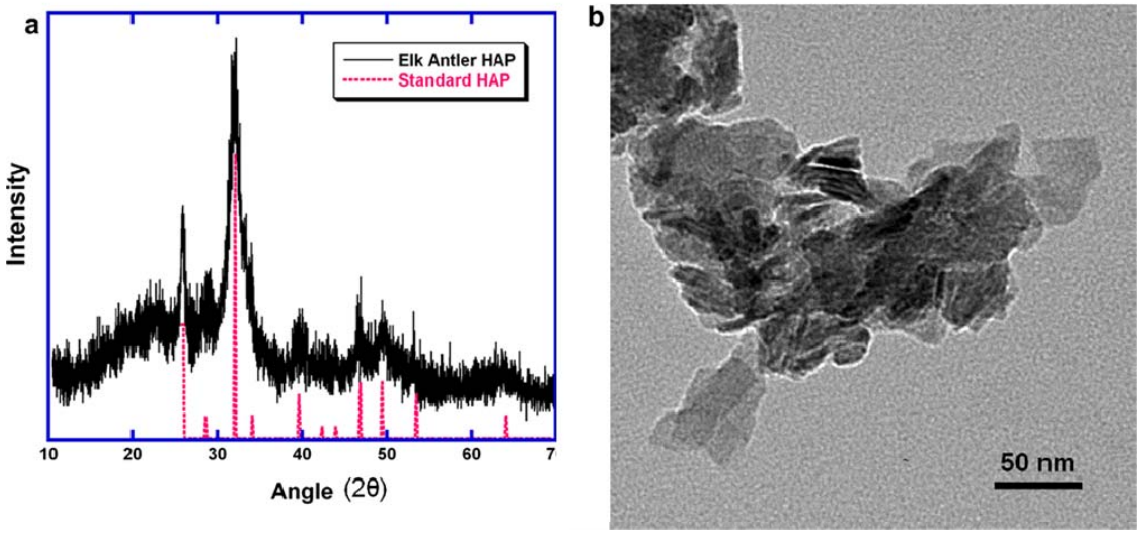

***Figure 4**. a) X-ray diffraction patterns from the compact elk antler bone. All peaks correspond to the Joint Committee on Powder Diffraction standards (JCPDS) file 00-001-1008 for hydroxylapatite and b) TEM micrograph of the hydroxyapatite crystals (from Chen et al., 2009).*

The collagen protein is the most abundant found in the body in different connective tissues, in both calcified and non-calcified. Bone is mostly composed of type I collagen, but some collagen type V is also present. Type I collagen comprises the 90% of the total collagen found in the body (Paschalis *et al*., 2001).

The bone collagen molecule has been characterized and its characteristic bands have been well identified by FT-IRM. The amide I and amide II from collagen have frequencies of vibration in the range of 1595 to 1720 cm^{-1} (see Figure 3) (Camacho *et al*., 1999).

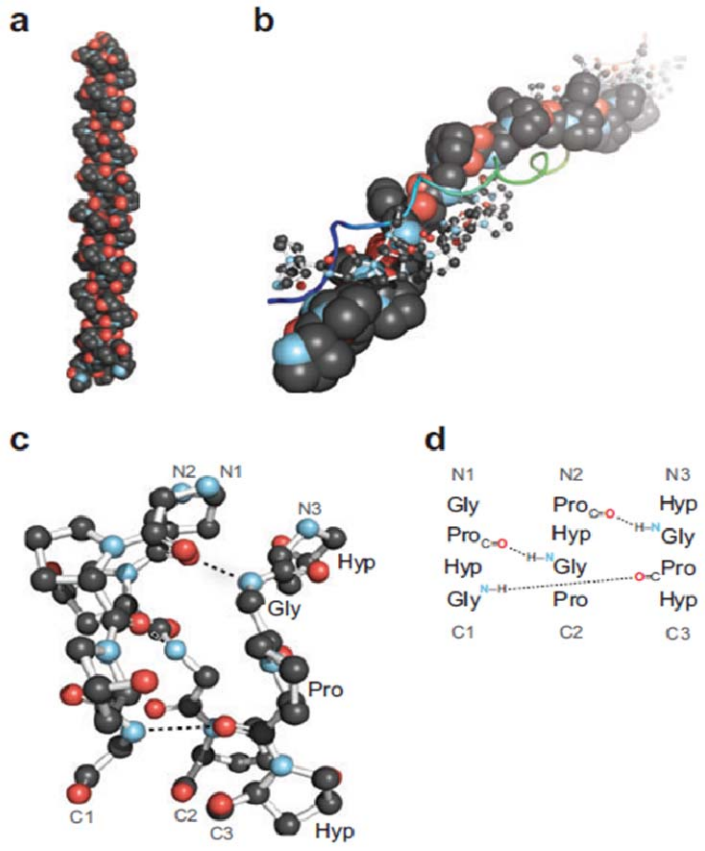

Figure 5. *Overview of the collagen triple helix. a) First high-resolution crystal structure of a collagen triple helix, formed from (ProHypGly)$_4$-(ProHypAla)-(ProHypGly)$_5$. b) View down the axis of a (ProProGly)$_{10}$ triple helix with the three strands depicted in space-filling, ball and stick, and ribbon representation. c) Ball-and-stick image of a segment of collagen triple helix, highlighting the leader of interstrand hydrogen bonds. d) Stagger of the three strands in the segment in panel c (from Shoulders and Raines, 2010).*

Collagen consists of tropocollagen molecules formed by two identical and one dissimilar α chains (($\alpha 1)_2\alpha 2$) within its tropocollagen molecule which has lengths of ~ 280 nm and diameters of ~ 1.5 nm. Staggered arrays of tropocollagen molecules form fibrils, which arrange to form collagen fibers. The structural features of collagen ranges from the aminoacid sequence, tropocollagen molecules, collagen fibrils to collagen fibers (Figure 6) (Robinson and Watson, 1952; Hing, 2004; Buehler, 2006).

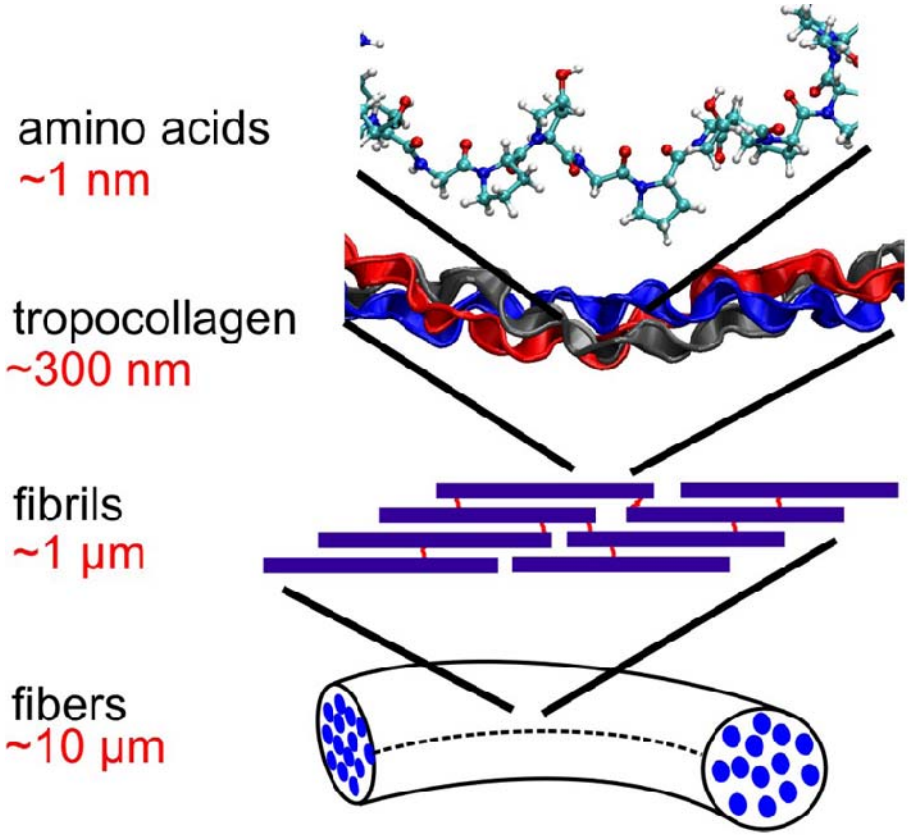

Figure 6. *Hierarchical design of collagen. Multi-scale model describing the mechanical properties of collagen fibrils using a hierarchical milti-scale scheme that starts from the atomistic level of aminoacids (from Buehler, 2006).*

The non-collagenous proteins (NCPs) are produced by bone cells and are believed to regulate bone mineralization and remodeling. They are comprised of sulphated and acid mucopolysacharides. Four NCPs are of special interest: osteocalcin (OC), bone sialoprotein (BSP), osteopontin (OP) and osteonectin (ON),

but only OC and BSP are bone specific. All of these NCPs appear to be multi-functional and is believed that their relative composition within the bone matrix is self-regulated through a feedback effect on the expression of NCPs by osteoclasts (Hing, 2004).

II.1.1.3 Water

Although water is a minor constituent (~ 10 wt%) has an important function, it contributes to the overall toughness of the bone, acting like plasticizer. Mechanical measurements of dry bone are different from those of wet bone (Weiner and Wagner, 1998; Olszta *et al*., 2007).

II.1.2 Hierarchical assembly

Materials found in nature often feature hierarchical structures ranging from the atomistic and molecular scales to macroscopic scales (Buehler, 2006). Bone has been explained in several hierarchical levels. A very detailed description of the bone hierarchy has been reported by Weiner and Wagner (1998). The authors explained the hierarchical structure of bone in seven levels (Figure 7). The *first level* is constituted by its major components, the hydroxyapatite crystals, the type I collagen fibrils and water (see sections II.1.1.1 – II.1.1.3 for a description of each of them).

The *second level* is formed by the mineralized collagen fibrils. The hierarchical assembly of nano-fibrils in mineralized collagen includes an orderly deposition of hydroxyapatite minerals within the type I collagen matrix (Cui *et al*., 2007). During the early stages of mineralization, the matrix host limits crystal growth and keeps the crystals separate from each other, at least along the length of the fibril. The crystals continue growing, compressing the collagen molecules, and eventually join together to form extended sheets. Definitely, the mechanical properties of the collagen fibrils change considerably under such conditions (Weiner and Wagner, 1998).

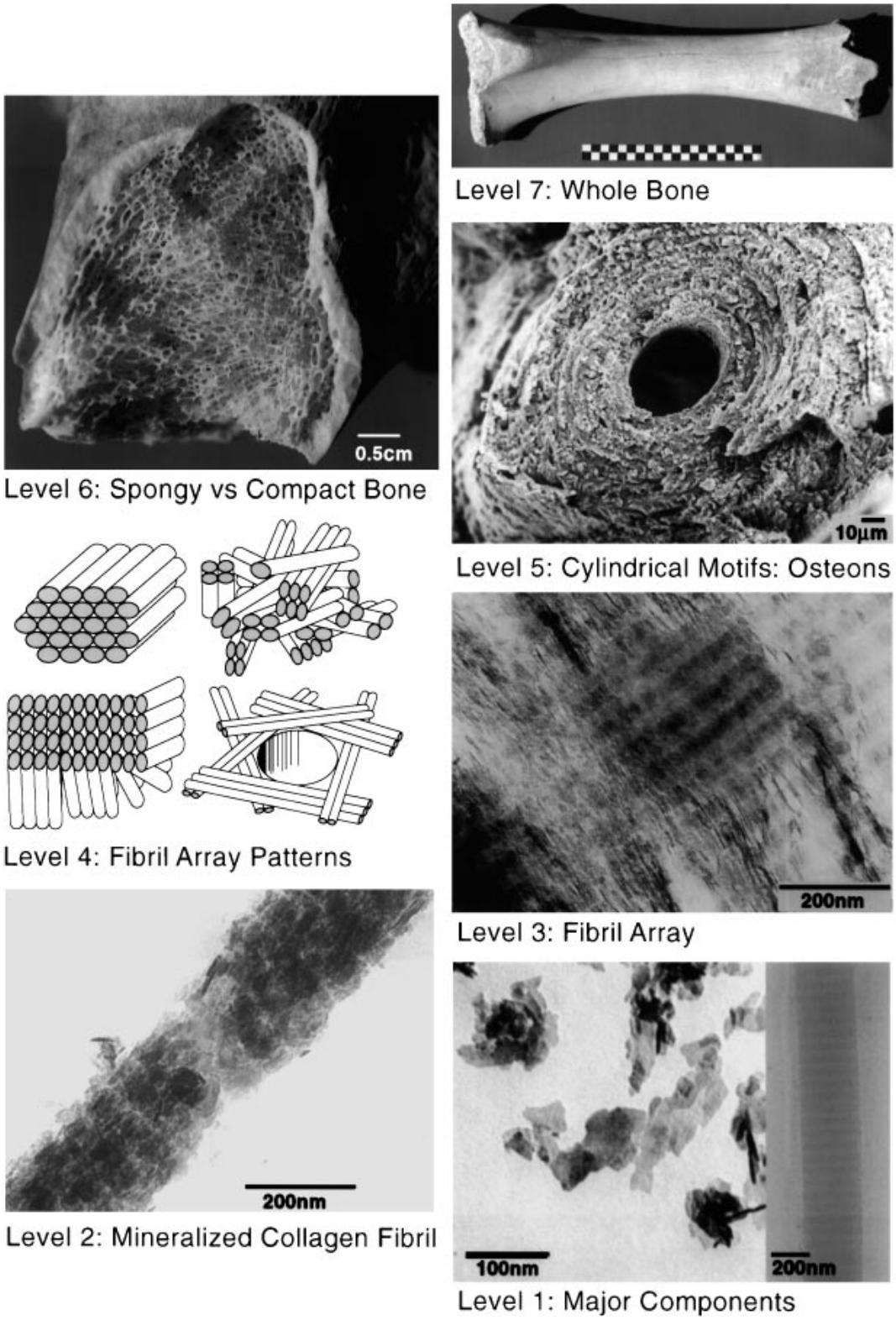

Figure 7*. The bone hierarchy at seven levels of organization. Whole bovine bone scale: 10 cm (from Weiner and Wagner, 1998).*

Landis *et al*. (1993) have studied the mineralization process on turkey tendon. They figured out a schematic representation of the process (Figure 8) based on *ex situ* observations using a combination of high-voltage TEM and tomographic reconstruction imaging. In their schematic, the cylindrical rods represent tropocollagen units composed of triple helical collagen molecules that assemble into fibrils in a quarter-staggered manner, which leads to periodic gaps and grooves within the fibrils. The combination of a 40 nm hole and 27 nm overlap zone gives as a result a 67 nm repeat (64 nm when dehydrated). The space between assembled tropocollagen units is 0.24 nm.

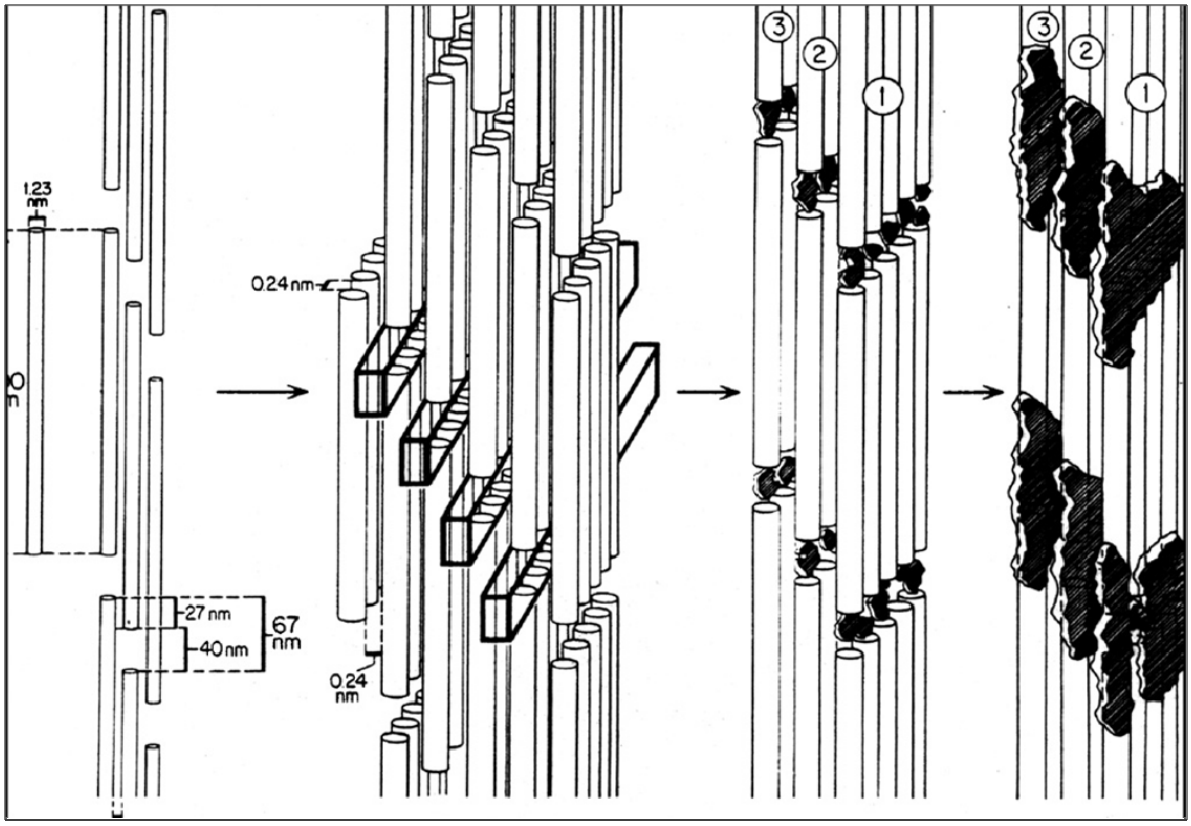

Figure 8*. Schematic representation of the mineralization of turkey tendon (from Landis et al., 1993).*

The *third level* consists of the fibril arrays, which are always almost present in bundles or arrays aligned along their lengths. Fibers from one bundle may fuse with a neighboring bundle (Weiner and Wagner, 1998). The team of Cui and co-workers has synthetically prepared nano-fibrils of mineralized collagen as a self-assembly model system. They used different compositions of monomeric collagen and solutions containing calcium and phosphate ions, and then used either pH or temperature to induce the formation of the collagen fibrils. The collagen fibrils bundles obtained were more than 1 μm long. Each collagen fibril is surrounded by a layer of hydroxyapatite nanocrystals grown on the surface of the collagen fibrils. The hydroxyapatite crystals had a preferential alignment in the *c*-axis with the collagen fibril longitudinal axis (Figure 9) (Ciu *et al*., 2007).

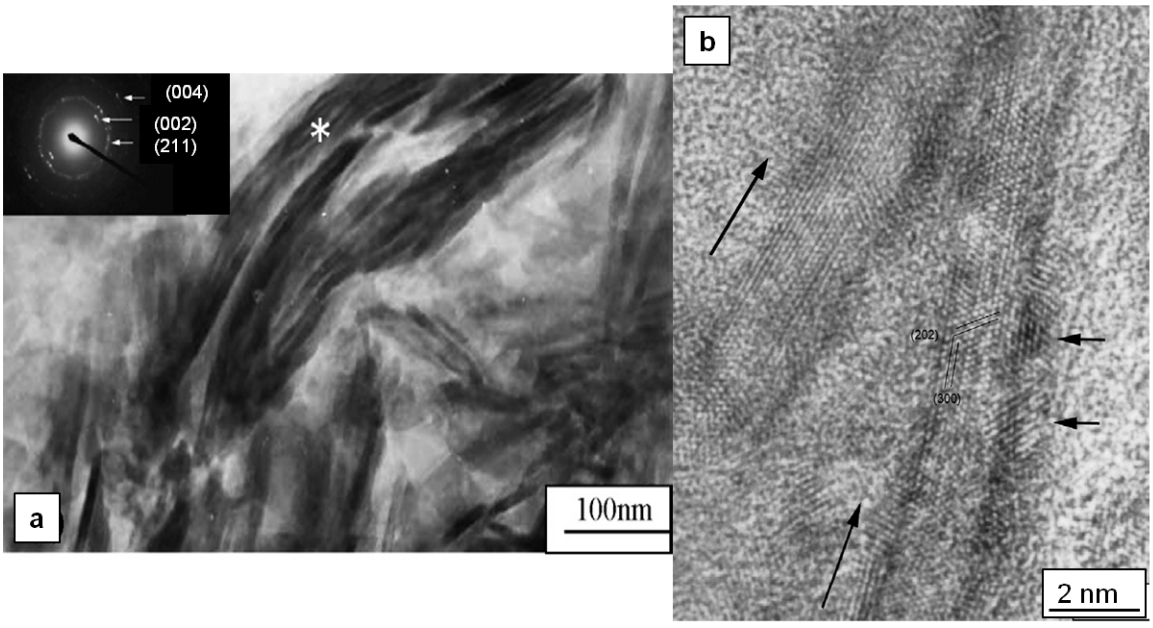

Figure 9. *TEM image of mineralized collagen fibrils. The insert shows a selected area electron diffraction pattern of the mineralized collagen fibrils. The two long arrows indicate the longitudinal direction of the collagen fibrils and, the two short arrows indicate two hydroxyapatite crystals (from Cui et al., 2007).*

The *fourth level* comprises the diversity in fibril arrays in organizational patterns. The most common are four (Figure 10). a) The parallel fibrils pattern is basically an extension of the Level 3. It is characteristically found in the bovid family. During early development, bone of this type is formed very rapidly. Parallel-fibered bone is first laid down with the fibrils more or less parallel to the bone long axis. b) The woven fiber structure is the exactly the opposite to the parallel fibril array. The fibrils are arranged into bundles with diameters up to 30 μm. The bundles are loosely packed and poorly oriented. There is large proportion of non-collagenous material in woven bone. The initially formed layers are disordered, but they get more order as the spaces between the initially formed layers are filled in. This bone is common in the skeletons of amphibian and reptiles and the skeleton of mammalian embryo. Woven bone is formed very rapidly and during development, is then replaced by other types of bone. Also, it is the first bone type that is formed after fracture or in other pathologic cases. c) The plywood-like pattern is present in the lamellar bone and is characterized by sets of parallel fibrils and/or fiber bundles present in discrete layers. The fibril orientation in each layer is different. d) The radial fibril array is found in dentin. The collagen fibrils are almost all in the plane parallel to the surface at which dentin formation takes place in the pulp cavity. Its fracture properties are anisotropic, in contrast to the elastic properties which are isotropic (Weiner and Wagner, 1998).

The *fifth level* refers to osteons, which are cylindrical motifs. The structure of an osteon is basically onion-like in cross-section with layers of lamella surrounding a central hole; they are cylindrical in the longitudinal section (Figure 11). Have a preferentially orientation along the growth direction (Weiner and Wagner, 1998).

The *levels 6 and 7* are concerning to trabecular and cortical bones and, the whole bone, respectively. Cortical and trabecular bones will be described in the next section.

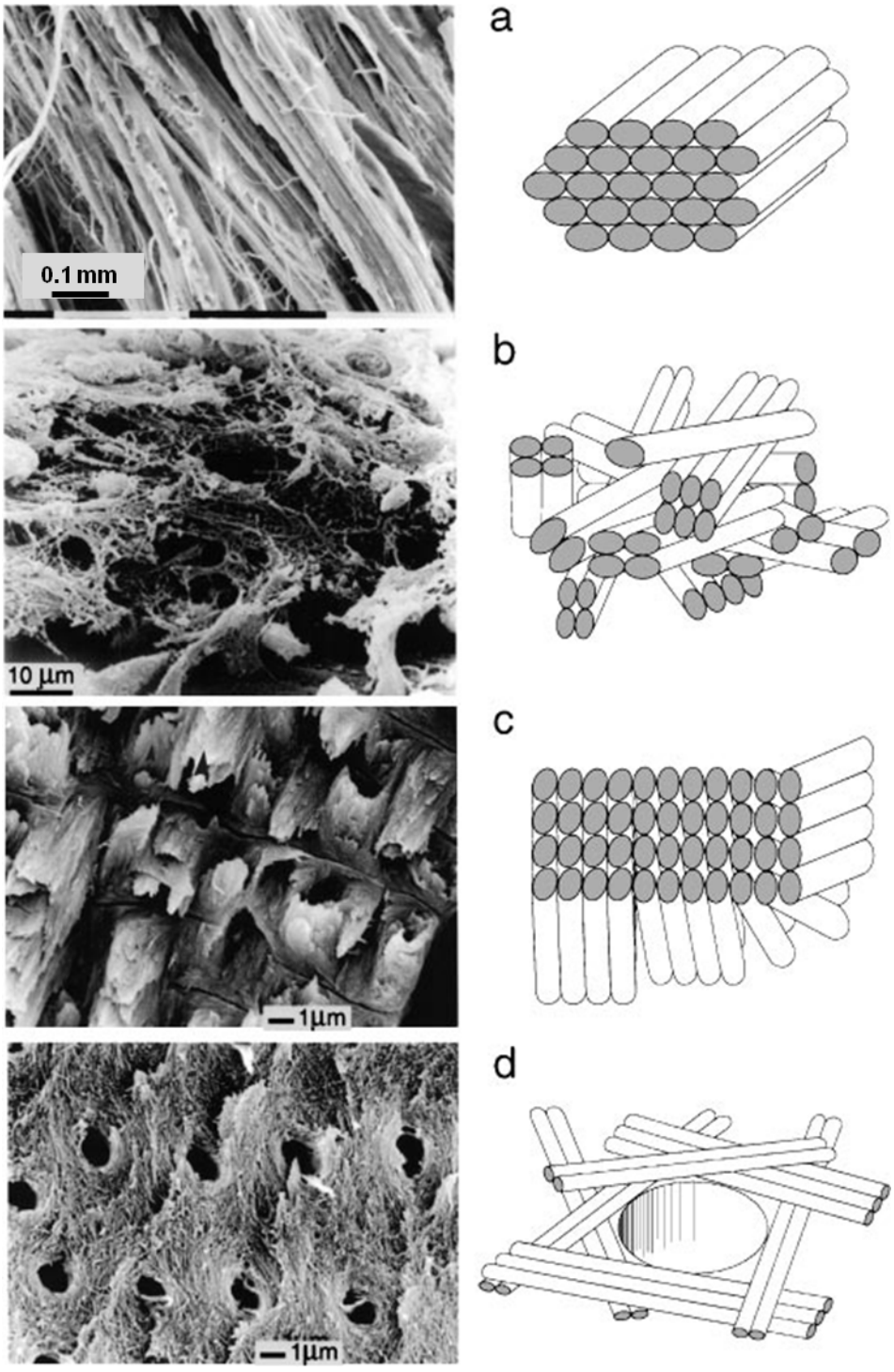

Figure 10. *Fibril array organizational patterns of bone. a) parallel fibrils, b) woven fiber, c) plywood-like structures and, d) radial fibril arrays (from Weiner and Wagner, 1998).*

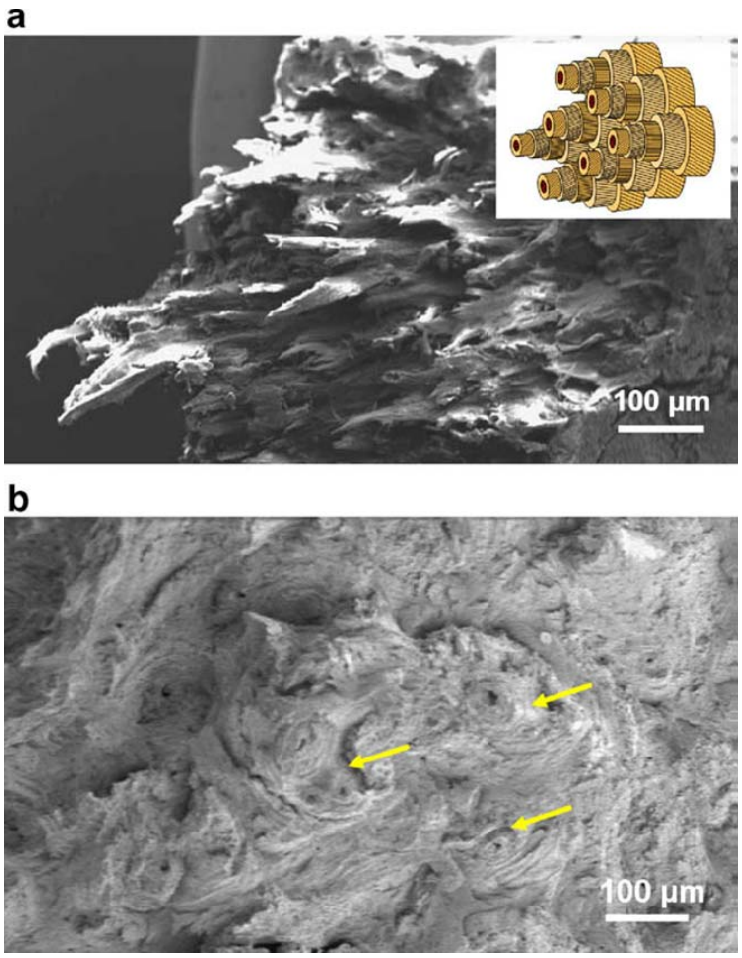

Figure 11. *SEM micrographs of a fractured deer antler bone showing the osteons. a) Side view of the fracture showing its fibrous nature, b) top surface showing the osteons. The arrows indicate the places where delamination around the osteons occurred (from Chen et al., 2009).*

II.1.3 Types of bone: trabecular and cortical

There are two types of bone: trabecular (also named cancellous, porous or spongy) and cortical (compact). The trabecular bone is highly porous (Figure 12), and it is located in parts of the body that need resistance to impact loading. For example, the skull and the head of the femur are largely composed of this bone (Chen *et al*., 2009). Trabecular bone is the site of bone marrow synthesis, and

exhibits anisotropy as a result of its rod and plate organization (Audersik and Audersik, 1996).

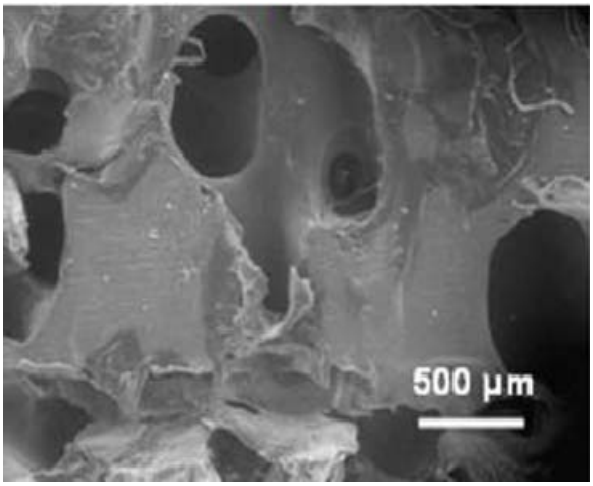

Figure 12. *SEM imaging of the trabeculae in trabecular antler bone (from Chen et al., 2009).*

Cortical bone is highly compact and orthotropic due to the circular nature of the osteons that make up its structure. Cortical bone contains only microscopic channels trough the center of the osteons (Figure 13).

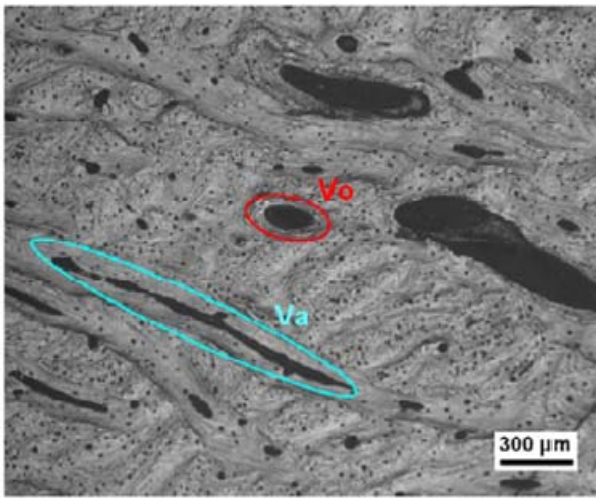

Figure 13. *Cortical bone. Optical micrograph of longitudinal area of bovine femur bone. Vo, Volkmann canals; Va, vascular canals (from Chen et al, 2009).*

The Ca/P molar ratio in cortical bone is close to that of the stoichiometric apatites, while it is appreciably reduced in trabecular bone. Cortical and trabecular differ in the structure and chemistry of their mineral phases. Therefore, functional differences in cortical and trabecular bones can be attributed to the differences both in the matrix and in the mineral component (Bigi *et al*., 1997).

II.2 Antlers

II.2.1 Growth, structure and function

Antlers offer an interesting area of study because they are one of the most impact resistant and energy absorbent of all biomineralized materials. Antlers are the bony protuberances that grow on the heads on animals from the Cervidae (deer). Commonly, antlers grow on male deer not including the reindeer, where antlers appear on both males and females. There are two sources of blood supply to the growing antlers: from the velvet (a highly vascularized tissue) on the surface of the antler and internally through the pedicle (the base of the antler), which results in an extraordinary growth rate. Actually, elk antlers are one of the fastest growing tissues in the animal kingdom. It grows as much as 14 kg in 6 months, with a peak growth rate of 2-4 cm per day. Once antlers are fully grown, the velvet is shed leaving the antler bare. Figure 14 shows optical micrographs of the cross-section of an antler. The subvelvet is 100-150 μm thick and has a layered structure. The cortical bone is under the subvelvet. Next, is the transition zone moving from cortical to trabecular bone which pore size ranges from 300 μm (Chen *et al.*, 2008).

Antlers have two primary functions: they serve as visual signs of social rank within bachelor groups and they are used in combat, as both a shield and a weapon (Chen *et al*., 2008; Chen *et al*., 2009).

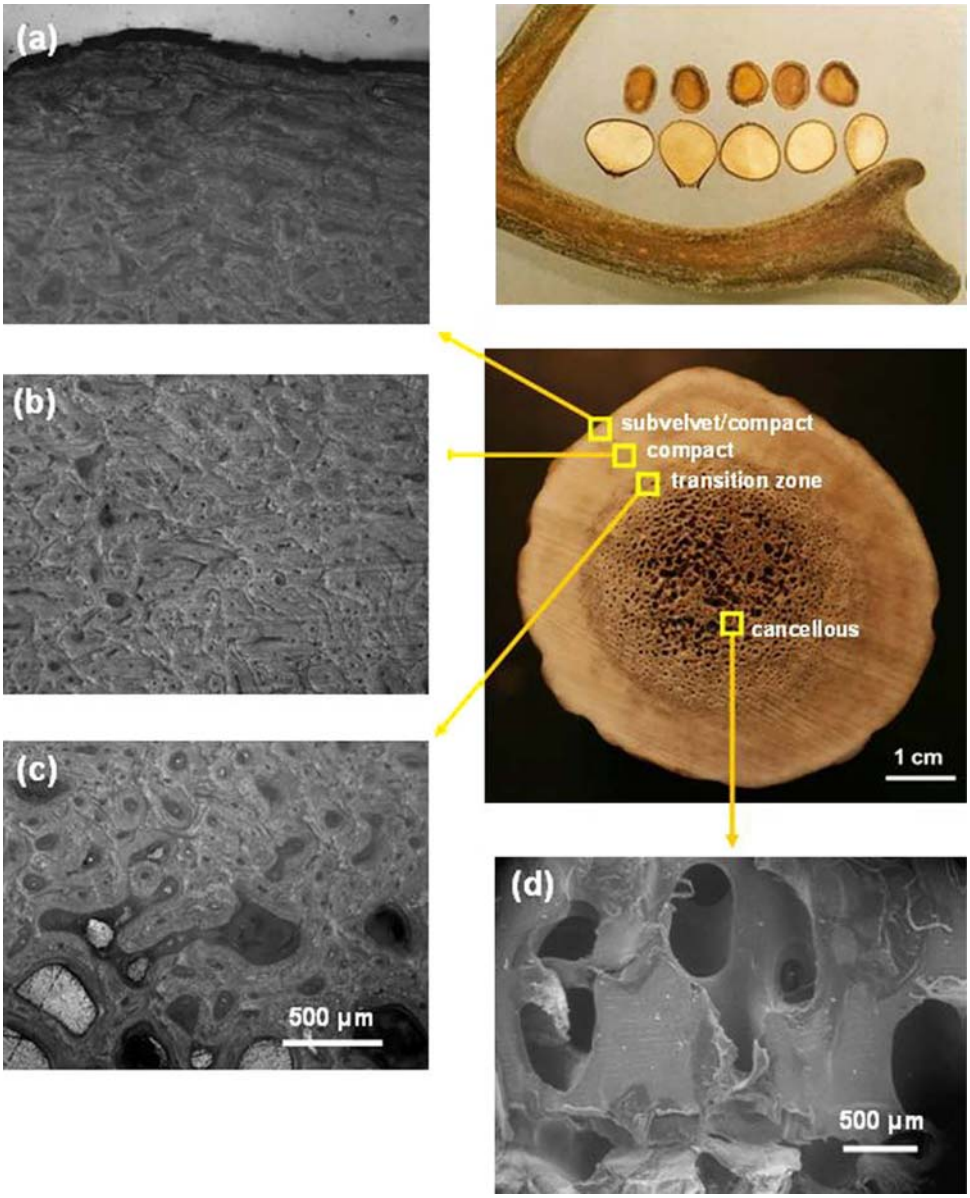

Figure 14. *Optical micrographs of the cross-section of an elk's antler. a) subvelvet/cortical interface, b) cortical and c) cortical to trabecular transition zone, d) SEM micrograph of a trabecular antler bone (from Chen et al., 2009).*

II.2.2 Mammalian bones and antler bones

Antlers have a composition and structure similar to other mammalian long bones, but there are distinct differences. Bones contain essential interior fluids

(blood and marrow). Skeletal bones supply structural support and protection of organs while antlers provide neither. Bones produce vital cells and minerals required for the body. In contrast, antler growth necessitates a large amount of calcium and phosphorous. Table I shows the density and mineral content of cortical and trabecular antler, as well as its chemical composition. The trabecular bone has a smaller weight fraction of the elements (Table I) (Chen *et al*., 2008; Chen *et al*., 2009). Table II shows the chemical composition of the mammalian bones. As see, they contain higher mineral composition; either they are cortical or trabecular.

Table I*. Chemical composition of cortical and trabecular antler bone (from Chen et al., 2009).*

Property	**Cortical bone**	**Trabecular bone**	**Total antler**
Density (g cm^{-3})	1.72 ± 0.04	0.50 ± 0.05	1.35 ± 0.10
Mineral content			
Wt%	56.9 ± 1.0	43.4 ± 0.4	50.1 ± 0.5
Volume fraction	0.36	0.25	0.30

Chemical composition (wt%) *E* = element

	Cortical				Trabecular			
	Pedical	*E*/Ca	Tine	*E*/Ca	Pedical	*E*/Ca	Tine	*E*/Ca
Ca	20.02	1.00	20.08	1.00	15.17	1.00	13.81	1.00
P	8.92	0.46	8.59	0.43	6.09	0.40	6.19	0.45
Sr	0.68	0.03	0.60	0.03	0.48	0.03	0.50	0.04
Na	0.43	0.02	0.57	0.03	0.44	0.03	0.54	0.04
Mg	0.33	0.02	0.42	0.02	0.28	0.02	0.31	0.02
Ba	0.12		0.07		0.07		0.07	
K	0.03		0.03		0.18		0.09	
C	20.19		28.55		31.20		37.46	
O	48.81		41.22		46.21		41.17	

***Table II**. Chemical composition of mammalian bones (from Boskey, 2001).*

Chemical composition	Percentage
Ca	26.70
P	12.47
CO_3	3.48
Na	0.73
Mg	0.44

II.3 Bone demineralization

Demineralization implies loss of the mineral content, and can naturally occur in certain organisms, or can be the cause of a disease. But also, demineralization can be induced in the laboratory for research purposes. Next, a concise description of each of these cases is presented.

II.3.1 Physiological demineralization

Physiological demineralization occurs during bone growth, teeth eruption and fracture healing. But demineralization is also necessary for the maintenance of an appropriate level of calcium in blood. Osteoclasts are the cells responsible for the bone resorption in normal and pathologic states. At normal physiological conditions bone resorption depends on the formation, by the osteoclasts, of an acidic extracellular compartment wherein mineral is degraded. Demineralization of bone involves acidification of the isolated extracellular microenvironment, and the process is mediated by a vacuolar enzyme known as H^+-adenosine triphosphatase (H^+-ATPase) in the open membrane of the cell. The intra-osteoclastic pH is maintained, in the presence of abundant proton transport, by an energy-independent Cl^-/HCO_3^{2-} exchange on the antiresoptive surface of the cell. Finally,

electroneutrality is preserved by an opened Cl^- channel on the membrane charge-coupled to the H^+-ATPase. The result of these ion transporting events is the secretion of HCl into the resorptive microenvironment, generating a pH of approximately 4.5. This acidic milieu first mobilizes bone mineral in the process of demineralizing the organic component of the bone which is subsequently degraded by a lysosomal protease (Ehrlich *et al*., 2008).

The demineralization process is also carried out by organisms like fungi, algae and cyanobacteria encountered in aquatic systems. These organisms are capable of growing on calcareous substrates which they dissolve possibly through the development of a microenvironment in which the conditions (saturation) are favorable for the dissolution of calcium carbonate (Ehrlich *et al*., 2009).

II.3.2 Pathological demineralization

From a biological point of view, bone is a specialized form of connective tissue that serves as both a tissue and an organ system within higher vertebrates. As such, its basic functions include locomotion, protection, and mineral homeostasis. Its cellular makeup includes osteoblasts, osteocytes, bone lining cells, and osteoclasts and, as all mineralized tissues, its matrix contains an organic and an inorganic component. Functionally, trabecular bone is more closely associated with metabolic capabilities than cortical, whereas cortical bone generally provides greater mechanical strength (Guyton and Hall, 2006).

As previously mentioned on Chapter I (p. 2), rarefaction of bone (osteoporosis) can occur when mineral homeostasis produced by the bone is lost (Carter and Hayes, 1976). The World Health Organization (WHO) defines osteoporosis as ‘a disease characterized by low bone mass and micro-architectural deterioration of bone tissue’, leading to enhanced bone fragility and a consequent increase in fracture risk (WHO, 1994) (see Figure 15).

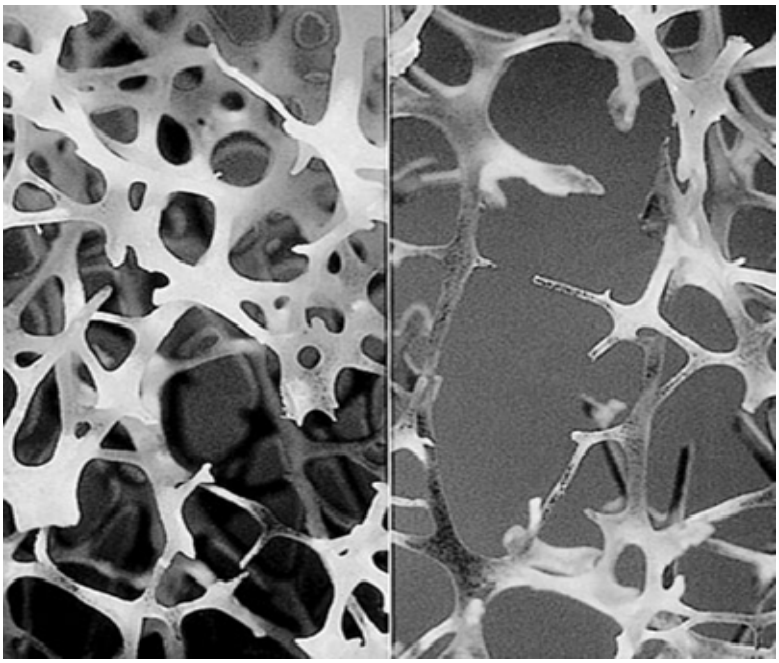

***Figure 15**. Normal (left) and osteoporotic bone (right) (from Theobald, 2005).*

Osteoporosis is present in many pathological conditions and is a common finding in bedridden or elderly patients. In all types of osteoporosis, the earliest and most striking change is in trabecular bone, where the porous become thin and sparse (Carter and Hayes, 1976).

Osteoporosis is a complex bone disease, and there are many causes than can give this condition as a consequence: 1) *lack of physical stress on the bones* because of inactivity; 2) *malnutrition* to the extent that sufficient protein matrix cannot be formed; 3) *lack of vitamin C*, which is necessary for the secretion of intercellular substances by all cells, including formation of osteoid by the osteoblasts; 4) *postmenopausal lack of estrogen secretion* because estrogens decrease the number and activity of osteoclasts; 5) *old age*, in which growth hormone and other growth factors diminish greatly, plus the fact that many of the protein anabolic functions also deteriorate with age, so that the bone matrix cannot be deposited satisfactorily; and 6) *Cushing's syndrome*, because massive quantities of glucocorticoids secreted in this disease cause decreased deposition

of protein throughout the body and increased catabolism of protein metabolism can cause osteoporosis (Guyton and Hall, 2006).

There are two other bone demineralization associated diseases. *Osteomalacia* causes defects in the bone mineral (Bhan *et al*., 2010). While osteoporosis refers to the degeneration of already synthesized bone, making it brittle, osteomalacia is an abnormality in the synthesizing process of the bone, making it soft. On the other hand, *rickets* occurs mainly in children. It results from calcium or phosphate deficiency in the extracellular fluid, usually caused by lack of vitamin D (Guyton and Hall, 2006).

II.3.3 *In vitro* demineralization

In vitro, or laboratory, or applied demineralization occurs when a chemical reagent is used in order to isolate an organic component from any natural biomineralized material and can be used for practical goals, such as the use of demineralized bone as scaffold for bone repair (Chakkalkal *et al*., 2001) and for tissue engineering (Li *et al*., 2006; Mauney *et al*., 2005), or scientific interest relating to the isolation and investigation of the organic matrix (Figure 16). In Materials Science, bone demineralization has been performed in order to study the mechanical properties of its organic component (Currey, 1969; Broz *et al*., 1995; Bowman *et al*., 1996; Catanese *et al*., 1999), because the mineral phase on bone plays an extremely important role in the mechanical properties of bone, please see Figure 2, which shows that mechanical resistance of bone to an applied stress directly depends on its mineral content.

Much attention of bone demineralization has been paid on its effect on the mechanical properties of bone therefore, there are scarce reports of the *in vitro* bone demineralization kinetics, which would provide information about rate of mineral depletion occurs under certain conditions of temperature, concentration of the demineralization agent, and type of bone (cortical or trabecular). The obtained information can be related to the structural characteristics of each type of bone.

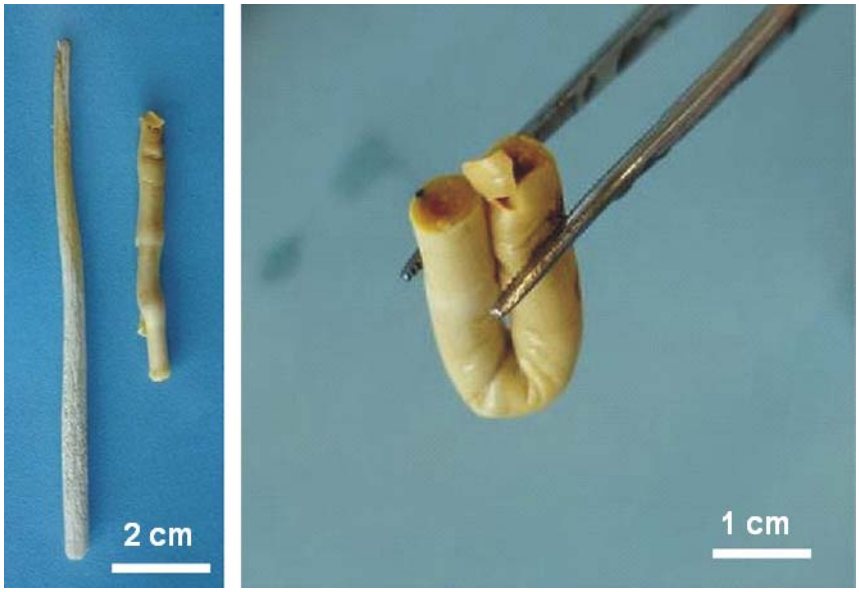

Figure 16. *In vitro demineralization of the stony hard calcite skeleton of the sea pen coral (Pennatulaceae). Demineralization was carried out by Osteosoft (EDTA) solution, which leaded to loss of the mineral phase (left), producing a highly flexible organic matrix (right) (from Ehrlich et al., 2008).*

II.3.3.1 Kinetics of bone *in vitro* demineralization

Most studies concerning to demineralization kinetics have been mainly focused on the kinetics of diffusion of the demineralizing agent, generally in tooth (Birkedal-Hansen, 1974a; Birkedal-Hansen, 1974b; Patel *et al*., 1987; Moreno and Zahradnik, 1974; Margolis *et al*., 1999). For studies performed in bone, the cortical has been the most analyzed (Lewandrowski *et al*., 1996). The diffusion coefficient of HCl into the organic matrix and the rate of penetration of the HCl demineralization front were studied in elephant ivory dentine. Depending on the geometrical shapes of the samples, the distance penetrated by the HCl solution was directly proportional to the square root of time, as described by Birkedal-Hansen (1974a, 1974b). A quantitative methodology for studying demineralization was proposed by Patel *et al.* (1987). They found that weak acids do not influence either the apparent solubility or the surface reaction process of the enamel. However, Moreno and Zahradnik (1974) showed that under acidic conditions, a

slight dissolution of the enamel surface does occur. In other studies, the kinetics of human cortical bone demineralization was examined using HCl. The advance of the reaction front *versus* immersion time was analyzed using mathematical models based on diffusion mass transfer to predict demineralization process. These authors found that the model for planar geometry is applicable to demineralization of cortical bone allografts of irregular shapes, and that the model for cylindrical geometry fitted well for curved surfaces (Lewandrowski *et al*., 1996). However, the rate constant, order of reaction, and activation energy were not included in those investigations. Margolis *et al.* (1999) reported a general model to describe the influence of organic acid type and activity on enamel demineralization. Rate constant values reported were on the order of 10^{-6}. However, no units for rate constant were indicated therefore, the order of demineralization reaction cannot be deduced from these data.

II.4 Bone *in vitro* deproteinization

Bone *in vitro* deproteinization has been performed using different chemical methods, such as hydrazine (Termine *et al*., 1973; Bertazzo and Bertran, 2008), NaOCl (Broz *et al*., 1997) and NaOH (Fattibene *et al*., 2006) has been used.

Termine *et al*. (1973) investigated physical and chemical properties of deproteinated bone by X-ray diffraction, infrared and TEM. Figure 17 shows TEM micrographs of hydrazine-deproteinated rat tibia. Although the effectiveness of hydrazine for bone deproteinization, there was some controversy about alterations produced to bone mineral caused by hydrazine deproteinization. For this reason, Bertazzo and Bertran (2008) performed a comprehensive discussion of the effects of using this reagent for the deproteinization of rat femur. The authors demonstrated that deproteination of bone by hydrazine does not alter bone mineral composition or morphology, even though there is a slight indication that its crystallinity is scarcely altered.

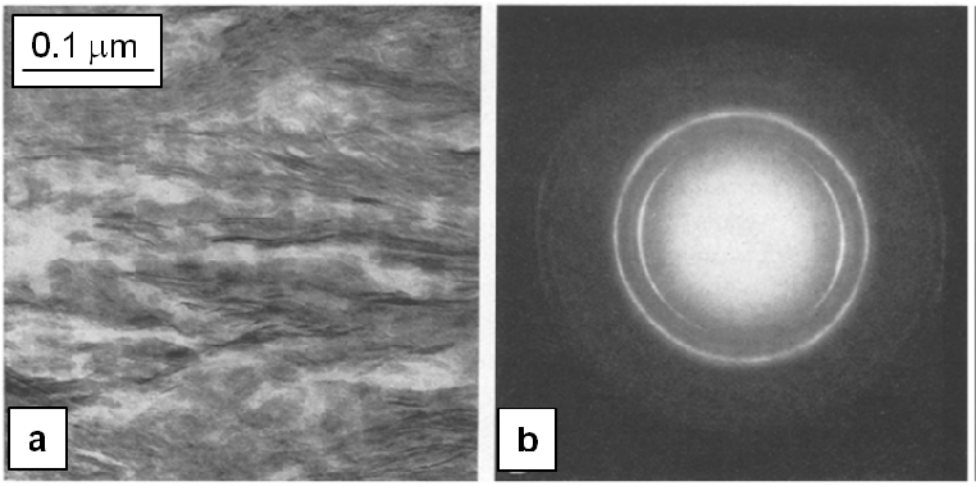

Figure 17. *a) Transmission electron micrograph (Ax70,000). b) Bone apatite electron diffraction pattern, showing the c-axis orientation of crystallites in three-month-old rat tibia (from Termine et al., 1973).*

Broz *et al*. (1997) immersed bovine cortical bone at different times for the selective removing of the collagen phase within the bone using 5.25% NaOCl. The effect of the collagen removing on the mechanical behavior on the bone was evaluated using macroscopic and microscopic experimental techniques. The mechanical behavior in three anatomical directions on bones became increasingly characteristic of a brittle ceramic material. The site-specific properties and the mineralization of the cores were not significantly affected by the treatment; however, according to the authors, the crystallite interlocking was destroyed after the removing of the organic phase with NaOCl. Therefore, this method was not suitable for the study of the mechanical behavior of deproteinizated bone.

Fattibene *et al*. (2006) studied the effect of sample preparation on dentine electron paramagnetic resonance (EPR) spectra. They performed analysis on tooth enamel and dentine. A solution of 5 M NaOH at 60-70°C was used for deproteinization. The authors found that the EPR spectrum of dentine is influenced by the sample preparation procedure used. No reports concerning to bone deproteination kinetics were found until the time of the elaboration of the present document (March, 2011).

From the present review of the literature it is seen that most of the attention has been paid on the study of the mineral and the collagen as individual components of the bones. Several of the reports on demineralization are related to the diffusion of the demineralizing agent, and most of them have been performed in teeth, probably because the presence of weak acids provokes demineralization of dental enamel. No kinetic parameters were found for specifically bone demineralization. The literature related to bone deproteinization process was scarcer. Most of the reports have been dedicated to the study of the mineral phase left on the bone after deproteinization. Others deal with the comparison of different bone deproteinization methods and the interferences they could provoke for the performing of further analysis of the bone samples. No reports on kinetics of bone deproteinization were found. However, demineralized and deproteinizated bone matrixes have been used as scaffolds for bone repair and for oral implants. Therefore, there are important applications for these biological materials.

On the other hand, the reports revised in this document show that the studies have been performed on the individual bone components (mineral and protein). But no studies with a physicochemical focus have been done, in a parallel manner, for the comparison of cortical and trabecular bones. Therefore, a physicochemical study of the bone demineralization and deproteinization processes, mainly focus on its kinetics parameters, will give new insights on how the bone inner matrix structure differences on trabecular and cortical bones affects demineralization and deproteinization processes, since the major bone components, mineral, protein and water, are the same in both types of bone.

As a consequence, the hypothesis and goals of this thesis work are next presented based on the previous literature review.

Research hypothesis and goals

Research hypothesis:

Considering the distinct structural architecture between cortical and trabecular bone, significant differences are expected in the kinetic parameters such as, the rate constant and the activation energy, in the *in vitro* bone demineralization and deproteinization reactions between cortical and trabecular bone.

General goals:

1. Develop a method to quantitatively measure of the mineral and the protein contents in bone.
2. Contribute to the interpretation of the mechanisms involved in the *in vitro* demineralization and deproteinization processes in cortical and trabecular bones.

Specific goals:

1. Demineralize cortical and trabecular bovine femur bones at different temperatures and acidity levels; and calculate the rate constant and the activation energy for each set of experimental conditions. Compare the results, with those obtained for the demineralization of the deer antler bone.
2. Deproteinize cortical and trabecular bovine femur bones at different temperatures; and calculate the rate constant and the activation energy according to the experimental conditions.

Chapter III

Kinetics of the *in vitro* demineralization of bovine femur bone and antler bone

This chapter describes the methodology used for the quantitative measurement of the mineral (calcium) content in bovine femur bone (trabecular and cortical). The kinetic parameters (order of reaction, rate constant and activation energy) of the demineralization reaction are calculated and discussed. Since the kinetics of bovine bone demineralization is relatively unknown, the cortical deer antler has been also studied, and the results compared with cortical femur bone wherever possible.

III.1 Materials and methods

III.1.1 Sample preparation

Bovine femur bone was purchased from a local butcher (Ensenada, Baja California, México). The slaughter age was approximately 24 months. The main beam was cut into sections (~5 cm) by a hand saw and followed by fine section. For experiments, 100 pieces were cut (5 mm x 5 mm x 5 mm) from both cortical and trabecular sections. The bovine femur was carefully cleaned to remove any marrow and lipid components. The trabecular bone was cleaned using pressurized stream of compressed air and water, as previously reported by other authors (Fantner *et al*., 2005; Thurner *et al*., 2009). All samples were air-dried and weighed before the demineralization treatment.

The Cervus canadensis antler was purchased from Into the Wilderness Trading Company (Pinedale, WY). The antler was shed approximately 1 year before it was

obtained for testing. The main beam was cut into sections (~5 cm) using a rotating diamond wheel saw. For analysis, 100 samples were cut (5 mm x 5 mm x 5 mm), only from the cortical section.

III.1.2 Demineralization experiments

The cortical and trabecular sections of bovine bone and the cortical section of antler (trabecular section of antler was not included) were placed in 50 ml centrifuge tubes containing 40 ml of 0.1 N, 0.6 N or 1.0 N HCl. Three temperatures were used: 0°C, 20°C and 37 °C. For experiments at 0°C, a refrigerator was used. Experiments at 20°C were performed at room temperature. For demineralization at 37°C, a water bath was used. The HCl solutions were refreshed after 0.5, 1.5, 3, 6, 9, 12, 16, 20, 24 h, and subsequently at 4 h intervals until the demineralization was complete (see Table III). The method used to determine when complete demineralization occurred is described in the following section. The refreshed HCl solution was saved for calcium concentration measurement. All experiments were done in triplícate.

Table III. *Time (h) required for reaching complete demineralization of bone specimens.*

	Time (h)								
	0.1 N HCl			0.6 N HCl			1.0 N HCl		
	0°C	20°C	37°C	0°C	20°C	37°C	0°C	20°C	37°C
Cortical bovine bone	---	---	---	52	48	32	36	32	28
Trabecular bovine bone	44	40	32	28	24	20	28	20	16
Cortical antler bone	---	---	---	44	40	36	32	28	24

III.1.3 Calcium content measurement

The amount of calcium from the dissolved minerals in the HCl solution was calculated by using Inductively Coupled Plasma Spectroscopy (ICP Emission Spectrometer, Varian Liberty 110, Palo Alto, CA, USA).

Parts per million (ppm) units were obtained from ICP calcium measurements and were converted to mg l^{-1} (1 ppm = 1 mg l^{-1}). The initial calcium concentration $[Ca]_0$ in mole l^{-1} was determined by dividing mg l^{-1} by the atomic weight of Ca (40.08 g mol^{-1}). $[Ca]_0$ was then calculated by adding the amount of dissolved calcium from each testing interval up to the complete demineralization time t_c given by:

$$[Ca]_0 = [Ca]_{0.5} + [Ca]_{1.5} + \bullet\bullet\bullet + [Ca]_{tc}, \quad (1)$$

where $[Ca]_0$ is the initial calcium concentration (before HCl treatment), $[Ca]_{0.5}$ is the calcium concentration at sampling time of 0.5 h, after which the solution was refreshed (see Section III.1.2 and Table 1 for the time of each HCl refresh). After the next sampling time, at 1.5 h, the concentration $[Ca]_{1.5}$ was measured and the solution refreshed. The procedure was continued until $[Ca]_{tC} = 0$, where t_C is the time at which demineralization was completed. This procedure is graphically explained in Figure 18. The calcium concentration $[Ca]_{t^*}$ at time t* is given by:

$$\left[Ca\right]_{t^*} = \sum_{t=0.5}^{t^*} \left[Ca\right]_t , \quad (2)$$

$[Ca]_{t^*}$ is the concentration reported at any time during the demineralization process.

III.1.4 Determination of the order of reaction

The rate equation was used to determine the kinetic parameters for demineralization, given by (Brown, 1991; Chang, 1998, Masel, 2001):

$$rate = \frac{d[Ca]}{dt} = k[Ca]^n, \quad (3)$$

where k is the rate constant of the reaction and is a function of the acid concentration and temperature, [Ca] is the concentration of the reactant (mol m^{-3}), and n is the order of the reaction. The order of demineralization reaction was obtained by plotting $-([Ca]_0 - [Ca]_{t^*})$ for zero order reaction, ln $([Ca]_{t^*}/[Ca]_0)$ for a first-order reaction and, $(1/[Ca]_0) - (1/[Ca]_{t^*})$ for a second-order reaction, as a function of time. The plot that is the most linear indicates the order of the reaction.

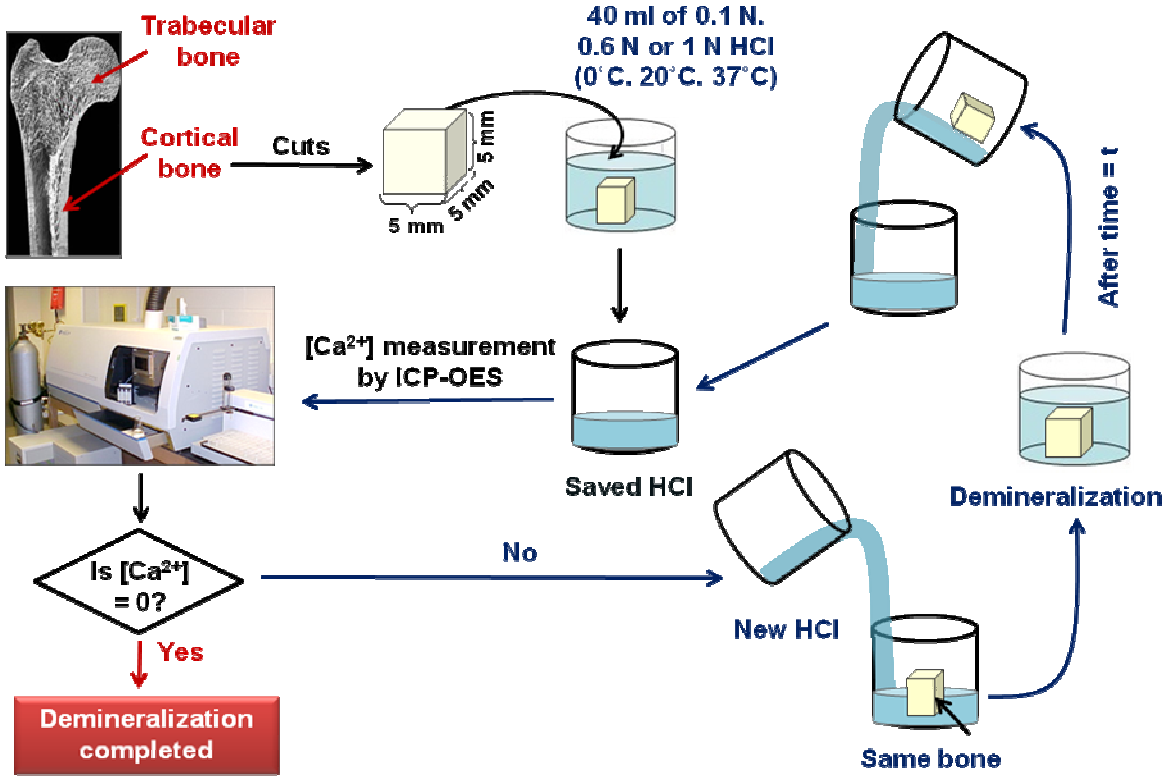

Figure 18. *Schematic representation of the trabecular and cortical bovine bone and deer antler demineralization experiments.*

III.1.5 Calculation of the activation energy

The dependence of the rate constant on temperature is expressed by the Arrhenius equation (Brown, 1991; Chang, 1998):

$$k = A\exp\left(-\frac{E_a}{RT}\right), \quad (4)$$

where A is a constant that indicates how many collisions lead to products, and is known as the frequency factor. E_a is the activation energy, R is the gas constant and T is the absolute temperature at which the reaction takes place. The activation energy is calculated from the slope of the plot of ln k as a function of reciprocal temperature.

III.1.6 Scanning electron microscopy (SEM)

Micrographs were obtained using a field emission scanning electron microscope (FE-SEM) (FEI-XL30, FEI Company, Oregon, USA). Samples were subjected to the critical point drying procedure in order to avoid excessive shrinkage. For imaging, samples were mounted on aluminum sample holders and air dried. Bone samples were sputter-coated with gold-platinum before observation. The electron beam was used with an accelerating voltage of 20 kV.

III.1.7 Statistical analysis of results

In order to determine the differences in mean values based on the three experimental replications, a Student's t-test was used. Significance level was determined at the 95% probability level. Microsoft Excel and Origin Pro 6.1 were employed for data processing and statistical analysis on the results as well.

III.2 Results

III.2.1 Demineralization reaction order

Plots of $-([Ca]_0 - [Ca]_{t^*})$ for zero-order kinetics, $\ln([Ca]_{t^*}/[Ca]_0)$ for first-order reaction, and $(1/[Ca]_0) - (1/[Ca]_{t^*})$ for second-order reaction versus time are shown in Figure 19. The slope of the plot is the rate constant of the reaction (Brown, 1991; Chang, 1998, Masel, 2001). As shown, the data fitted first-order kinetics (Figure 19(b)). Rate constant values calculated for all the demineralization treatments are presented in Table IV. Rate constants were significantly different between the cortical and trabecular bones (Table IV). Although the data plotted in Figure 19(b) fell along straight line, there was some variability noticed mainly at the start and end of the reaction. To further investigate the rate constant, k_1 can be plotted as a function of time, using the method of Van't Hoff (Masel, 2001):

$$k_1 = \frac{1}{t^*} \ln\left(\frac{[Ca]_{t*}}{[Ca]_0}\right), \tag{5}$$

where k_1 is the rate constant for a first-order reaction, t^* is the time at which the calcium concentration was evaluated. The method of Van't Hoff indicates the sensitivity of the rate constant as a function of time. Plotting k_1 versus time revealed three stages for all demineralization conditions, as shown in Figure 20:

a) First stage: the rate constant increased.

b) Second stage: demineralization occurred on a steady state. *All the kinetic parameter calculations were done based on data from the steady stage*.

c) Third stage: rate constant diminished.

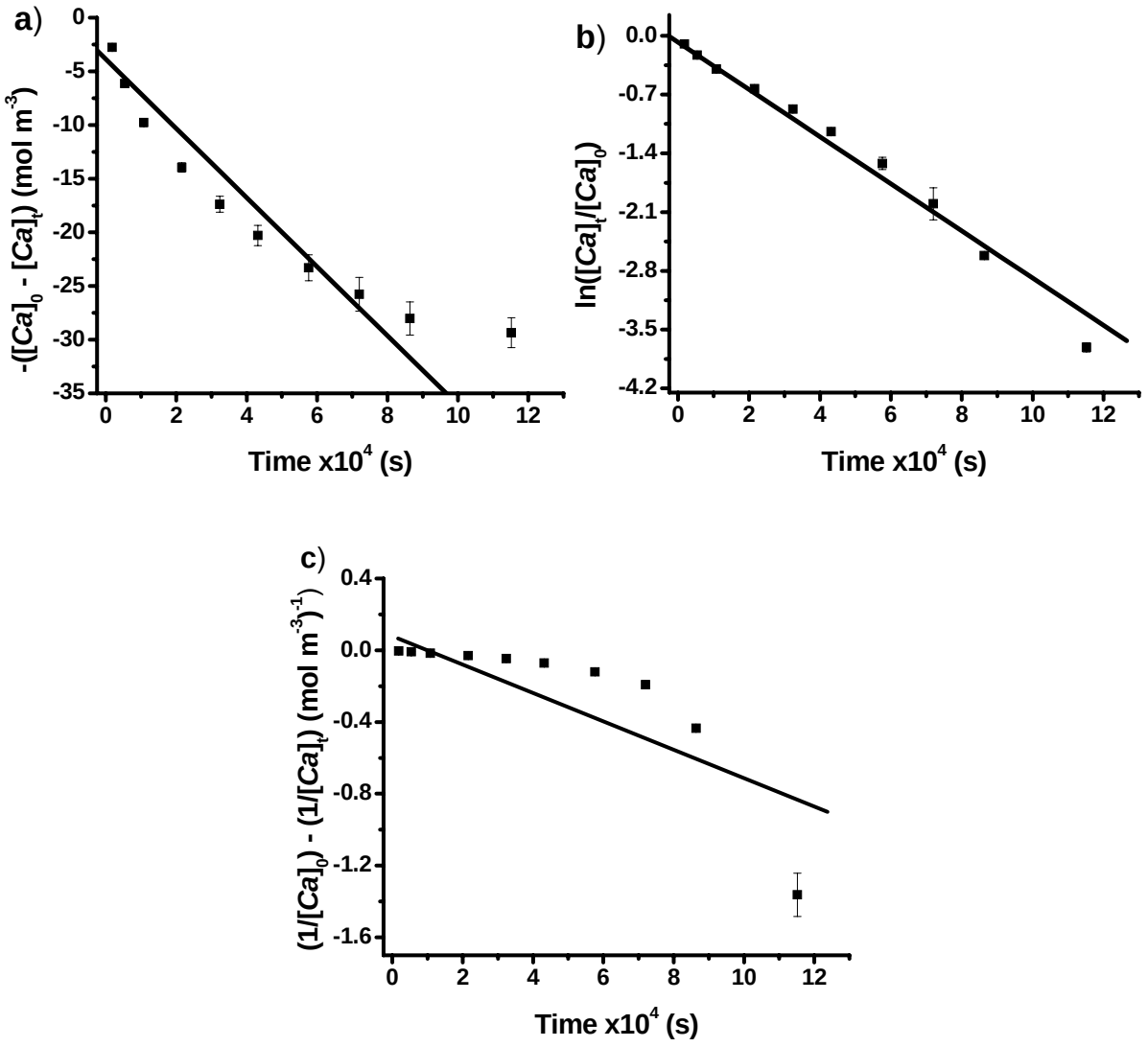

Figure 19. *Plots of a) –([Ca]$_0$ – [Ca]$_{t*}$) for zero-order reaction, b) ln([Ca]$_{t*}$/[Ca]$_0$) for first-order reaction, and c) (1/[Ca]$_0$) – (1/[Ca]$_{t*}$) for second-order reaction versus time for demineralization of cortical bovine femur bone, using 0.6 N HCl at 0°C.*

Table IV. *Rate constant, k_1 x 10^{-5} (s^{-1}) calculated for demineralization of bone as a function of HCl concentration (n = 3). Numbers in parenthesis are the standard deviation of the average rate constants.*

	k_1 x10^{-5} (s^{-1})								
	0.1 N HCl			**0.6 N HCl**			**1.0 N HCl**		
	0°C	**20°C**	**37°C**	**0°C**	**20°C**	**37°C**	**0°C**	**20°C**	**37°C**
Cortical bovine bone	N.D.	N.D.	N.D.	2.69 ±0.30[a]	2.86 ±0.02[a]	3.91 ±0.49[a]	3.58 ±0.48[a]	5.64 ±0.10[a]	9.08 ±0.47[a]
Trabecular bovine bone	2.41 ±0.17	2.84 ±0.48	4.07 ±0.89	4.80 ±0.38[b]	10.9 ±1.80[b]	13.8 ±1.20[b]	5.61 ±1.40[b]	11.8 ±0.03[b]	20.5 ±0.27[b]
Cortical antler bone	N.D.	N.D.	N.D.	3.72 ±0.18[c]	4.98 ±0.21[c]	7.42 ±0.74[c]	4.29 ±0.12[b]	5.67 ±0.36[a]	9.04 ±1.20[a]

[a]Averages with different superscript in a column are significantly different ($p < 0.05$).

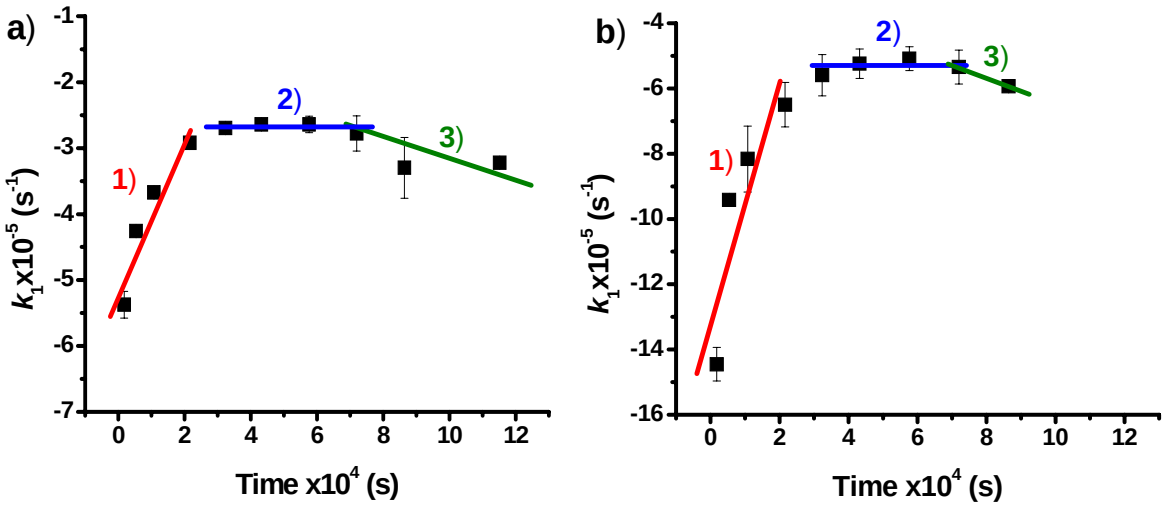

Figure 20. *The rate constant (k_1) of the first-order demineralization of a) cortical bovine femur bone and, b) trabecular bovine femur bone, using 0.6 N HCl at 0°C. Three stages were identified: 1) rate increased as HCl advanced from the periphery of the specimen to the core, 2) demineralization is on steady stage on the central part of the sample and, 3) rate diminished as calcium concentration on the sample also diminished. Further kinetics calculations were done from data on steady state.*

III.2.2 Effect of the temperature on bone demineralization

Results for cortical and trabecular bovine femur bones demineralized with 1 N HCl are presented in Figure 21. These are representative of the analysis done under the different conditions used in this work. The rate of reaction (slope) increased as the temperature increased for both types of the bones (Table IV). It is important to mention that the cortical antler bone and the trabecular bovine femur bone demineralized at 37°C using 0.6 N and 1.0 N HCl, experienced a permanent deformation of its structure after completing the demineralization process, this is, samples completely shrank, reducing their volume from ~125 mm^3 to ~8mm^3. This indicated that the combination of high temperature (37°C) and high HCl concentration ([HCl]) (0.6 N and 1.0 N), adversely affected the architecture of the bone samples, therefore these conditions are not recommended for further mechanical tests, such as the compression testing, followed by demineralization under the previous conditions mentioned.

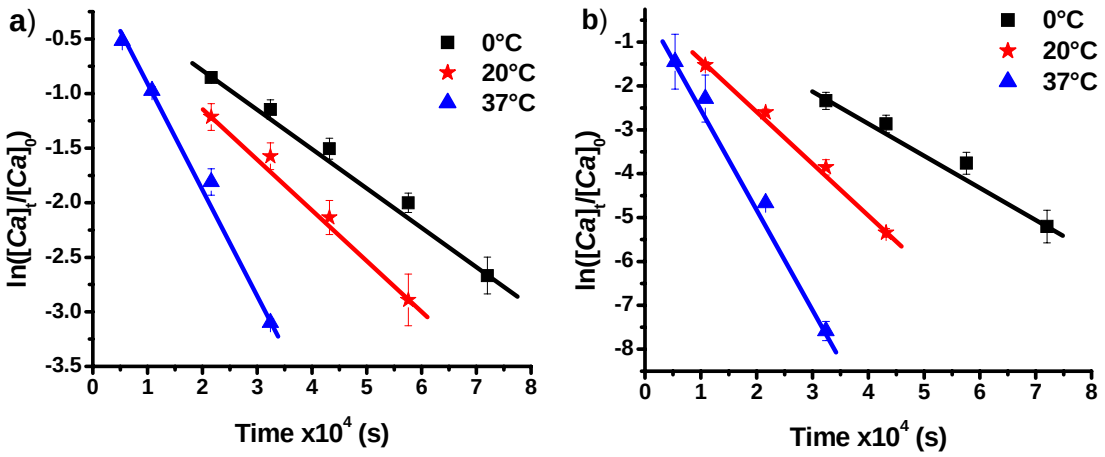

Figure 21. *Effect of temperature on demineralization of a) cortical bovine femur bone and b) trabecular bovine femur bone, using 1.0 N HCl. The data corresponds to the steady state demineralization.*

III.2.3 Effect of HCl concentration on bone demineralization

Results of the demineralization rate of cortical bone treated in HCl at 37°C are presented in Figure 22. The same procedure was applied for all different conditions used in the present work. The demineralization rate constant increased as HCl concentration increased.

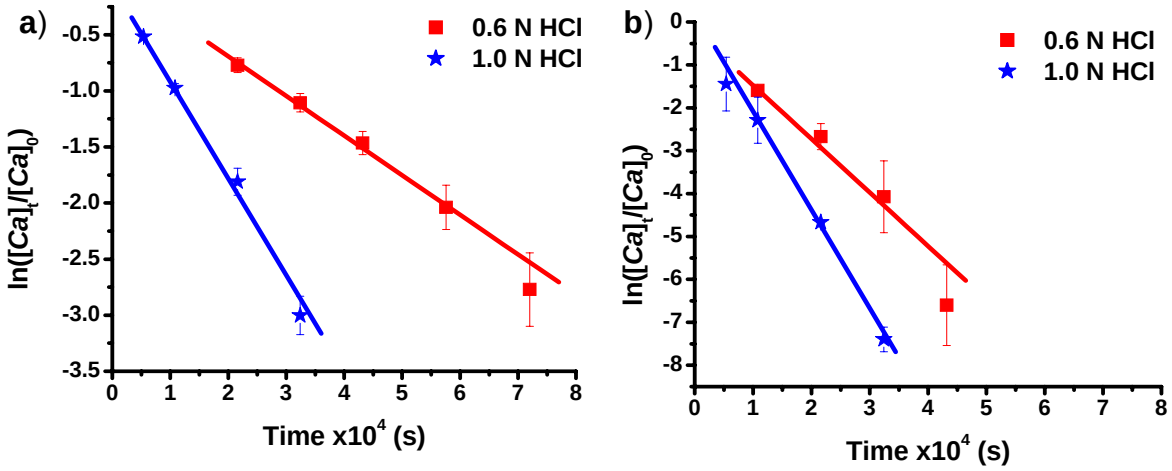

Figure 22. *Effect of HCl concentration on demineralization at 37°C of a) cortical bovine femur bone and b) trabecular bovine femur bone. The data corresponds to steady state demineralization.*

III.2.4 Effect of the surface area (architecture) of the bone inner matrix on the demineralization rate

Values of surface area per bone volume of 2,500 $m^2\ m^{-3}$ and 20,000 $m^2\ m^{-3}$, for cortical and trabecular bones respectively, were reported by Jee (1983). Previous rate constant values (Table IV) were multiplied by their corresponding bone surface area (Table V). For all practical purposes, the same surface area per bone volume was used for cortical bone and for cortical antler bone, since no data were found for the antler bone as such.

Table V. *The rate constant multiplied by the surface area of cortical and trabecular bone respectively, As · k_1 x 10^{-9} (m^2 s^{-1}), calculated for demineralization of bone as a function of HCl concentration (n = 3). Numbers in parenthesis are the standard deviation of the average rate constants*

	As · k_1 x10^{-9} (m^2 s^{-1})								
	0.1 N HCl			**0.6 N HCl**			**1.0 N HCl**		
	0°C	**20°C**	**37°C**	**0°C**	**20°C**	**37°C**	**0°C**	**20°C**	**37°C**
Cortical bovine bone	N.D.	N.D.	N.D.	1.01 ±0.11[a]	1.07 ±0.007[a]	1.47 ±0.18[a]	1.34 ±0.18[a]	2.12 ±0.03[a]	3.41 ±0.17[a]
Trabecular bovine bone	16.9 ±1.19	19.9 ±3.36	28.5 ±6.23	33.6 ±2.66[b]	76.3 ±12.60[b]	96.6 ±8.40[b]	39.3 ±9.80[b]	82.6 ±0.21[b]	144.0 ±1.89[b]
Cortical antler bone	N.D.	N.D.	N.D.	1.40 ±0.07[c]	1.87 ±0.08[c]	2.78 ±0.28[c]	1.61 ±0.04[b]	2.13 ±0.13[a]	3.39 ±0.45[a]

[a]Averages with different superscript in a column are significantly different ($p < 0.05$).

III.2.5 Activation energy

The dependence of the rate constant on temperature is expressed by Eq. (4). The activation energy for each set of experimental conditions was determined by plotting the logarithm of k_1 as a function of the reciprocal of the temperature, by the linear expression of the Arrhenius equation given by:

$$\ln k = -\frac{E_a}{RT} + A\,, \tag{6}$$

In Figure 23, k_1 was plotted as a function of T^{-1} for the demineralization of cortical and trabecular bovine femur bones using 1.0 N HCl. The activation energy was calculated from the slope (Table VI). The activation energy was higher for the trabecular bone compared to the cortical bone.

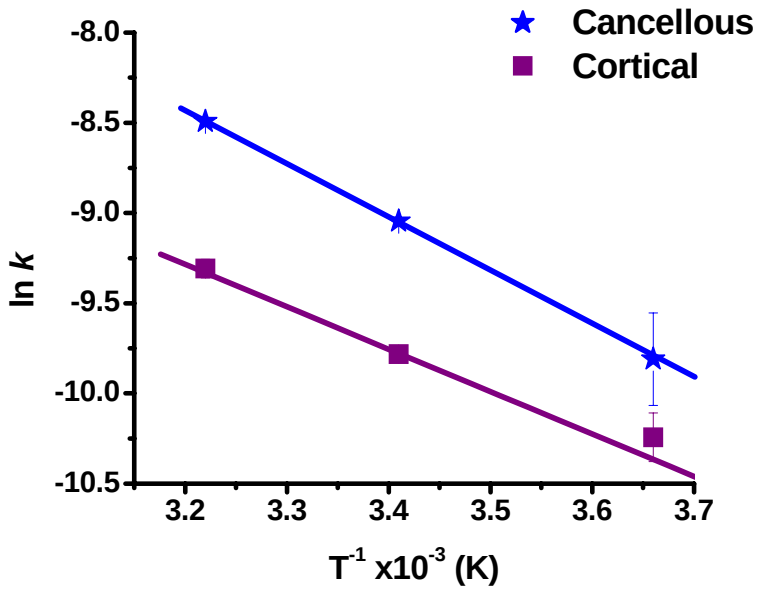

Figure 23. *The rate constant, k_1 as a function of 1/T for demineralization of cortical and trabecular bovine femur bones with 1.0 N HCl. The slope of the plot is $-E_a/R$.*

Table VI. *Activation energy calculated for demineralization of bone as a function of HCl concentration. Numbers in parenthesis are the standard deviation of the average activation energy.*

	Activation energy (kJ mol^{-1})		
	0.1 N HCl	**0.6 N HCl**	**1.0 N HCl**
Cortical bovine bone	N.D.	6.8±0.06[a]	17.6±1.7[a]
Trabecular bovine bone	9.5(3.0)	20.4±0.3[b]	25.1±4.8[b]
Cortical antler bone	N.D.	12.9±0.9	13.8±1.97

[a]Averages with different superscript in a column are significantly different ($p < 0.05$).

III.2.6 Fitting of demineralization data

Since data at three different HCl concentrations for trabecular bovine femur bone demineralized at 37°C are presented in this work, we were able to plot the

demineralization rate constants calculated for each HCl concentration. Figure 24 shows that demineralization rate constant fits well a linear tendency.

III.2.6.1 Demineralization equation

Keeping in mind the linear tendency relationship of the rate constant as a function of [HCl] and, from previous Eq. (4), we obtain a rate equation that incorporates [HCl]:

$$k_1 = A'[\mathrm{HCl}]exp\left(-\frac{E_a}{RT}\right), \tag{7}$$

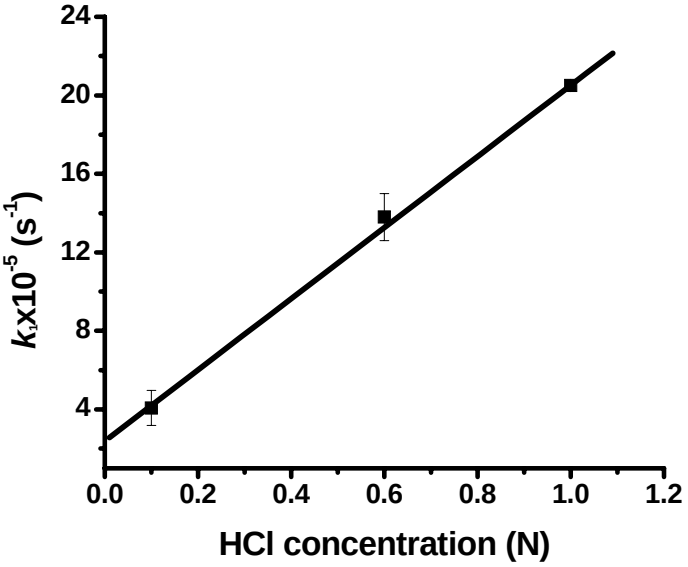

Figure 24. *Relationship of the rate constant, k_1 as a function of the HCl concentration for trabecular bovine femur bone demineralization at 37°C. Data plotted from Table IV.*

Assuming that the steady state rate constant can be expressed by the multiplication of the acid concentration with the temperature dependence, an equation that incorporates calcium concentration depletion in trabecular bovine

femur bone as a function of [HCl] and the temperature is obtained by combining Eqs. (5) and (7):

$$\frac{1}{t}\ln\left(\frac{[Ca]_t}{[Ca]_0}\right) = -A'\,[HCl]\,exp\left(-\frac{E_a}{RT}\right), \qquad (8)$$

The slope obtained by plotting $\frac{1}{t}\ln\left(\frac{[Ca]_t}{[Ca]_0}\right)$ as a function of $-[HCl]exp\left(-\frac{E_a}{RT}\right)$, will give the collision factor, *A'*.

III.2.6.2 Example using Eq. (8)

As an example using Eq. (8), the value of A' has been calculated for the cortical bovine femur bone demineralized with 1 N HCl (the slope in Figure 25) and solved Eq. (8) for the three temperatures used in this work (Table VI). The variation between the numbers experimentally obtained (*i.e.* by plotting $\ln([Ca]_t/[Ca]_0)$ as a function of time) and the values calculated by Eq. (8) were less than 10% (Table VI), which indicated that the calculation of the calcium depletion by using Eq. (8) gives values confidentially near to those experimentally calculated.

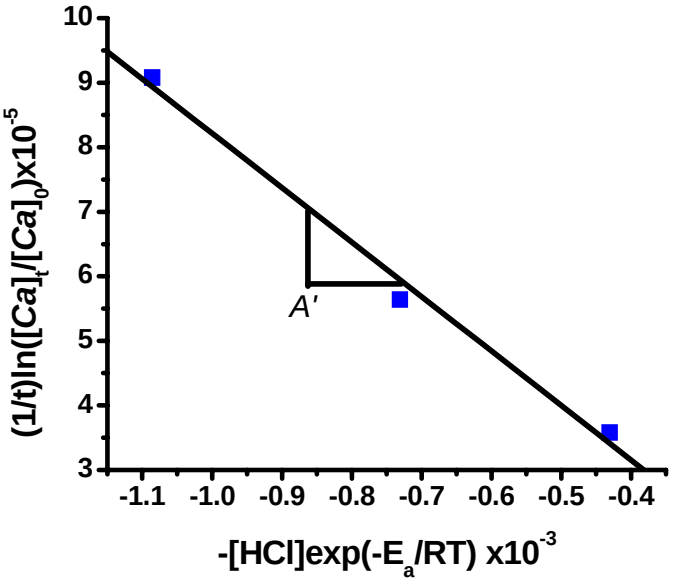

Figure 25. *Finding of A' (collision factor) for cortical bovine femur bone demineralized with 1 N HCl. A' = 0.084. Data plotted from Table VI.*

Table VII. *Kinetics data for the demineralization with 1 N HCl of cortical bovine femur bone (data from Table IV and Table VI as an example using eq. (8).*

$$\frac{1}{t}\ln\left(\frac{[Ca]_t}{[Ca]_0}\right) = -A'[HCl]\exp\left(-\frac{E_a}{RT}\right) \qquad \text{Eq. (8)}$$

$-[HCl]\exp\left(-\frac{E_a}{RT}\right)$	T(K)	Experimental $\frac{1}{t}\ln\left(\frac{[Ca]_t}{[Ca]_0}\right)$ x10^{-5} (s^{-1})	Calculated from eq. (8) $\frac{1}{t}\ln\left(\frac{[Ca]_t}{[Ca]_0}\right)$ x10^{-5} (s^{-1})	Variation coeficient* (%)
-4.3x10^{-4}	273.15	3.58	3.62	1.78
-7.3x10^{-4}	293.15	5.64	6.14	6.00
-1.08x10^{-3}	310.15	9.08	9.12	0.31

*Shows the variation (%) between the depletion of calcium calculated from eq. (8) and the value obtained experimentally from the plotting of $\ln([Ca]_t/[Ca]_0)$ vs. time.

III.2.7 SEM imaging

SEM micrographs of untreated cortical bovine femur bone are shown in Figure 26 a–b, which clearly shows the mineralized collagen fibers. The protein phase alone was observed when bones where treated with 0.6 N HCl at 20 °C until complete demineralization was reached (Figure 26 c–d).

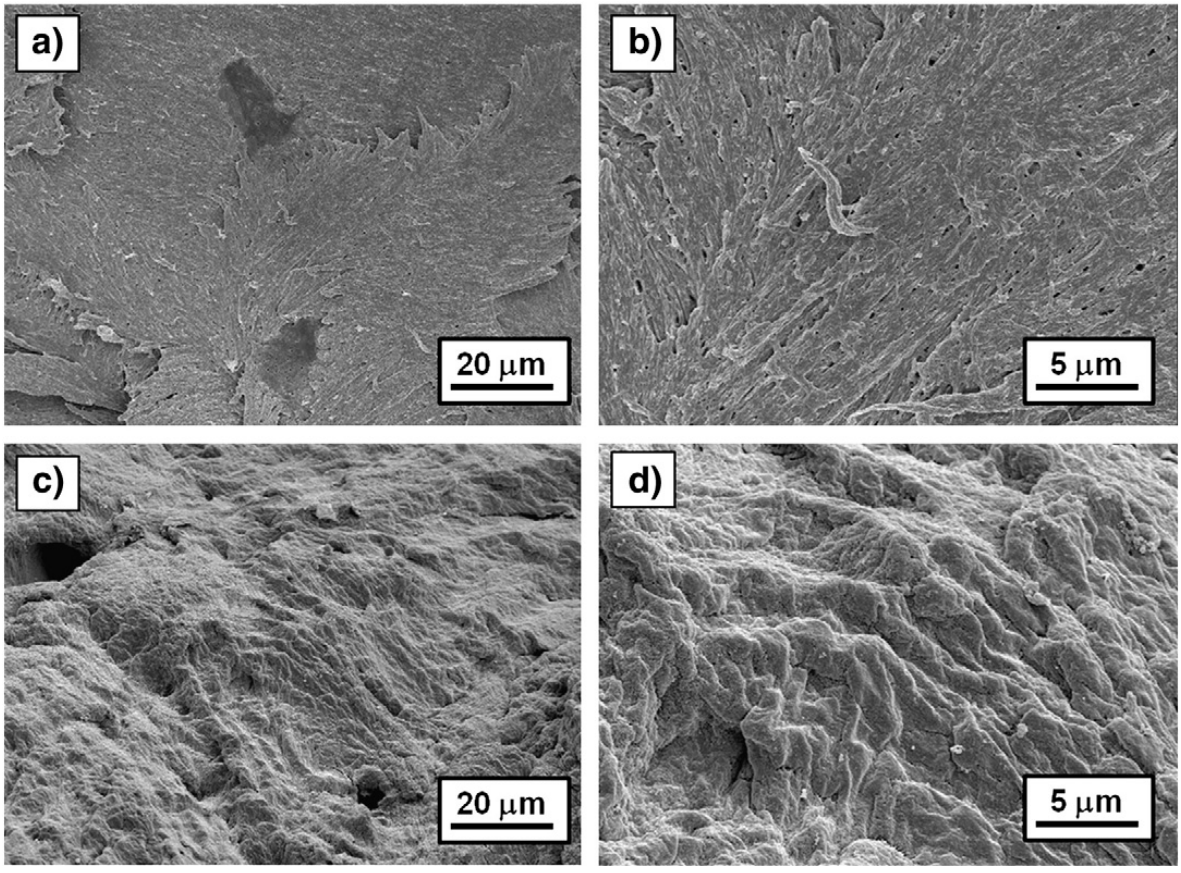

Figure 26. *Scanning electron microscopy images of a-b untreated, and c-d completely demineralized cortical bone.*

III.3 Discussion

Bone demineralization was found to fit a first order reaction, and the analysis of the demineralization kinetics of cortical antler bone corroborated the results obtained for cortical bovine femur bone.

Three different demineralization stages were identified for cortical and trabecular bones. In the first stage of bone demineralization, the rate increased as the HCl advanced from the periphery to the core of the sample. In the second stage, steady rate constant values were calculated indicating that demineralization occurs on a steady state. According to Brain (1966) demineralization requires longer time to be completed in the central part than in the peripheral part of a bone sample. Therefore, this steady state should correspond to the central part of the bone. Finally, in the third stage, the rate constant diminishes as the calcium concentration in the bone also becomes depleted.

The first stage of demineralization was more pronounced in the trabecular bone than in the cortical. This can be attributed to the structural differences observed between cortical and trabecular bones (Biggi *et al*., 1997; Chappard *et al*., 2001; Thurner *et al*., 2009). The pores of the trabecular bones could facilitate the mobility of the HCl molecules leading to a longer first stage, which corresponds to the periphery of the bone.

The rate of demineralization increased with increasing HCl concentration. This can be explained as follows: according to Eq. (9), chlorine and calcium ions react with each other by:

$$Ca_{10}(PO_4)_6(OH)_2 + 20HCl \rightarrow 10CaCl_2 + 6H_3PO_4 + 2H_2O, \qquad (9)$$

From the chemical kinetics theory of collisions, it is known that the rate of a reaction is directly proportional to the number of molecular collisions per second (Brown, 1991; Chang, 1998). This relation explains the dependency of the reaction rate on the reactant concentration. As HCl concentration increases, the probability

to have more successful collisions between chloride and calcium ions is higher. Therefore, the reaction rate increases with increasing HCl concentration. In addition, the increment of the rate constant was more notorious in trabecular than cortical bone. The higher porosity of the internal matrix of trabecular bone, as well as its higher surface area, improved the contact of the HCl molecules with the inner section of trabecular bone, this could led as a consequence, to a higher effect of the HCl concentration on the rate of demineralization for trabecular compared to cortical bone.

The demineralization rate constants increased with temperature. At higher temperature, the HCl molecules increase their energy; therefore the demineralization reaction is more likely to occur. Thus, as a consequence, the rate constant has been observed to increase (Brown, 1991; Chang, 1998). However, the effect of the temperature is more apparent in trabecular than cortical bone. This could be attributed to the dilatation of the pores in trabecular bones. Studies relating to the porosity and the temperature on other minerals, such as the silicates, have shown that the porosity of the material increases with temperature (Cultrone *et al*., 2004). In addition, it has been previously reported that the porous microarchitecture of the trabecular bones suffers adaptations due to biomechanical and metabolic changes (Chappard *et al*., 2001), and it also adapts during aging (Parfitt *et al*., 1983), which shows the capability of trabecular bone to change its architecture as a function of the environmental conditions, the temperature increment, in this case. This characteristic of the trabecular bones could facilitate the expansion of its pores, promoting the diffusion of the demineralizing solution (HCl) as a consequence, which increased the efficiency of the contact of the HCl molecules with the inner matrix of the trabecular bone as the temperature increased, compared to cortical bone.

Demineralization rate constants for cortical bone increased one order of magnitude, while the increment for trabecular bone was of two orders of magnitude after considering the surface area per bone volume corresponding to each type of

bone. This is completely reasonable, since surface area of trabecular bone is approximately 87% higher than the one for cortical bone. From a merely chemical focus, as the contact area between the reactant (bone) and the demineralizing agent (HCl) increase, the rate of the reaction also increases. But, bones are very complex systems, and other factors must be considered. Trabecular and cortical bones have the same chemical composition: hydroxyapatite (mineral) and collagen (protein), however demineralization rate constants for trabecular bone are significantly higher than those of the cortical. Meier *et al*. (1984) studied the rate of loss of trabecular and cortical bones through the years in healthy men. They found that cortical bone mineral content falls much less rapidly than vertebral trabecular content with age. In this work, trabecular and cortical bone samples were subjected to a rapid mineral loss by the action of different concentrations of HCl, as well as the increment of temperature. Therefore, our results are corroborated by previous findings by other authors (Meier *et al*., 1984) that indicate that trabecular bone is more susceptible to bone loss (mineral content depletion) and fracture, as a consequence, even in healthy bones. This marked disparity in bone (mineral) loss depletion is directly related to chemical, structural, functional and metabolic differences. Bigi *et al*. (1997) reported a reduced carbonate content and Ca/P molar ratio in trabecular bone compared to cortical. While the Ca/P molar ratio is close to that of stoichiometric apatites, in trabecular bones it is significantly reduced. These authors also reported that trabecular bone has a lower degree of maturation with respect to cortical bone. Noris Suarez *et al*. (1996) reported differences in the nonreducible cross-links in the collagen fibrils, which could affect the nucleation site for mineral formation, or the site where mineral deposition occurs. Therefore, the differences found in this work for rate of mineral depletion in trabecular and cortical bones can be attributed not only to differences in the inner matrix architecture between the two types of bones, but also to differences in the mineral component.

The activation energy values were calculated from the slope of the plots of ln *k* as a function of the reciprocal temperature. Activation energy was calculated to be

not only higher for trabecular than for cortical bone, but also increased as the HCl concentration increased. We could have expected the contrary since mineral depletion seems to be easier in trabecular than cortical bone (rate constants were higher for trabecular bone, and they increased as the HCl concentration was higher). However, our results may indicate that other factors should be considered, which could be due to differences in their inner matrix architecture. Noris Suarez *et al*. (1996) reported that the collagen of cortical and trabecular bones, in the rat, has different extents in posttranscriptional modifications, which indicates that the matrix of each types of bones has a different network organization. Therefore, the type of mineral and its association with the collagen scaffold leading to the mineralized collagen matrix might not be exactly the same, which produces bones with different functional features. The functional differences in cortical and trabecular bones might be based on molecular differences. It is important to consider the previous molecular information because it indicates that energy requirements for demineralization reaction to occur should be different, and that those differences are intrinsically related to the distinct matrix network of cortical and trabecular bones. Thus, our activation energy results might be attributed to the differences in the inner matrix between both types of bones. From one perspective, the demineralization in trabecular bone is favored by its high surface area, which allows a greater amount of bone to be in contact with the demineralizing solution (HCl) compared to cortical bone. However, as the demineralization reaction occurs along the trabecular inner matrix, the mineral-collagen bonds might be harder to access by the HCl solution, and they might become highly protected from hydrolysis, as a consequence. This hypothesis can be supported by the fact that activation energy values increased as the HCl concentration was higher, although the rate constants also increased under these conditions. As the HCl concentration was higher, the access to the mineral-collagen bonds became more difficult as the HCl solution penetrated the bone matrix. These results are corroborated by the activation energy values calculated for cortical antler bone. Our results suggest that the differences in the inner matrix architecture between the two bones, in

conjunction with their chemical differences, are responsible for these different activation energy requirements.

On the other hand, SEM images of the demineralized and the untreated bones shows that the structural features are well preserved after HCl treatment.

These exceptional findings concerning to the physicochemical characteristics of bone demineralization can be corroborated by the kinetic parameters of deproteinization, which will be analyzed in the next chapter.

III.4 Conclusions

Demineralization experiments were performed on cortical and trabecular bovine femur bones, and cortical antler bone. Kinetic parameters of the rate equation were determined at three temperatures (0°C, 20°C and 37°C), using three HCl concentrations (0.1 N, 0.6 N and 1.0 N). The following conclusions were obtained from this research:

1. An efficient method for the quantitative measurement of the bone mineral (calcium) content was used.
2. As the HCl concentration or temperature increases, the rate of demineralization also increases.
3. Bone demineralization occur in three stages:
    a. First stage: the rate constant increased as HCl solution demineralized the peripheral part of the sample.
    b. Second stage: demineralization occurs at a steady state. This steady state corresponds to demineralization of the central part of a bone sample.
    c. Third stage: at the end of the reaction, rate constant decreases as calcium concentration in the bone becomes depleted.
4. Statistical differences are found on the demineralization rate constants and activation energy values for trabecular and cortical bones. This is attributed to

the effect of the differences on the inner matrix architecture between the cortical and the trabecular bones.

5. A good linear fit was found for cortical bovine femur for the demineralization rate constant as a function of [HCl].

6. An Arrhenius equation that expresses demineralization as a function of [HCl] and temperature was proposed. By plotting this equation one can obtain the frequency factor, *A'*, which indicates how many collisions lead to products:

$$\frac{1}{t}\ln\left(\frac{[Ca]_t}{[Ca]_0}\right) = -A'\,[HCl]\,exp\left(-\frac{E_a}{RT}\right)$$

7. The structural features on demineralized bones are well preserved as observed by SEM.

Chapter IV

Kinetics of the *in vitro* deproteinization of bovine femur bone

In this chapter, the Lowry method is used for the quantification of the protein based on a bovine collagen-extracted reference curve. The complete methodology developed for the quantitative measurement of the protein content in cortical and trabecular bovine femur bones, as well as the construction of the standard curve used as reference for protein quantification, along with its characterization by X-ray and infrared spectroscopy are described. The rate constant and the activation energy of the deproteinization reaction are calculated and discussed.

IV.1 Materials and methods

IV.1.1 Sample preparation

A whole piece of bovine femur bone was purchased from a local butcher (Ensenada, México). The slaughter age of the cattle was approximately 24 months. The femur was cut into approximately 1 cm slices by a Torrey® meat saw. The femur was carefully cleaned by hand to remove any marrow and lipid content using a pressurized stream of compressed air and water, as previously reported (Fantner *et al.*, 2005; Thurner *et al*., 2009). Cortical and trabecular bones were sectioned into small cubes (5 mm x 5 mm x 5 mm) using a rotating diamond wheel saw. For the experiments, 100 pieces of cortical and trabecular bones were used.

IV.1.2 Deproteinization experiments

The bones were immersed into 40 ml of 6% NaOCl. Three temperatures were used: 37°C, 50°C and 60°C in order to analyze the effect of the temperature on the rate of deproteinization in cortical and trabecular bones. For each experimental condition, triplicate set of samples were maintained. Each temperature condition was reached and maintained using a convection oven (Blue M Electric Company, Model OV-560A-2, Blue Island, Illinois, USA). In order to determine rate of protein depletion for each bone and temperature condition, a triplicate of bone samples were removed from the solution at different times (Table VIII). After removed, bones were rinsed with distilled water and air dried. Cortical bone has a denser structure therefore, refreshing of the NaOCl solution was done for deproteinization assays at 50°C (21.6 h) and 60°C (14.4 h), the solutions were not refreshed for the 37°C experiments. Refreshing of the deproteinization solution was not necessary for trabecular bone, since saturation of the NaOCl solution did not occurred (Figure 27a). The refreshing time was selected from previous visual analysis of the solution when was saturated.

Table VIII. *Deproteinization evaluation times (h) for each type of bovine femur bone at the different treatment temperatures.*

	Time (h)	
Temperature (°C)	**Cortical bovine femur bone**	**Trabecular bovine femur bone**
37	4, 9, 22.5, 27.5, 33.	1.5, 3, 4.5, 6, 8, 10, 12, 14, 16, 18.
50	7.2, 14.4, 21.6^{R}, 24.1, 29.1, 31.6	3.6, 7.2, 10.8, 14.4, 21.6, 25.2, 28.8, 36.
60	4.8, 9.6, 14.4^{R}, 19.2, 24, 28.8^{R}, 43.2, 48.	2,4, 4.8, 7.2, 9.6, 12, 14.4, 19.2, 24.

^{R}Refreshing of the 6% NaOCl solution

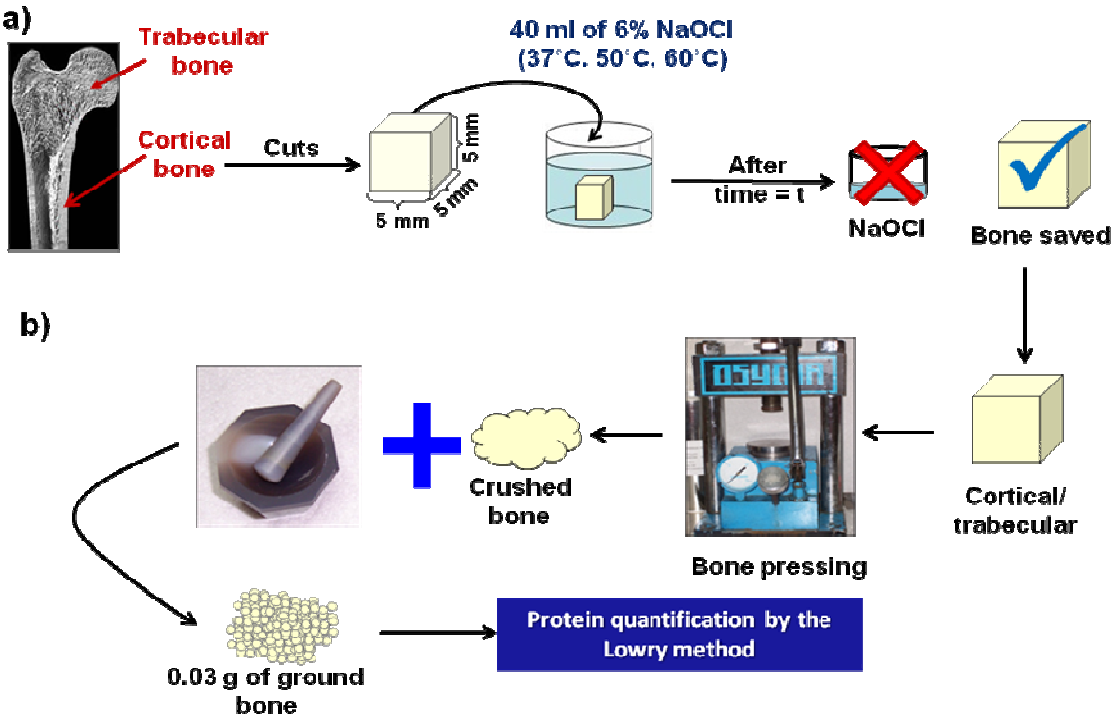

Figure 27. *a) Procedure used for bovine bone deproteinization with NaOCl at three temperatures. b) Preparation of the deproteinized bones for the protein quantification.*

IV.1.3 Protein quantification

Protein content left into the bone sample after deproteinization was quantified by the Lowry method (Lowry *et al*., 1951), with the following modifications: the cortical and trabecular bones deproteinized at different times (Table VIII) were crushed in a hydraulic press and then ground with a mortar and pestle (Figure 27b). The protein quantification was performed in two steps: 1) *protein extraction*: 0.03 g of trabecular and cortical ground bone were collected corresponding to each time and temperature of the deproteinization assays. Protein from the ground bone was extracted using 3 ml of 0.5 N NaOH at 100°C (in order to accelerate the removal of the protein from the bone) for 15 min. These conditions were previously determined by analyzing protein extraction using 0.1 N, 0.6 N and 1 N NaOH and measuring protein concentration after a first extraction (15 min) and a second extraction (15 min more). Results indicated that the best conditions were 0.5 N

NaOH and no second extraction was necessary since all of the remaining protein in the samples was removed by the first extraction. Samples were then cooled using a cold water bath, then centrifuged at 4000 rpm at 5°C for 5 min ((Figure 28a). 2) *Protein quantification*: protein was quantified by taking 1 ml of supernatant liquid and mixing it with 5 ml of an alkali solution (2% Na_2CO_3 in 0.1 N NaOH, 0.5% CuSO4·5$H_2$0 and, 1% $KNaC_4H_4O_6 \cdot 4H_2O$ mixed in a 100:1:1 ratio). Samples were left to react for 10 min. Then, 0.5 ml of 50% folin phenol reagent (in water) was added to the previous mixture. Samples were left to react for 1.5 h in dark environment (the folin reagent is sensitive to the light). Absorbance was read at 750 nm, using a halogen gas-filled tungsten lamp, in a HACH® spectrophotometer (Model 4000 UV). Protein content, in mole l^{-1}, was calculated by interpolating the absorbance data at 750 nm (Figure 28b) in a bovine bone protein reference curve (Section IV.1.5).

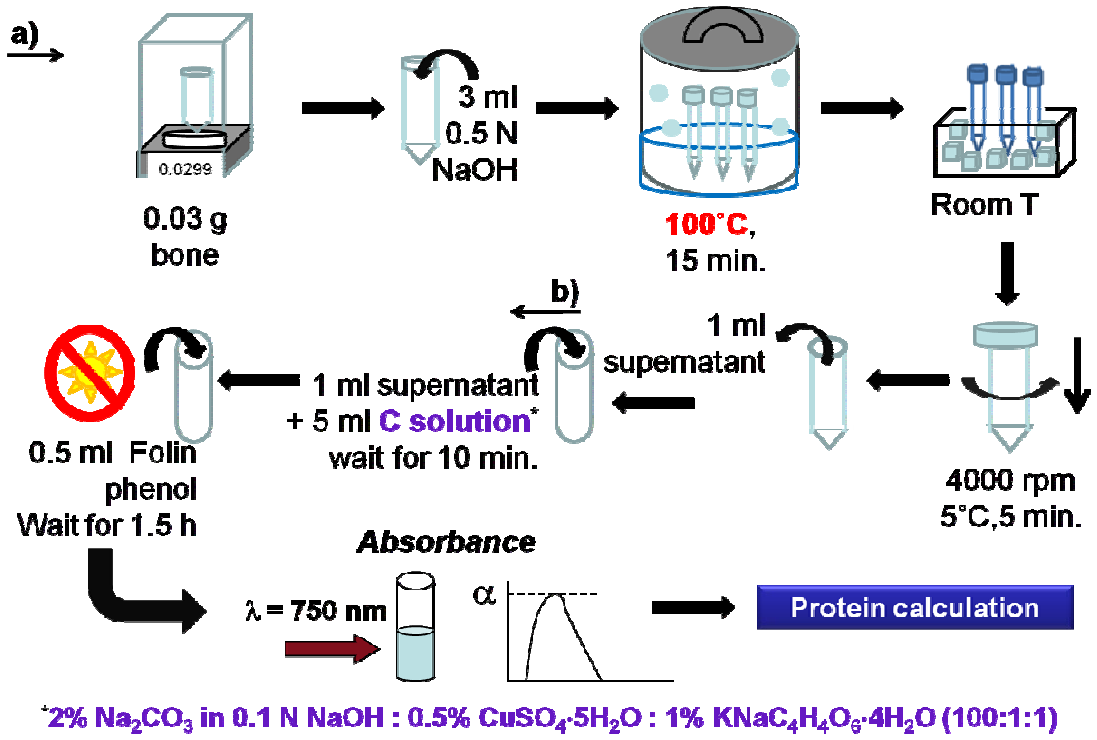

Figure 28. *a) Bone protein extraction procedure. b) Application of the Lowry method (Lowry, 1951) for the quantification of the bone protein extracted at different times and temperatures (see Figure 27 and Table VIII).*

IV.1.4 Construction of a protein reference curve

A protein reference curve was used in order to quantify the protein content remaining in each bone sample after each deproteinization time (Table I). The curve was prepared using a solution of protein from cortical bovine bone. We preferred to prepare our own protein reference curve from bovine bone extracted protein, since Bovine Serum Albumin (BSA) - the reference most used for protein quantification- is not the perfect reference for collagen quantification. In this point, is important to mention that all the calculations presented in this work are based on the bovine type-I collagen data; the non-collagenous proteins were neglected. The protein was extracted as previously described in the section IV.1.3, step 1 (see also Figure 28a). The supernatant recovered from the extraction step (Figure 28a) contained the bone protein. The concentration of the protein solution was calculated using the Beer-Lambert law (Rosenberg, 1996):

$$A = \varepsilon \mathrm{l} \left[P \right], \tag{10}$$

where A is the absorbance of the protein solution at 280 nm, ε is the molar absorption coefficient [(mol l^{-1})$^{-1}$ cm^{-1})], ℓ is the pathlength (cm), and $\left[P\right]$ is the protein concentration (mol m^{-3}) of the protein solution extracted from the bone. $\left[P\right]$ was converted into mol m^{-3} for further calculations.

The ε value was calculated according to Pace *et al*. (1995):

$$\varepsilon\,(\mathrm{M^{-1}cm^{-1}}) = (\#\mathrm{Trp})(5{,}500) + (\#\mathrm{Tyr})(1{,}490) + (\#\mathrm{Cys})(125)\,, \tag{11}$$

where #Trp, #Tyr and, #Cys are the number of the tryptophan, tyrosine and cystine amino acids residues, respectively. The numbers: 5,500; 1,490 and, 125 are the molar absorption coefficients [(mol/l) $^{-1}$ cm^{-1})] at 280 nm for Trp, Tyr and, Cys, respectively (Pace *et al*., 1995).

The amino acid sequences for bovine collagen type-I α1 chains (NCBI Reference Sequence: NM_001034039.1) and α2 chain (NCBI Reference Sequence: NM_174520.2) used for the calculations presented in this work were obtained from the National Center for Biotechnology Information (NCBI, 2010).

A gradient of the protein solution was prepared based on the concentration $[P]$ calculated by Eq. (10), in mol m^{-3}. Then, the Lowry method (Lowry *et al*., 1951) (see section IV.1.3, step 2) was used in order to measure the absorbance at 750 nm corresponding to each solution of the prepared gradient of solutions. A reference curve was constructed by plotting the absorbance at 750 nm as a function of the bone protein concentration (Figure 29).

IV.1.4.1 Characterization of the protein reference solution

The protein solution extracted from cortical bovine femur bone used for the construction of the reference curve (section IV.1.5) was freeze dried for 5 days using a lyophilizer (Labconco, Kansas, MO, Model 75018-18). The powder was used for X-ray diffraction and infrared (IR) analyses in order to verify the absence of the bone mineral phase. An untreated powdered sample of cortical bovine femur was used as reference for comparison.

X-ray diffractograms were recorded by a Phillips X'pert equipment, operated at 45 kV and 40 mA, using Cu Kα radiation (λ = 0.154060 nm). Scanning was performed in continuous mode at 0.02°/s acquisition speed, and between 10° to 60° 2θ. IR spectra were obtained from the powders. The scans were performed between 4000 and 400 cm^{-1}, after 32 accumulations, at 4 cm^{-1} resolution. A ThermoNicolet (Model Nexus) spectrometer was used.

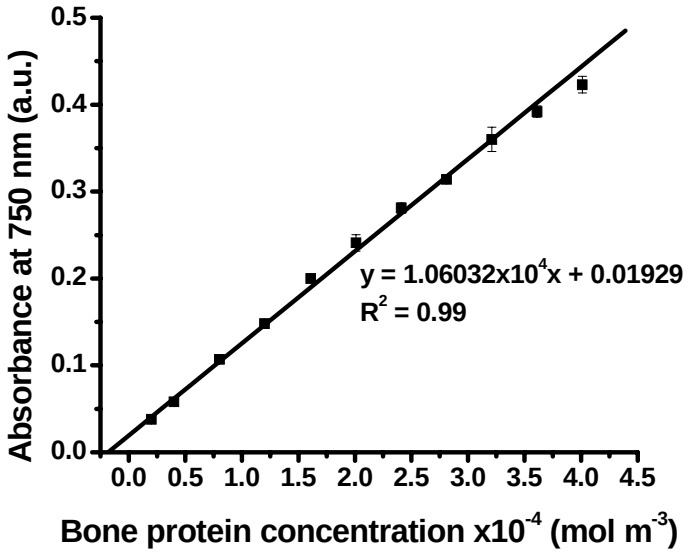

Figure 29. *Standard curve for the Lowry protein assay. A cortical bovine femur soluble protein extract was used as a reference.*

IV.1.5 Measurement of the particle diameter of the powdered bones

The homogeneity of the powdered bones (Section IV.1.3) was evaluated by measuring the particle size diameter of a representative set of cortical and trabecular samples (each in triplicate) using a particle counter Beckman Coulter (Model Multisizer 3, Brea, CA). A suspension prepared with 0.015 g of bone sample in 15 ml of 0.9% NaCl was used for the particle diameter measurements.

IV.1.6 Kinetics of deproteinization

The rate of protein depletion was calculated based on the rate law, described by:

$$rate = \frac{d[P]}{d\mathrm{t}} = A_s k [P]^n , \qquad (12)$$

where $\left[P\right]$ is the protein concentration (mol m^{-3}), t is the time (s), *k* is the rate constant, *n* is the order of reaction and A_S is the surface area per bone volume: 20,000 m^2 m^{-3} for trabecular bone, and 2,500 m^2 m^{-3} for cortical bone (Jee, 1983). The order of reaction was determined by plotting $-(\left[P\right]_0 - \left[P\right]_t)$ for zero order reaction, $\ln(\left[P\right]_t / \left[P\right]_0)$ for first order, and $(1/\left[P\right]_0) - (1/\left[P\right]_t)$ for second order kinetics as a function of time. The plot most linear indicates the order of reaction. The rate constant was obtained from the slope of the plot. Since 0.03 g of either trabecular or cortical bone were weighted, and the density (ρ) for cortical and trabecular bone are known: 2,000 kg m^{-3} and, 865 kg m^{-3}, respectively; the volume, in m^3, of each bone was calculated. Each of these numbers were multiplied by either 2,500 or 20,000 m^2 m^{-3} to get the total surface area per 0.03 g of bone, $3.75x10^{-5}$ m^2 for cortical and $7x10^4$ m^2 for trabecular. There was assumed that the surface area did not change much during deproteinization.

The protein concentration $\left[P\right]$ was calculated based on linear equation obtained from the protein reference curve (Figure 29) by:

$$[P] = \frac{(A_{750}) - 0.01929}{1.06032x10^4}, \tag{13}$$

where $\left[P\right]$ is the protein concentration of the deproteinized sample, in mol m^{-3}, obtained by interpolating the absorbance (A_{750}), at each deproteinization time, in the reference curve (Figure 29).

IV.1.7 Activation energy calculation

The dependence of rate constant on temperature is expressed by the Arrhenius equation (Eq. 4) as previously described in the Section III.1.5.

IV.1.8 SEM imaging

Micrographs of untreated and completely deproteinizated bovine bone samples were prepared under the same conditions previously described in the Section II.1.6.

IV.1.9 Statistical analysis of the results

The statistical analysis of results was performed in the same way described in section III.1.7.

IV.2 Results

IV.2.1 Characterization of the protein extract used as reference

The protein reference curve (Figure 29) fit well to a linear relationship (R^2 = 99). The linear equation obtained from this curve was used to calculate the protein concentration (mol m^{-3}) by interpolating the absorbance read at 750 nm corresponding to any of the times stated in Table VIII.

The presence of collagen and the absence of the mineral phase (hydroxyapatite) in the lyophilized protein reference were demonstrated by X-ray analysis. The diffractogram of the untreated bone (Figure 30a) shows the hydroxyapatite phase (Joint Committee on Powder Diffraction Standards, JCPDS, card file No. 00-001-1008). While for the lyophilized protein reference (Figure 30(b)) it is clear that the hydroxyapatite was completely eliminated and only the NaOH (JCPDS card file No. 00-0030-1194) phase was identified.

IR analysis was used to confirm the X-ray studies. The IR characteristic peaks for the mineral phase, PO_4^{3-} and CO_3^{2-}, were identified in the untreated bone spectrum (Figure 31a) at the regions of 900-1200 cm^{-1} and 840-890 cm^{-1}, respectively. A peak on the region of 1595-1720 cm^{-1}, corresponding to the amide I frequency was also identified. The IR spectrum of the lyophilized protein reference (Figure 31b) corroborates with the X-ray analysis. Peaks at the mineral phase regions were absent.

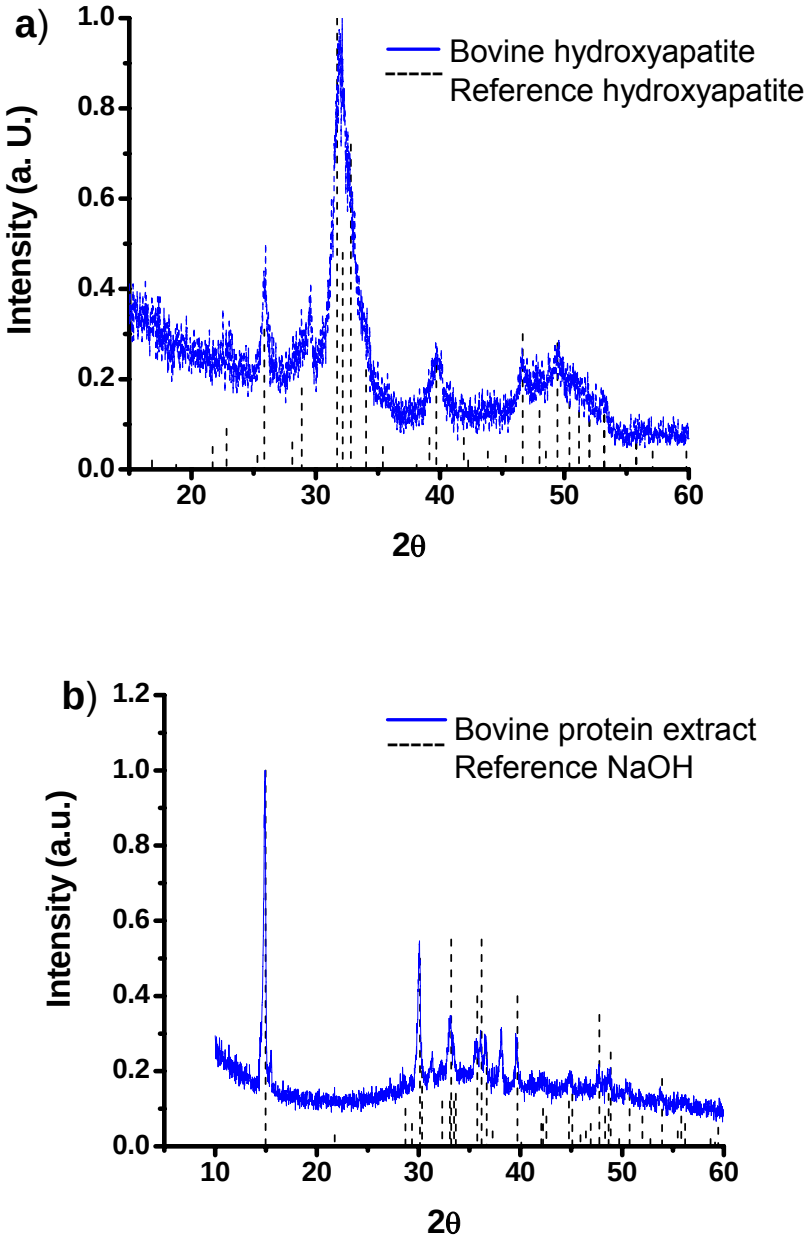

Figure 30. *X-ray diffractograms of a) untreated cortical bovine bone. Peaks correspond to Joint Committee on Powder Diffraction Standards (JCPDS) file 00-046-0905 for hydroxylapatite. b) Protein reference solution (lyophilized) from cortical bovine femur bone. Peaks correspond to JCPDS file 00-030-1194 for NaOH (the solution used for the extraction of the bovine protein).*

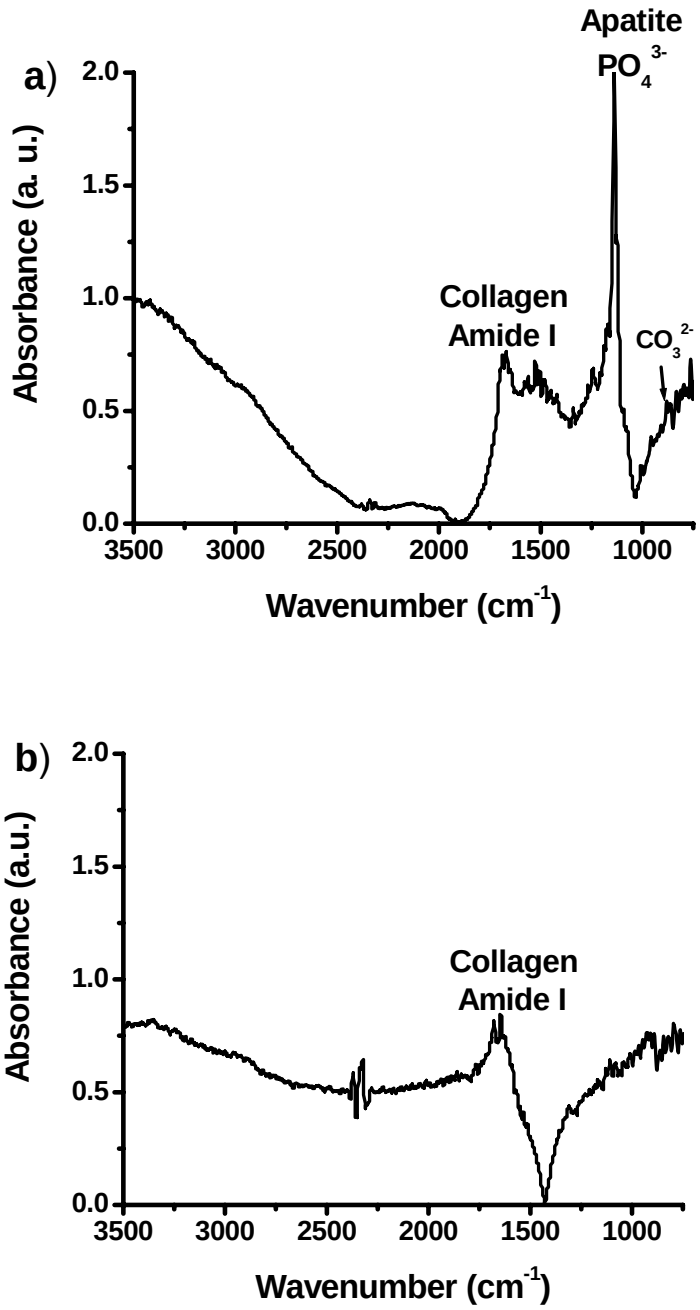

Figure 31. *Infrared spectra of bone. a) Intact, and b) protein extract from cortical bovine femur bone.*

IV.2.2 Size diameter of the powdered bones

The measurement of the diameters of the ground cortical and trabecular bones after being deproteinized at different times (Table VIII) varied from 3 to 25 μm and 3 to 35 μm for cortical and trabecular samples, respectively. The average size is 5.00±0.04 μm for cortical and 6.12±0.10 μm for trabecular bones. And the calculated mode values are 2.90±0.06, and 2.97±0.08, for cortical and trabecular, respectively (Table IX).

Table IX. *Representative particle size diameter (μm) (n = 3) of the ground bovine cortical and trabecular bones used for protein quantification (after deproteinization, Figure 27).*

	Size particle interval (μm)	**Size average (μm)**	**Mode**
Cortical bone	3 - 25	5.00±0.04	2.90±0.06
Trabecular bone	3 - 35	6.12±0.10	2.97±0.08

IV.2.3 Kinetics of deproteinization

Plots of $-([P]_0 - [P]_t)$ for zero order reaction, $\ln([P]_t/[P]_0)$ for first order, and $(1/[P]_0) - (1/[P]_t)$ for second order kinetics as a function of time for trabecular bone deproteinized at 50°C are showed in Figure 32, which indicate that deproteinization of bovine bone fitted well to zero order kinetics.. In Chapter III, it was showed that bone demineralization follows first order kinetics. The finding of different order of reaction for both processes is not surprising since demineralization and deproteinization are quite different reactions, although there is a synergistic effect in bone between mineral and protein.

Plots of the protein concentration (mol m^{-3}) as a function of time (s) were constructed for cortical and trabecular bones (Figure 33) in order to determine the rate of protein depletion for each bone at each temperature. As shown (Figure 33), there is a linear relationship between the protein concentration and time, where the

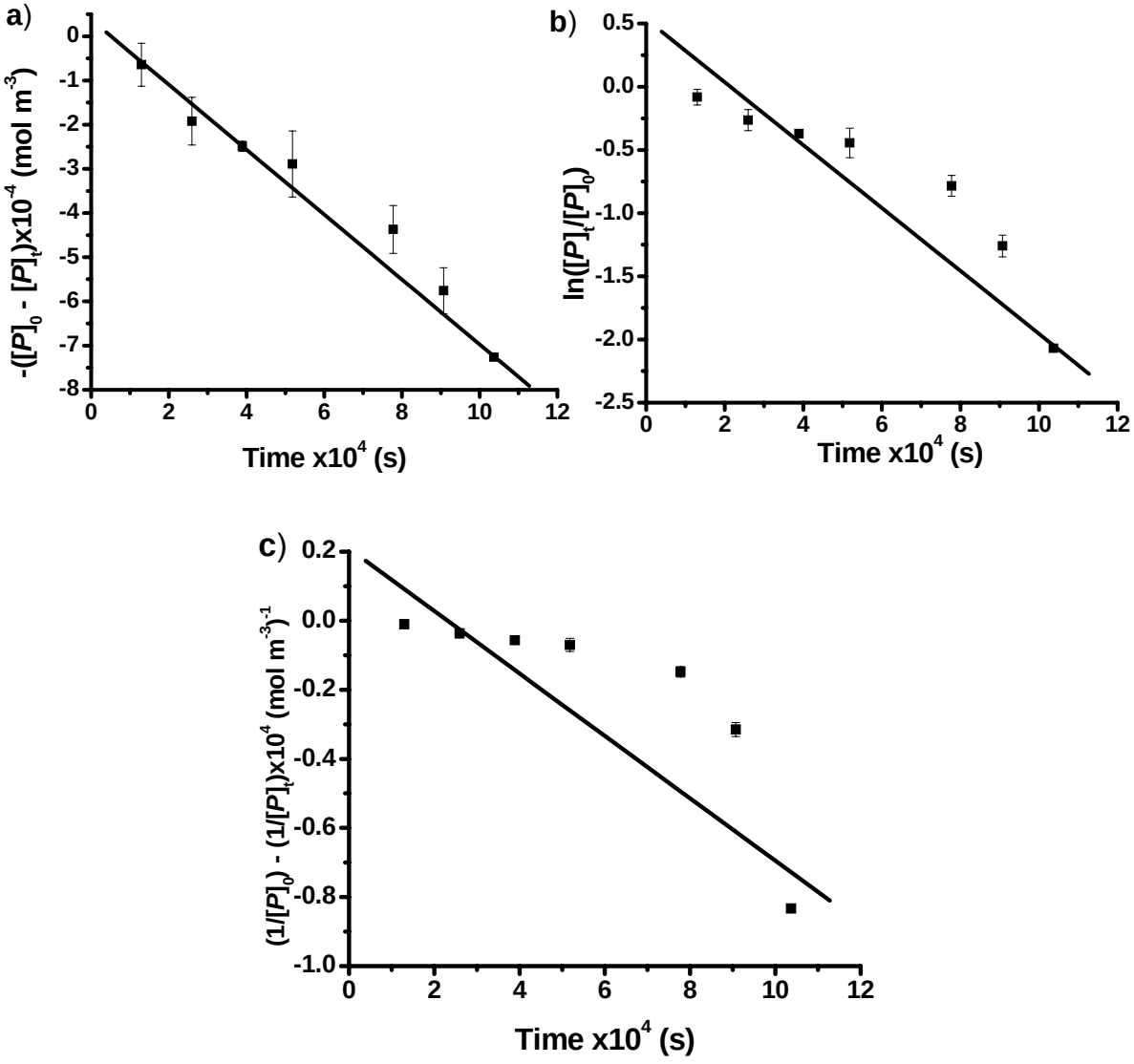

Figure 32. *Plots of a) –($[P]_0 - [P]_t$) for zero order reaction, b) ln($[P]_t/[P]_0$) for first order, and c) (1/ $[P]_0$) – (1/ $[P]_t$) for second order kinetics as a function of time for trabecular bone deproteinized at 50°C. Deproteinization fitted well to zero order kinetics.*

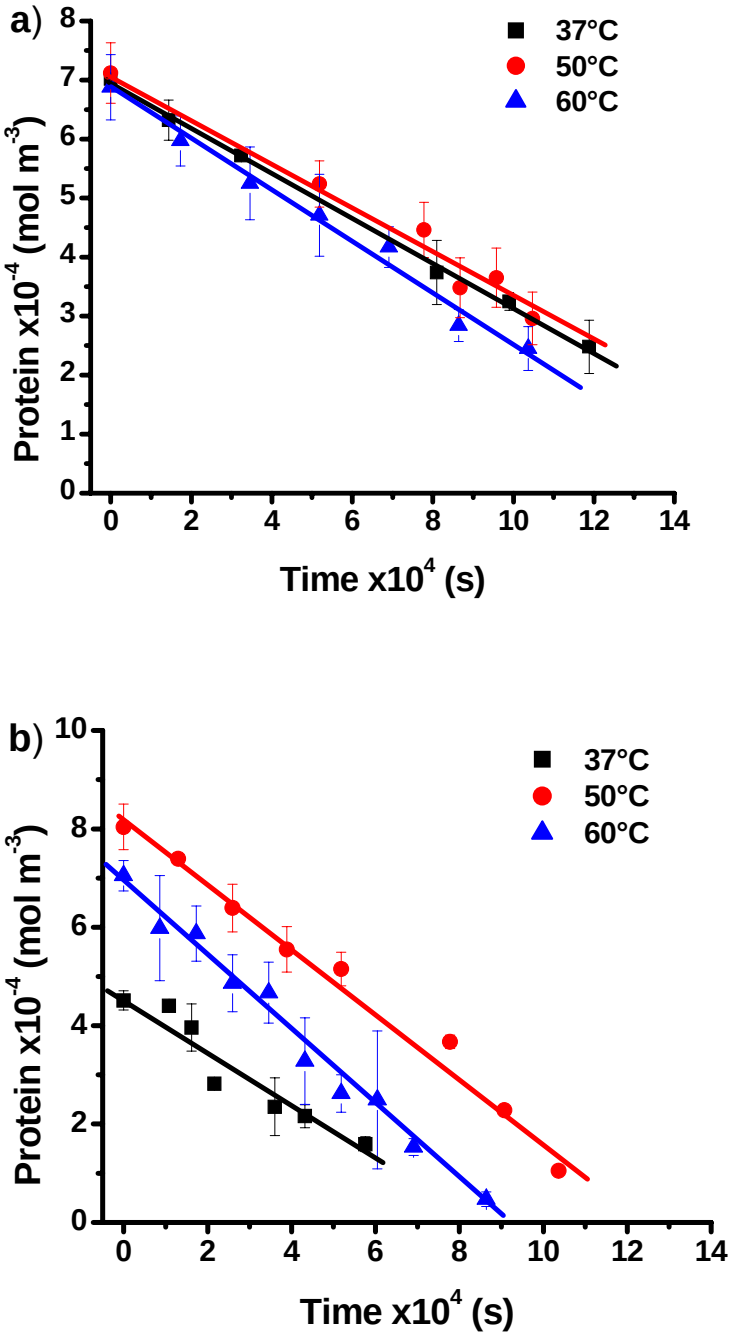

Figure 33. *Protein concentration depletion on a) cortical and b) trabecular bovine femur bones at different temperatures using 6% NaOCl.*

slope is the deproteinization rate constant, *k*, in mol m^{-1} s^{-1}. The product of the *k* values by the surface area corresponding to each type of bone are listed in Table X along with the activation energy values calculated for cortical and trabecular bones. The rate of deproteinization is higher as the temperature increases for both types of bones. It is interesting to note that there are no statistical differences between the rates of deproteinization values as the temperature increased in the cortical bone (Table III, Figure 33a), while statistical differences are found for trabecular bone deproteinization (Table IX, Figure 33b). The rate of deproteinization is significantly different between cortical and trabecular bones for all temperature conditions (Table X). Other important finding to remark is that no significant differences were found on the protein concentration between cortical and trabecular bone (Table X). The response of the rate constant to the temperature increments in both types of bones was evaluated by the activation energy calculus (Figure 34). The activation energy is significantly different for cortical and trabecular bone (Table X).

Table X. *Protein concentration and kinetic parameters calculated for deproteinization of bovine femur bone using 6% NaOCl (n = 3) considering the surface area (A_S) of trabecular and cortical bone. Numbers in parenthesis are the standard deviation.*

	Untreated bone [*P*] x10^{-4} (mol m^{-3})	**$A_S \cdot k$ x10^{-13} (mol m^{-1} s^{-1})**			**E_a kJ mol^{-1}**
		37°C	**50°C**	**60°C**	
Cortical bone	7.10±0.50[a]	1.42±0.14[a]	1.55±0.30[a]	1.61±0.12[a]	5.0±0.64[a]
Trabecular bone	7.54±0.65[a]	39.3±2.24[b]	44.0±4.44[b]	54.6±8.73[b]	13.7±2.4[b]

[a]Averages with different superscript in a column are significantly different ($p < 0.05$).

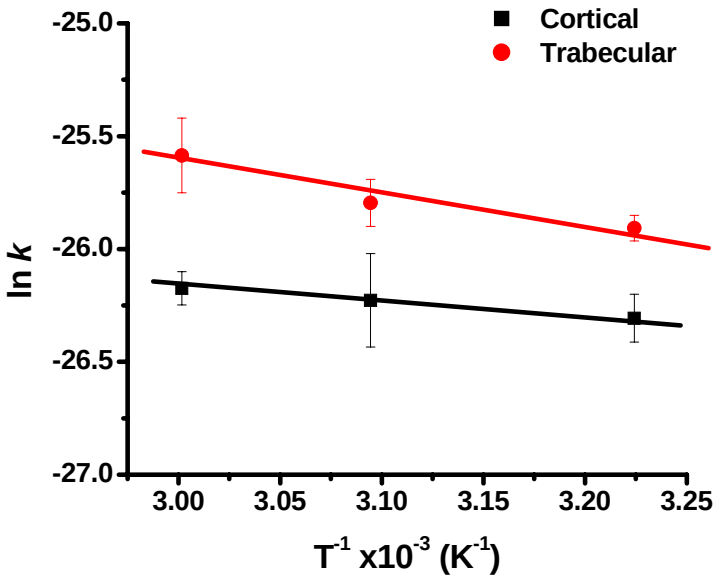

Figure 34. *The rate constant, k as a function of T^{-1} for deproteinization of cortical and trabecular bovine femur bones using 6% NaOCl. The slope of the plot is $-E_a/R$.*

IV.2.4 Scanning electron microscopy

Scanning electron microscope (SEM) micrographs obtained from untreated and completely deproteinizated (37°C) cortical bovine femur bones are shown in Figs. 35 a-b and c-d, respectively. The removal of the protein was clearly visible even at a large scale (Figure 35 c)) when compared with the untreated sample (Figure 35 a). The untreated bone shows a solid-compact surface morphology (Figure 35a-b) with the minerals arranged along the collagen fibers and between them. During the deproteinization process, minerals remain their arrangement, although collagen is being progressively removed (Figure 35 c-d). While the micrographs after deproteinization show the plaques of the bone mineral (calcified filamentous clusters) (Figure 35 e-f).

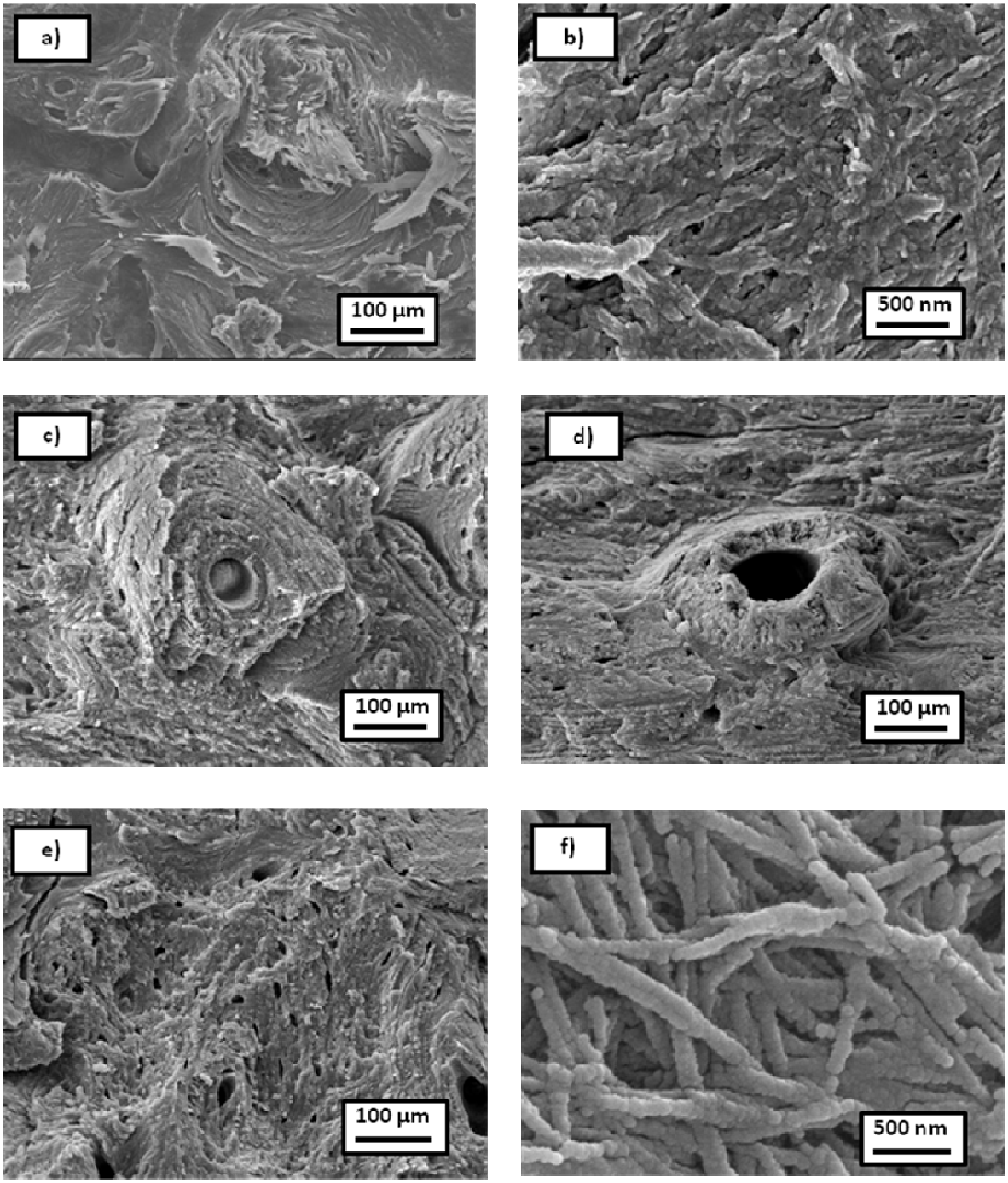

Figure 35. *Scanning electron microscopy (SEM) images of a-b untreated, c-d partially deproteinized, and e-f completely deproteinized (37°C) cortical bovine femur bone.*

IV.4 Discussion

The untreated bones and the bone protein extract were compared by X-ray and IR analyses in order to verify the removal of the mineral phase in the bone protein extract. The X-ray diffractogram of the untreated bone completely corresponded to untreated bone diffractograms previously reported (Bertazzo and Bertran, 2008; Chen *et al*., 2009). The X-ray diffractogram of the protein extract showed only peaks corresponding to NaOH crystals. No peaks corresponding to hydroxyapatite crystals were found in accordance to what was expected. This shows that no bone mineral was present in the bone protein extract. X-ray diffractograms for the untreated bone and the protein extract showed an amorphous band through them, which is attributed to the presence of the organic matrix in both samples (Bertazzo and Bertran, 2008). Results obtained by X-ray were confirmed by IR analysis. For the untreated bone, IR spectrum showed peaks at 1595-1790 cm^{-1} corresponding to the amide I frequency, and peaks at 840-890 cm^{-1} and 900-1200 cm^{-1} for the CO_3^{2-} and the PO_4^{3-}, respectively, which are characteristic of the mineral phase in bone (Camacho *et al*., 1999; Bertazzo and Bertran, 2008). For the bone protein extract, peaks corresponding to the mineral phase were absent, but the characteristic peak of the amide I (from the collagen molecules) was present, this clearly confirmed the removal of the mineral phase in the protein extract previously showed by X-ray analysis.

After the deproteinization procedure, all the bone samples were hand ground in order to do more efficient the extraction of the protein remaining in the bone after every deproteinization time (for the rate constant calculation). The analysis of the particle size of the ground bones showed variations from 3 to 25 μm for cortical and 3 to 35 μm for trabecular bones. The statistical analysis of the data showed that the mode (the size particle that most frequently occurred) was ~ 3 μm for cortical and trabecular bones. This means that the majority of the ground bone particles have a diameter size of ~ 3 μm, even though the particle interval size was large. The homogeneity of the bone samples used for the protein quantification

after each deproteinization time is demonstrated since this particle size was reproducible along the ground bone samples (the standard deviation was calculated to be less than 3%).

Trabecular bone deproteinizes approximately 12 times faster (considering the surface area per bone volume) than cortical. Bigi *et al*. (1997) investigated the mineral phase in cortical and trabecular bones by X-ray diffraction, and infrared spectroscopy. The authors found several significant differences – crystallite size, Ca/P ratio and carbonate content were smaller for trabecular bone tha in cortical bone. They attributed these differences to the different extents of collagen posttranscriptional modifications (chemical modifications of a protein after being decoded by the ribosome in order to produce a specific amino acid chain) between the two types of bones. Differences in the collagen between trabecular and cortical bones were reported by Noris Suarez *et al*. (1996). They found that trabecular bone collagen fibrils have a reduced stability (higher amount of hydroxylysine residues and pyridinium cross-links concentration), whereas cortical bone matrix is more stable since has a larger number of nonreducible cross-links, which confers mechanical strength to the bone structure. Therefore, deproteinization of cortical bone would be expected to occur at a slower rate than trabecular, which corroborates the obtained results.

On the other hand, the rate of deproteinization increases as the temperature is higher. But the temperature effect was more marked in the trabecular than the cortical bone, which was the same tendency formerly noted on demineralization experiments (Section III.2.2). As previously discussed (Section III.3), this effect is attributed the expansion of the porous in the trabecular bones, as well as its capability to change its internal network architecture as a function of the environmental conditions (the temperature increment, in this case). However, the temperature effect was more notorious in deproteinization experiments than previous demineralization assays. This can be attributed to the different intervals of temperature studied. Demineralization experiments were performed at 0°C, 20°C

and 37°C, while deproteinization was done at 37°C, 50°C and 60°C. Therefore, as the temperature was increased, the expansion of the porous of the trabecular bones was more notorious.

The logarithmic plots representing the rate constants as a function of the reciprocal temperature were used to determine the activation energy for deproteinization of trabecular and cortical bones. Activation energy calculated for cortical was found to be 5.4±0.02 kJ mol^{-1} and 16.3±0.87 kJ mol^{-1} for trabecular bone. Thus, our results indicate that the minimal energy required to start deproteinization is almost three times higher for trabecular than cortical bones. This was the same tendency found for activation energy of demineralization (Section III.3). As previously mentioned, the contrary results were expected because protein depletion seems easier in trabecular bones (the rate constant was higher) than cortical. Also, as previously mentioned, cortical bone collagen fibrils are more stable than those of trabecular (Noris Suarez *et al*., 1996). However, once again, these results indicate that other factors need to be considered. Noris Suarez *et al*. (1996) reported chemical differences in the collagen bonding between cortical and trabecular bones, which directly affects the association of the mineral with the collagen scaffold. These differences led to distinct inner matrix architectures between the two types of bones. The deproteinization in trabecular bone is favored by: 1) its high surface area, which confers a greater extent of bone to be in contact with the deproteinizing solution (NaOCl) compared to cortical bone, and 2) trabecular collagen fibrils appear to have reduced stability. Nevertheless, as the deproteinization reaction occurs along the trabecular inner matrix, the mineral-collagen bonds might be harder to access from water and NaOCl, and they might become highly protected from hydrolysis, as a consequence. Certainly, these structures in trabecular bones are well protected from hydrolysis due to their lipid (marrow) content, which is scarcely present in cortical bone. This characteristic of trabecular bone might confer it a hydrophobic shell which prevents the diffusion of both water and NaOCl. Although trabecular bone was carefully cleaned before experiments, their lipid nature may perhaps be preserved. In addition, it is possible

to propose that lipoproteins content might be higher in trabecular than cortical bone, which could be required to the metabolic function of trabecular bone. Also, mineral-collagen conformations might be different between cortical and trabecular bones, which also would lead to their different activation energy requirements. Percot *et al*. (2003) studied the deproteinization of shrimp shell. They found that it occurs in three different stages. Although the rate constants diminished along the three steps, the activation energy was calculated to be smaller as the reaction advanced (contrary to what was expected). The authors attributed their findings to the weak accessibility of the protein as the reaction advanced, as well as to the presence of lipoproteins remaining in the system, which made the proteins well protected to hydrolysis due to their hydrophobic characteristic.

Although the effect of the temperature on cortical and trabecular bones was markedly different, the protein concentration calculated for both types of bones was almost the same. Eurell and Kazarian (1983) measured protein content in trabecular and cortical bone of vertebrae from the lumbar region of male Wistar rats (approximately 83 days of age). They used fast green staining for the measurement of collagen. The authors found similar collagen content between trabecular and cortical bone. The results obtained in the present study indicate that the differences on the internal architecture of cortical and trabecular bones, its mineral concentration, and its bonding with the collagen matrix are the responsible factors that influence the different physicochemical characteristics found in this study, and not the protein content by itself. Although the protein content was found statistically in the same quantity in cortical and trabecular bones, the deproteinization rate constant values were significantly different. This also corroborates that the differences of the internal architecture of the cortical and trabecular bones directly influence their physicochemical characteristics.

SEM micrographs show the bone mineral plaques of the completely deproteinized bone. The micrograph at higher resolution (500 nm) shows hydroxyapatite platelets ranging in width from 50 to 70 nm and length from

approximately 60 to 70 nm. These dimensions are similar to those reported for human bone (25 to 50 nm) (Weiner and Wagner, 1998) measured from TEM micrographs. However, dimensions measured from AFM studies showed widths and lengths from 30 to 200 nm (Hassenkam *et al*., 2004). Our results are also similar to elk antler hydroxyapatite crystals length, which varied from 20 to 70 nm (Chen *et al*., 2009) measured from TEM micrographs.

IV.5 Conclusions

The present chapter shows the effect of the temperature, as well as the influence of the differences in the inner geometry of cortical and trabecular bones on their deproteinization kinetic parameters. The following conclusions were obtained:

1. An experimental method for determining the *in vitro* bone deproteinization kinetics was developed.

2. Protein depletion occurs at a higher rate in trabecular than cortical bone. This is directly attributed to the differences in the internal matrix of the two types of bones.

3. The deproteinization rate constant increases as the temperature increased. However, the effect of temperature is larger in trabecular bone, which could be due to the dilatation of the trabecular bone porosity, which increased the deproteinization efficiency in comparison to cortical bone at each temperature increment.

4. The activation energy is found to be higher for trabecular than cortical bone. This is attributed to a different network organization of the matrix in the two types of bones, which could led to weak accessibility from water and NaOCl molecules to the collagen, in part due to the high complex architecture of the trabecular bone, and also to its high lipid content nature. Certainly, it is possible that trabecular bone possess higher lipoproteins content related to its metabolic role.

5. The protein concentration values are almost the same for cortical or trabecular bovine bone. These results confirm that the individual inner matrix geometry of trabecular and cortical bones and their characteristics such as the mineral concentration and its cross-linking with collagen fibers, are the responsible factors that control the extraordinary physicochemical properties observed for each type of bone, and not due to the protein concentration.

6. This work clearly demonstrates that although cortical and trabecular bones are constituted by the same components: mineral, protein and water, the differences in the internal architecture between these systems directly affect their deproteinization kinetic parameters.

7. These results indicate that protein depletion in trabecular and cortical bones are regulated independently from each other.

Chapter V

Summary of results and conclusions

The present thesis work has been based on the research hypothesis that considering the distinct structural architecture between cortical and trabecular bone, significant differences are expected in the kinetic parameters such as, the rate constant and the activation energy, in the *in vitro* bone demineralization and deproteinization reactions between cortical and trabecular bone.

In order to verify this hypothesis, cortical and trabecular bovine femur bones were submitted to *in vitro* demineralization and deproteinization processes. The main results and conclusions obtained from both sets of studies are presented below.

V.1 Summary of results

Cortical and trabecular bovine femur bones were demineralized using 0.1 N, 0.6 N and 1N HCl at 0°C, 20°C and 37°C. Deproteinization was carried out using 6% NaOCl at 37°C, 50°C and 60°C. The kinetic parameters (rate constant and activation energy) were calculated, and the surface area of each type of bone was considered. A statistical analysis of the rate constants shows that cortical bones demineralize and deproteinize at a slower rate than trabecular bones (Figure 36), which is attributed to the chemical and structural differences that exist between cortical and trabecular bones. According to the protein quantification experiments obtained, the protein concentration values are almost the same for both types of bones (Figure 37). This indicates that factors such as the differences in the inner network between cortical and trabecular bones, the mineral composition, along with the collagen binding cross-links, directly influence the different physicochemical characteristics found in this study, and not the protein content by itself. The results here obtained, indicate that

demineralization and deproteinization in trabecular and cortical bones are independently modulated.

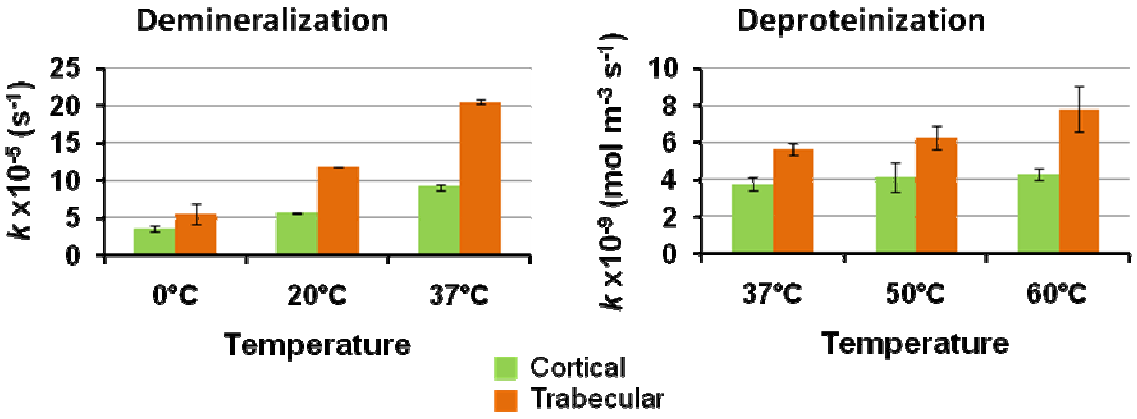

Figure 36. *Summary of the rate constant results for cortical and trabecular bovine femur bones, demineralized with 1 N HCl and deproteinized with 6% NaOCl.*

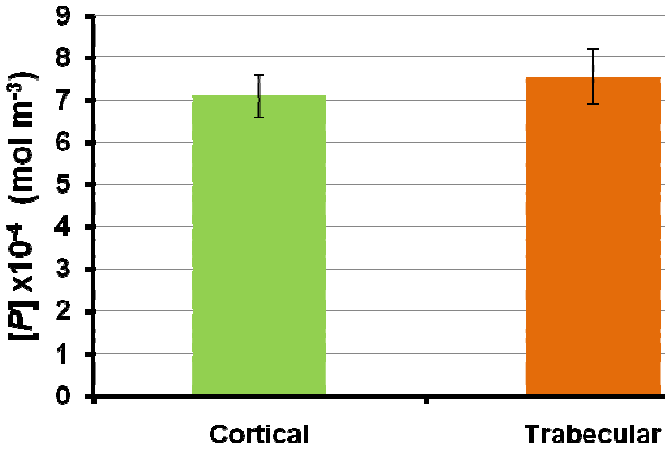

Figure 37. *The protein content measured was almost the same in trabecular and cortical bones*

V.2 Summary of conclusions

1. Efficient methods for the quantitative measurement of the mineral and the protein contents in bone were developed.

2. Demineralization is found to occur in three stages:

    a. First stage: the rate constant increased as HCl solution demineralized the peripheral part of the sample.
    b. Second stage: demineralization occurs at a steady state. This steady state corresponds to demineralization of the central part of a bone sample.
    c. Third stage: at the end of the reaction, rate constant decreases as calcium concentration in the bone becomes depleted.

3. Statistical differences are found on the demineralization and deproteinization kinetic parameters (rate constants and activation energy) between trabecular and cortical bones. This is attributed to the effect of the differences on the inner matrix architecture between the cortical and the trabecular bones.

4. No statistical differences were found in the protein concentration for cortical and trabecular bovine femur bones, indicating that the mineral concentration and its cross-linking with the collagen are the responsible factors that influence the different characteristics on mineralized tissues and not the protein content by itself.

5. The microstructural features on demineralized and deproteinized bones remain well preserved.

6. The results obtained in this work indicate that protein depletion in trabecular and cortical bones are independently regulated.

7. The research hypothesis is accepted, based on the analysis of the obtained results. Therefore, this work clearly demonstrates that although cortical and trabecular bones

are constituted by the same components: mineral, protein and water, the differences in the internal architecture between these systems directly affect their deproteinization kinetic parameters.

Chapter VI

Contributions and future work

VI.1 Contributions

The present work is the first one that presents the physicochemical characteristics of the *in vitro* bone demineralization and deproteinization. This study has been performed at three different temperatures, and comprehensively analysis at the same time the results for cortical and trabecular bones.

Protein quantification is not an easy subject. There is no a precise technique for protein measurement. Here is reported a complete methodology for bone protein extraction and its measurement. A procedure for the obtaining, as well as the construction of a bovine collagen reference curve especially designed and used for bone protein quantification has been described in detail.

The results presented in this work show how the differences of the geometry of the inner matrix between cortical and trabecular bones affect its physicochemical characteristics, which was an issue not previously considered in other works. The present thesis provides valuable data and analysis to the scientific community.

VI.2 Future work

The study of bones is a vast issue, and its study requires the involving of physicians, biologists, chemists and materials science engineers.

The present thesis work has opened the door to the study of the *in vitro* kinetics of two important processes that a bone can get through: demineralization and deproteinization. It would be interesting to investigate if there is a modification of the sizes of the porous along the process of deproteinization.

It would be interesting to apply a methodology for the measurement of the force required for the separation of the protein from the mineral, and statistically analyze the results obtained for cortical and trabecular bones.

Since there is a synergistic effect between protein and mineral in bone, it would be interesting to parallel study if there are changes in the protein concentration while demineralization is occurring, and vice versa.

From the knowledge learned during the development of the present investigation, the interest to further investigate bone has personally arisen. The next stage could be to fabricate bioinspired bone composites, which will have potential use as bone implant materials.

References

- Audersik T. and Audersik G. 1996. Biology, Life on Earth. 4th Edition. Prentice-Hall, New Jersey. 947 pp.

- Bhan A., Rao A.D. and Rao D.S. 2010. Osteomalacia as a result of vitamin D deficiency. Endocrinol. Metab. Clin. North Am. 39:321-331.

- Benke, D., Olah, A. and Möhler, H. 2001. Protein-chemical analysis of Bio-Oss bone substitute and evidence on its carbonate content. Biomaterials. 22:1005-1012.

- Bertazzo S. and Bertran C.A. 2008. Effect of hydrazine deproteination on bone mineral phase: A critical review. J. Inorg. Biochem. 102:137-145.

- Bigi A., Cojazzi G., Panzavolta S., Ripamonti A., Roveri N., Romanello M., Noris Suarez K. and Moro L. 1997. Chemical and structural characterization of the mineral phase from cortical and trabecular bone. J. Inorg. Biochem. 68:45-51.

- Birkedal-Hansen H. 1974a. Difusion of $H^{36}Cl$ in decalcified ivory dentine. J. Histochem. Cytochem. 22:428-433.

- Birkedal-Hansen H. 1974b. Kinetics of acid demineralization in histologic techniques. J. Histochem. Cytochem. 22:434-441.

- Boskey A. 2001. Bone Mineralization. Cowin SC, editor. Bone Biomechanics Handbook. CRC Press LLC. Boca Raton.

- Bowman S.M., Zeind J., Gibson L.J., Hayes W.C. and McMahon A. 1996. The tensile behavior of demineralized bovine cortical bone. J. Biomech. 29:1497-1501.

- Brain E. 1996. The Preparation of Decalcified Sections, Charles C. Thomas, Springfield. 206 pp.

- Brown T.L., LeMay H. E. and Bursten B. E. 1991. Chemistry the Central Science. 5th Edition. Prentice-Hall, New Jersey. 1159 pp.

- Broz J.J., Simske S.J. and Greenberg A.R. 1995. Material and compositional properties of selectively demineralized cortical bone. J. Biomech. 28:1357-1368.

- Broz J.J., Simske S.J. Corley W.D. and Greenberg A.R. 1997. Effects of deproteinization and ashing on site-specific properties of cortical bone. J. Mater. Sci. - Mater. Med. 8:395-401.

- Buehler M. 2006. Nature designs though collagen: Explaining the nanostructure of collagen fibrils. P. Natl. Acad. Sci. USA. 103:12285-12290.

- Camacho N.P., Rinnerthaler S., Paschalis E.P., Mendelsohn R., Boskey A.L. and Fratzl P. 1999. Complementary information on bone ultrastructure from scanning small angle X-ray scattering and Fourier-transform infrared microspectroscopy. Bone 25:287-293.

- Carter D.R. and Hayes W.C. 1976. Bone compressive strength: the influence of density and strain rate. Science. 194:1174-1175.

- Carter, D. H., Scully, A. J., Heaton, D. A., Young, M. P. J. and Aaron, J. E. 2002. Effect of deproteination on bone mineral morphology: implications for biomaterials and ageing. Bone. 31:389-395.

- Catanese J.C. III, Iverson E. P., Ng R.K. and Keaveny T. M. 1999. Heterogeneity of the mechanical properties of demineralized bone. J. Biomech. 32:1365-1369.

- Chakkalakal D.A., Strates B.S., Garvin K.L., Novak J.R., Fritz E.D., Moliner T.J. and McGuire M.H. 2001. Demineralized bone matrix as a biological scaffold for bone repair. Tissue Eng. 7:161-177.

- Chang R. 1998. Chemistry. 6th Edition. McGraw-Hill, New York. 995 pp.

- Chappard D., Legrand E., Haettich B., Chales G., Auvinet B., Eschard J-P., Hamelin J-P., Baslé M-F. and Audran M. 2001. Fractal dimension of trabecular bone: comparision of three histomorphometric computed techniques for measuring the architectural two-dimensional complexity. J Pathol. 195:515-21.

- Chen P.-Y., Lin A.Y.M., Lin Y.-S., Seki Y., Stokes A.G., Peyras J., Olevsky E.A., Meyers M.A. and McKittrick J. 2008. Structure and mechanical properties of selected biological materials. J. Mech. Behav. Biomed. Mater. I:208-226.

- Chen P.-Y., Stokes G.A. and McKittrick J. 2009. Comparison of the structure and mechanical properties of bovine femur bone and antler of the North American elk (*Cervus elaphus canadensis*). Acta Biomater. 5:693-706.

- Cui F.-Z., Li Y. and Ge J. 2007. Self-assembly of mineralized collagen composites. Mater. Sci. Eng., R. 57:1-27.

- Cultrone G., Sebastián E., Elert K., de la Torre M.J., Cazalla O. and Rodríguez-Navarro C. 2004. Influence of mineralogy and firing temperature on the porosity of bricks. J. Eur. Ceram. Soc. 24:547-564.

- Currey J. D. 1969. The mechanical consequences of variation in the mineral content of bone. J. Biomech. 2:1-11.

- Currey J.D. 1990. Physical characteristics affecting the tensile failure properties of compact bone. J. Biomech. 23:837-844.

- Dodds R.A., York-Ely A.M., Zhukauskas R., Arola T., Howell J., Hartill C., Cobb R.R. and Fox C. 2010. Biochemical and radiographic comparision of demineralized bone hydroxyapatite in a rabbit spinal fusion model. J. Biomater. Appl. 25:195-215.

- Downey P.A. and Siegel M.I. 2006. Bone biology and the clinical implications for osteoporosis. Phys. Ther. 86:77-91.

- Ehrlich H., Koutsoukos P.G., Demadis K.D. and Pokrovsky O.S. 2008. Principles of demineralization: modern strategies for the isolation of organic frameworks. Part I. Common definitions and history. Micron 39:1062-1091.

- Ehrlich H., Koutsoukos P.G., Demadis K.D. and Pokrovsky O.S. 2009. Principles of demineralization: modern strategies for the isolation of organic frameworks. Part II. Decalcification. Micron 40:169-193.

- Eurell J.A. and Kazarian L.E. 1983. Quantitative histochemistry of rat lumbar vertebrae following spaceflight. Am. J. Physiol. 244: R315-R318.

- Falini G., Fermani S., Foresti E., Parma B., Rubini K., Sidoti M.C., Roveri N. 2004. Films of self-assembled purely helical type I collagen molecules. J. Mater. Chem. 14:2297-2302.

- Fantner G.E., Hassenkam T., Kindt J.H., Weaver J.C., Henrikbirkedal, L. Pechenik, Cutroni J.A., Cidade G.A., Stuky G.D., Morse D.E. and Hansma P.K. 2005. Sacrificial bonds and hidden length dissipate energy as mineralized fibrils separate during bone fracture. Nat. Mater. 4:612-616.

- Fattibene P. Carosi A. De Coste V. and Onori S. EPR properties of intactc and deproteinated dentin. 2006. Radiat. Prot. Dosim. 120:216-220.

- Guyton A.C. and Hall J.E. 2006. Textbook of medical physiology. 11th edition. Elsevier Inc. Philadelphia, Pennsylvania. 1116 pp.

- Hassenkam T., Fantner G.E., Cutroni J.A., Weaver J.C., Morse D.E., Hansma P.K. 2004. High-resolution AFM imaging of intact and fractured trabecular bone. Bone 35:4-10.

- Hing, K. A. 2004. Bone repair in the twenty-first century: biology, chemistry or engineering? Phil. Trans. R. Soc. Lond. A. 362:2821-2850.

- Jee W.S.S. 1983. The skeletal tissues, p. 206-254. In: Weiss L. (ed.). Histology: cell and tissue biology. 5th edition. Macmillan Press, New York. 1952 pp.

- Kanis J.A., Johnell O., Oden A., Sembo I., Redlund-Johnell I., Dawson A., De Laet C. and Jonsson B. 2000. Long-term risk of osteoporotic fracture in Malmö Osteoporosis Int. 11:669-674.

- Landis W.J., Song M.J., Leith A., McEwen L. and McEwen B.F. 1993. Mineral and organic matrix interaction in normally calcifying tendon visualized in 3 dimensions by high-voltage electron-microscopic tomography and graphic image-reconstruction, J. Struct. Biol. 110:39-54.

- Lewandroski K.-U., Venugopalan V., Tomford W.W., Schomacker K.T., Mankin H.J. and Deutsch T.F. 1996. Kinetics of cortical bone demineralization: controlled demineralization- a new method for modifying cortical bone allografts. J. Biomed. Mater. Res. 31:365-372.

- Li X., Jin L., Balian G., Laurencin C.T. and Anderson D.G. 2006. Demineralized bone matrix gelatin as a scaffold for osteocondral tissue engineering. Biomater. 27:2426-2433.

- Lowry O.H., Rosebrough N.J., Farr A.L. and Randall R.J. 1951. Protein measurement with the folin phenol reagent. J. Biol. Chem. 193: 265-275.

- Margolis H.C., Zhang Y.P., Lee C.Y., Kent R.L. and Moreno E.C. 1999. Kinetics of enamel demineralization in vitro J Dent Res. 78:1326-34.

- Masel R. 2001. Chemical Kinetics and Catalysis. Wiley-Interscience, New York. 952 pp.

- Mauney J.R., Jaquiéry C., Volloch V., Heberer M., Martin I. and Kaplan D.L. 2005. *In vitro* and *in vivo* evaluation of differentially demineralized cancellous bone scaffolds combined with human bone marrow stromal cells for tissue engineering. Biomater. 26:3173-3185.

- Meier D., Orwoll E. and Jones J.M. 1984. Marked disparity between trabecular and cortical bone loss with age in healthy men. Measurement by vertebral

computed tomography and radial photon absorptiometry. Ann. Intern. Med. (United States). 101(5):605-612.

- Meyers M., Chen P.-Y., Lopez M.I., Seki Y. and Lin A.Y.M. 2010. Biological materials: A materials science approach. J. Mech. Behav. Biomed. Mater. doi:10.1016/j.jmbbm.2010.08.005.

- Mooren R.E.C.M., Dankers A.C.A., Merkx M.A.W., Bronkhorst E.M., Jansen J. A., Stoelinga P. J. W. 2010. The effect of platelet-rich plasma on early and late bone healing using a mixture of particulate autogenous cancellous bone and Bio-Oss®: an experimental study in goats. Int. J. Oral Maxilofac. Surg. 39:371-378.

- Mordenfeld A., Hallman M., Johansson C.B., Albrektsson T. 2010. Histological and histomorphometrical analyses of biopsies harvested 11 years after maxillary sinus floor augmentation with deproteinized bovine and autogenous bone. Clin. Oral. Impl. Res. 21: 961-970.

- Moreno E.C. and Zahradnik R.T. 1974. Chemistry of enamel subsurface demineralization in vitro. J. Dent. Res. 53:226-235.

- National Center for Biotechnology Information (NCBI) (http://www.ncbi.nlm.nih.gov/) July, 2010.

- Noris Suarez K., Romanello M., Bettica P., and Moro L. 1996. Collagen typeI of rat cortical and trabecular bone differs in the extent of posttranslational modifications. Calcif. Tissue Int. 58:65-69.

- Olszta M.J., Cheng X., Jee S.S., Kumar R., Kim Y.-Y., Kaufman M.J., Douglas E.P. and Gower L.B. 2007. Bone structure and formation: A new perspective. Mater. Sci. Eng., R. 58:77-116.

- Pace C.N., Vajdos F., Fee L., Grimsley G. and Gray T. 1995. How to measure and predict the molar absorption coefficient of a protein. Protein Sci. 4: 2411-2423.

- Parfitt A.M., Mathews C.H.E. Villanueva A.R., Kleebekoper M.,Frame B., and Rao D.S. 1983. Relationships between surface, volume, and thickness of iliac trabecular bone in aging and in osteoporosis. Implications for the microatomic and cellular mechanisms of bone loss. J. Clin. Invest. 72:1396-1409.

- Paschalis E.P., Verdelis K., Doty S.B., Boskey A.L., Mendelsohn R. and Yamauchi M. 2001. Spectroscopic characterization of collagen cross-links in bone. J. Bone Miner. Res. 16:1821-1828.

- Patel M.V., Fox J.L. and Higuchi W.I. 1987. Effect of acid type on kinetics and mechanism of dental enamel demineralization. J. Dent. Res. 66:1425-1430.

- Percot A., Viton C. and Domard A. 2003. Characterization of shrimp shell deproteinization. Biomacromolecules. 4:1380-1385.

- Robinson, R. A. and Watson, M. L. 1952. Collagen-crystal relationship in bone as seen in the electron microscope. Anat. Rec. 114:383-410.

- Rosenberg I. M. 1996. Protein analysis and purification. Benchtop techniques. Birkhäuser, Boston.

- Shoulders M. and Raines R.T. 2010. Collagen structure and stability. Annu. Rev. Biochem. 78:929-58.

- Sollazzo V., Palmieri A., Scapoli L., Martinelli M., Girardi A., Alviano F., Pellati A., Perrotti V. and Carinci F. 2010. Bio-Oss® acts on stem cells derived from peripheral blood. Oman Medical Journal. 25:26-31.

- Stavropoulos A. and Karring, T. J. 2010. Guided tissue regeneration combined with a deproteinized bone mineral (Bio-Oss) in the treatment of intrabony periodontal defects: 6 year results from a randomized-controlled clinical trial. Clin. Periodontol. 37:200-210.

- Termine J.D., Eanes E.D. Greenfield D.J. and Nylen M.U. 1973. Hydrazine-deproteinated bone mineral. Calc. Tiss. Res. 12:73-90.

- Theobald H.E. 2005. Dietary calcium and health. Nutrition Bulletin. 30:237-277.

- Thurner P.J., Erickson B., Turner P., Jungmann R., Lelujian J., Proctor A., Weaver J.C., Schitter G., Morse D.E. and Hansma P.K. 2009. The effect of NaF in vitro on the mechanical and material properties of trabecular and cortical bone. Adv. Mater. 21:451-457.

- Wang Z.-H., He X.-J., Yang Z.-Q. and Tu J.-B. 2010. Cartilage tissue engineering with demineralized bone matrix gelatin and fibrin glue hybrid scaffold: an in vitro study. Artif. Organs. 34:161-166.

- Weiner S. and Wagner H.D. 1998. The material bone: structure-mechanical function relations. Annu. Rev Mater. Sci. 28:271-298.

- WHO (World Health Organization). 1994 Assessment of Fracture Risk and Its Application to Screening For Postmenopausal Osteoporosis. Report of a WHO Study Group. WHO Technical Report Series 843. WHO: Geneva.

- You T-M., Choi B-H., Li J., Jung J-H., Lee H-J., Lee S-H., Jeong S-M. 2007. The effect of platelet-rich plasma on bone defects treated with Bio-Oss: a pilot study in the dog tibia. Oral Surg. Oral Med. Oral Pathol. Oral Radiol. Edod. 103:e8-e12.

Appendix A

Glossary

Anabolism: the phase of metabolism in which complex molecules, such as the proteins and fats that make up body tissue, are formed from simpler ones.

Bone lining cells: cells that are essentially inactive osteoblasts. They cover all of the available bone surface and function as a barriers for certain ions.

Catabolism: the set of pathways that breakdown molecules into smaller units and release energy.

Cushing's syndrome: is a hormone (endocrine) disorder caused by high levels of cortisol (hypercortisolism) in the blood. This can be caused by taking glucocorticoid drugs, or by tumors that produce cortisol or adrenocorticotropic hormone (ACTH).*Cushing's syndrome* refers to one specific cause, a tumor (adenoma) in the pituitary gland that produces large amounts of ACTH, which in turn elevates cortisol.

Glucocorticoid: any of a group of steroid hormones, such as cortisone, that are produced by the adrenal cortex, are involved in carbohydrate, protein, and fat metabolism, and have anti-inflammatory properties.

Homeostasis: the process used by an organism or a cell to maintain internal equilibrium by adjusting its physiological process.

Metabolism: the chemical processes by which cells produce the substances and energy needed to sustain life. As part of metabolism, organic compounds are broken down to provide heat and energy in the process called catabolism. Simpler molecules are also used to build more complex compounds like proteins for growth and repair of tissues as part of anabolism.

Osteoblast: a cell specialized in the formation of new bone. Osteoblasts produce osteoid, which is composed mainly of Type I collagen. Osteoblasts are also responsible for mineralization of the osteoid matrix. Zinc, copper and sodium are some of the many minerals produced. Bone is a dynamic tissue that is constantly being reshaped by osteoblasts, which build bone, and osteoclasts, which resorb bone. Osteoblast cells tend to decrease as individuals become elderly, thus decreasing the natural renovation of the bone tissue.

Osteoclast: a large multinucleate cell found in growing bone that resorbs bone tissue by removing its mineralized matrix and breaking up the organic bone. This process is known as *bone resorption*.

Osteocytes: bone cells that maintain bone tissue, and is the most abundant cell found in compact bone. Osteocytes are networked to each other via long cytoplasmic extensions that occupy tiny canals called canaliculi, which are used for exchange of nutrients and waste. They are actively involved in the routine turnover of bony matrix, through various mechanosensory mechanisms.

Osteoid: is the unmineralized, organic portion of the bone matrix that forms prior to the maturation of bone tissue. Osteoblasts begin the process of forming bone tissue by secreting the osteoid as several specific proteins. When the osteoid becomes mineralized, it and the adjacent bone cells have developed into new bone tissue

Resorbing cell: Bone resorbing cells are the osteoclasts. In general, a resorbing cell dissolves and assimilates for example, bone tissue.

Resorption: the organic process in which the substance of some differentiated structure that has been produced by the body undergoes lysis and assimilation.

Materials Science and Engineering C 31 (2011) 523–530

Contents lists available at ScienceDirect

Materials Science and Engineering C

journal homepage: www.elsevier.com/locate/msec

Kinetic studies of bone demineralization at different HCl concentrations and temperatures

A.B. Castro-Ceseña [a], E.E. Novitskaya [b], P.-Y. Chen [b], G.A. Hirata [c,*], J. McKittrick [b,d]

[a] Centro de Investigación Científica y de Educación Superior de Ensenada, Ensenada, Baja California, Carretera Ensenada-Tijuana No. 3918, Zona Playitas, 22860, Ensenada, B.C., México
[b] Materials Science and Engineering Program, UC San Diego, La Jolla, CA 92093, United States
[c] Centro de Nanociencias y Nanotecnología, UNAM, Km. 107 Carretera Tijuana-Ensenada, Apdo. Postal, 356, CP. 22800, Ensenada, B.C., México
[d] Mechanical and Aerospace Engineering UC San Diego, La Jolla, CA 92093, United States

ARTICLE INFO

Article history:
Received 28 June 2010
Received in revised form 11 October 2010
Accepted 8 November 2010
Available online 9 December 2010

Keywords:
Bone
Kinetics
Demineralization
Rate constant
Activation energy

ABSTRACT

The goal of this study was to contribute to the interpretation of the kinetics involved in the in vitro demineralization process of bone, which has clinical uses as bone grafts (demineralized bone matrix), as well as for materials science applications. Cortical and cancellous bovine femur bones and cortical antler were demineralized in dilute hydrochloric acid and the kinetic parameters of the demineralization reaction at different temperatures and HCl concentrations were calculated. The rate of demineralization increased with both HCl concentration and temperature. During the demineralization reaction experiments, three different stages were clearly identified: a) in the first stage, the rate constant increased as HCl advanced from the periphery to the core of the sample. b) In the second stage, the demineralization occurred at a steady state, and finally, c) in the third stage, the rate constant diminished. The activation energy for demineralization was calculated for both types of bones.

Published by Elsevier B.V.

1. Introduction

Bone is a composite material hierarchically structured. There are two types of bone: cancellous and cortical. Cancellous bone is highly porous, and it is located in parts of the body that need resistance to impact loading. For example, the skull and the head of the femur are largely composed of cancellous bone. Cancellous bone is surrounded by cortical bone, which is denser. Cortical bone is composed by osteons, which surround a central blood vessel. Both bones are composed of type I collagen fibrils. These fibrils are composed of tropocollagen, a triple helix of collagen molecules. Collagen fibrils have mineral (hydroxyapatite) dispersed between or along them [1–4] (Fig. 1).

The study of bone demineralization is considered important from two perspectives. From a biological point of view, bones supply ~99% of the calcium and ~90% of the phosphorous in the human body. Bones simultaneously absorb and release these minerals as required, keeping a constant concentration in the blood [5]. When this balance is lost, osteoporosis can arise as a consequence [6]. The World Health Organization (WHO) defines osteoporosis as 'a disease characterized by low bone mass and micro-architectural deterioration of bone tissue', leading to enhanced bone fragility and a consequent increase in fracture risk [7]. Another condition that degrades bone strength is osteomalacia, which causes defects in the bone mineral [8]. While osteoporosis refers to the degeneration of already synthesized bone, making it brittle, osteomalacia is an abnormality in the synthesizing process of the bone, making it soft. As a consequence, synthetic and natural bone graft substitutes prepared from demineralized bone matrix have been used as scaffolds for bone repair [9–13]. From the materials science perspective, the bone mineral phase has been studied due to its extremely important role in the mechanical properties of the bone. Currey performed studies about the relationship between the mineral content of the bone and the mechanical consequences of its variation [14]. In Fig. 2 (adapted from Ref. [14]), the relationship between the mineral content for various mineralized biological materials and the elastic modulus is shown. These results clearly indicate that the resistance of the bone material to stress is strongly related to the mineral content (Fig. 2). Therefore, a detailed study of the chemistry, specifically of the kinetics of the mechanism of bone demineralization has a great importance in the interpretation of the in vitro bone demineralization mechanism.

Most studies on demineralization kinetics have been focused mainly on the kinetics of diffusion [15–17]. The diffusion coefficient of HCl into the organic matrix and the rate of penetration of the HCl demineralization front were studied in elephant ivory dentine. Depending on the geometrical shapes of the samples, the distance penetrated by the HCl solution was directly proportional to the square root of time, as described by Birkedal-Hansen [15,16]. In other studies [17], the kinetics of human cortical bone demineralization was examined using HCl. The advance of the reaction front versus

* Corresponding author. Tel.: +52 646 174 46 04; fax: +52 646 174 46 03.
E-mail address: hirata@cnyn.unam.mx (G.A. Hirata).

0928-4931/$ – see front matter. Published by Elsevier B.V.
doi:10.1016/j.msec.2010.11.003

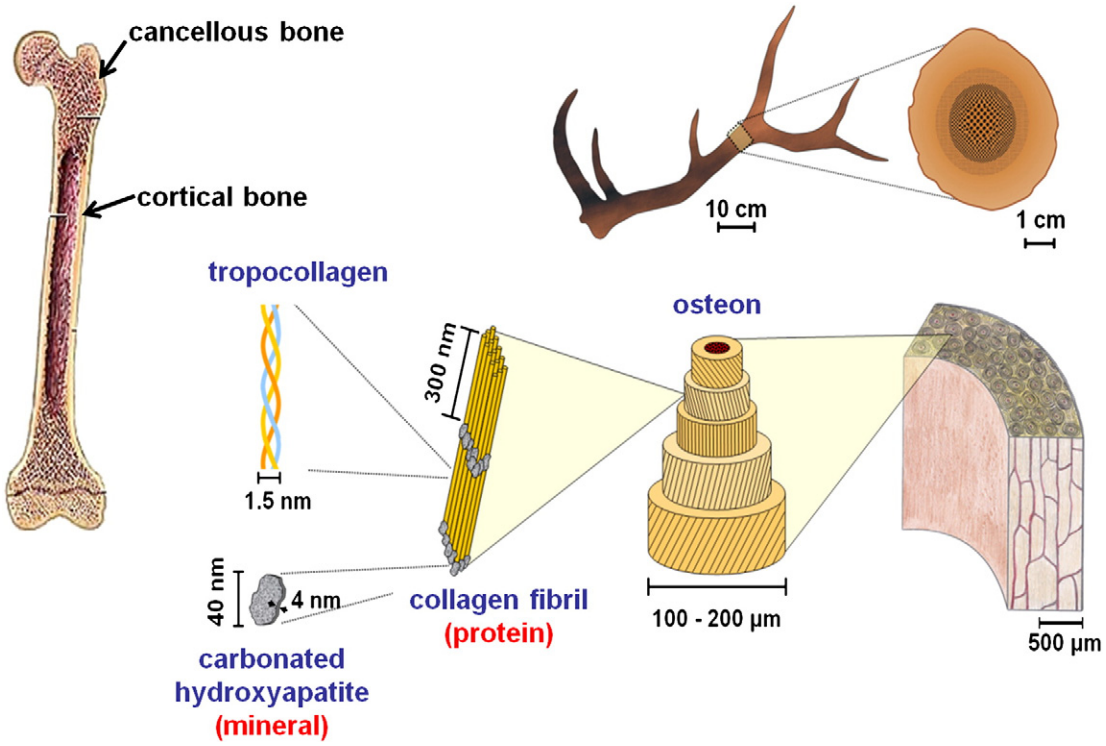

Fig. 1. Hierarchical structure of bone and antler. Cancellous section is surrounded by cortical section. Cortical section consists of osteons, which are concentric lamellae surrounding a central blood vessel. Each lamella has oriented type I collagen fibrils with mineral interspersed between or along them. Collagen fibrils are composed of tropocollagen. Modified from Chen et al. [4].

immersion time was analyzed using mathematical models based on diffusion mass transfer to predict the demineralization process. These authors found that the model for planar geometry is applicable to the demineralization of cortical bone allografts of irregular shapes, and that the model for cylindrical geometry fitted well for curved surfaces [17]. However, the rate constant, order of reaction, and activation energy were not included in those investigations.

Antler bone offers an interesting area of study because they are one of the most impact resistant and energy absorbent of all biomineralized materials [4].

The aim of the present work was to contribute to the interpretation of the kinetics involved in the in vitro demineralization process of the bone, which has clinical uses as bone grafts (demineralized bone matrix), as well as for materials science applications. For this purpose, cortical and cancellous bovine femur bones were demineralized with HCl at three different concentrations (0.1 N, 0.6 N and 1.0 N) at 0 °C, 20 °C and 37 °C. The kinetic parameters were calculated: order of reaction, rate constant and activation energy. Since the kinetics of bovine bone demineralization is relatively unknown, we also studied cortical antler and compared the results with cortical femur bone wherever possible.

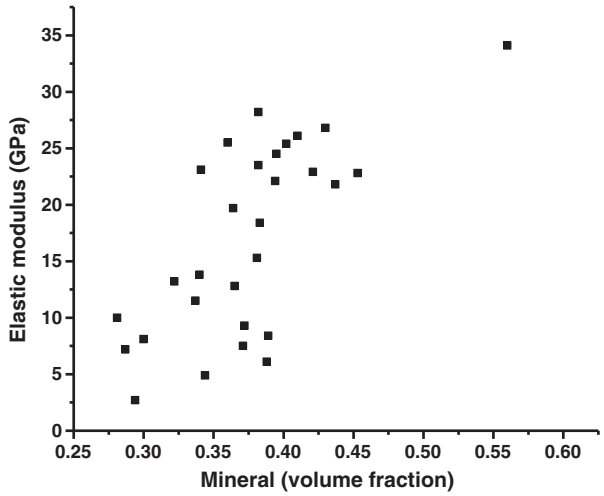

Fig. 2. Young's modulus as a function of mineral content for various mineralized biological materials. Data plotted from Currey [14].

2. Experimental techniques

2.1. Sample preparation

Bovine femur bone was purchased from a local butcher. The slaughter age was approximately 24 months. The main beam was cut into sections (~5 cm) by a hand saw and followed by fine section. For experiments, 100 rectangles were cut (mean size was 125 mm^3) from both cortical and cancellous sections. The bovine femur was carefully cleaned to remove any marrow and lipid components. The cancellous bone was cleaned using pressurized stream of compressed air and water, as previously reported by other authors [18,19]. All samples were air-dried and weighed before the demineralization treatment.

The *Cervus canadensis* antler was purchased from Into the Wilderness Trading Company (Pinedale, WY). The antler was shed approximately 1 year before it was obtained for testing. The main beam was cut into sections (~5 cm) using a rotating diamond wheel saw. For analysis, 100 rectangles were cut (mean was 125 mm^3), only from the cortical section.

2.2. Demineralization experiments

The cortical and cancellous sections of bovine bone and the cortical section of antler (cancellous section of antler was not included) were

placed in 50 ml centrifuge tubes containing 40 ml of 0.1 N, 0.6 N or 1.0 N HCl. Three temperatures were used: 0 °C, 20 °C and 37 °C. For experiments at 0 °C, a refrigerator was used. Experiments at 20 °C were performed at room temperature. For demineralization at 37 °C, a water bath was used. The HCl solutions were refreshed after 0.5, 1.5, 3, 6, 9, 12, 16, 20, 24 h, and subsequently at 4 h intervals until the demineralization was complete (see Table 1). The method used to determine when complete demineralization occurred is described in the following section. The refreshed HCl solution was saved for calcium concentration measurement. All experiments were done in triplicate.

2.3. Calcium content measurement

The amount of calcium from the dissolved minerals in the HCl solution was calculated by using Inductively Coupled Plasma Spectroscopy (ICP Emission Spectrometer,Varian Liberty 110, Palo Alto, CA, USA).

Parts per million (ppm) units were obtained from ICP calcium measurements and were converted to mg/l (1 ppm = 1 mg/l). The initial calcium concentration $[Ca]_0$ in moles/l was calculated by dividing mg/l by the atomic weight of Ca (40.08 g/mol) and then summing the amount of dissolved calcium from each testing interval to the complete demineralization time t_c given by:

$$[Ca]_0 = [Ca]_{0.5} + [Ca]_{1.5} + \bullet\bullet\bullet + [Ca]_{tc}, \quad (1)$$

where $[Ca]_0$ is the initial calcium concentration (before HCl treatment), $[Ca]_{0.5}$ is the calcium concentration at sampling time of 0.5 h, after which the solution was refreshed (see Section 2.2 and Table 1 for the time of each HCl refresh). After the next sampling time at 1.5 h, the concentration $[Ca]_{1.5}$ was measured and the solution refreshed. The procedure was continued until $[Ca]_{t_c} = 0$, where t_C is the time for complete demineralization. The calcium concentration $[Ca]_{t^*}$ at time t^* is given by:

$$[Ca]_{t^*} = \sum_{t=0.5}^{t^*} [Ca]_t. \quad (2)$$

$[Ca]_{t^*}$ is the concentration reported at any time during the demineralization process.

2.4. Determination of order of reaction

The rate equation was used to determine the kinetic parameters for demineralization, given by Ref. [20–22]:

$$\text{rate} = -\frac{d[Ca]}{dt} = k[Ca]^n, \quad (3)$$

where k is the rate constant of the reaction and is a function of the acid concentration and temperature, [Ca] is the concentration of reactant (mol/l), and n is the order of the reaction. The order of demineralization reaction was obtained by plotting $-[Ca]_0 - [Ca]_{t^*}$ for zero-order reaction, $\ln([Ca]_{t^*}/[Ca]_0)$ for a first-order reaction and, $(1/[Ca]_{t^*})[([Ca]_{t^*}/[Ca]_0) - 1)$ for a second-order reaction, as a function of time. The plot that is the most linear indicates the order of the reaction.

Table 1
Time (h) required to reach complete demineralization of bone specimens.

Time (h)	0.1 N HCl			0.6 N HCl			1.0 N HCl		
	0 °C	20 °C	37 °C	0 °C	20 °C	37 °C	0 °C	20 °C	37 °C
Cortical bovine femur bone	–	–	–	52	48	32	36	32	28
Cancellous bovine femur bone	44	40	32	28	24	20	28	20	16
Cortical antler bone	–	–	–	44	40	36	32	28	24

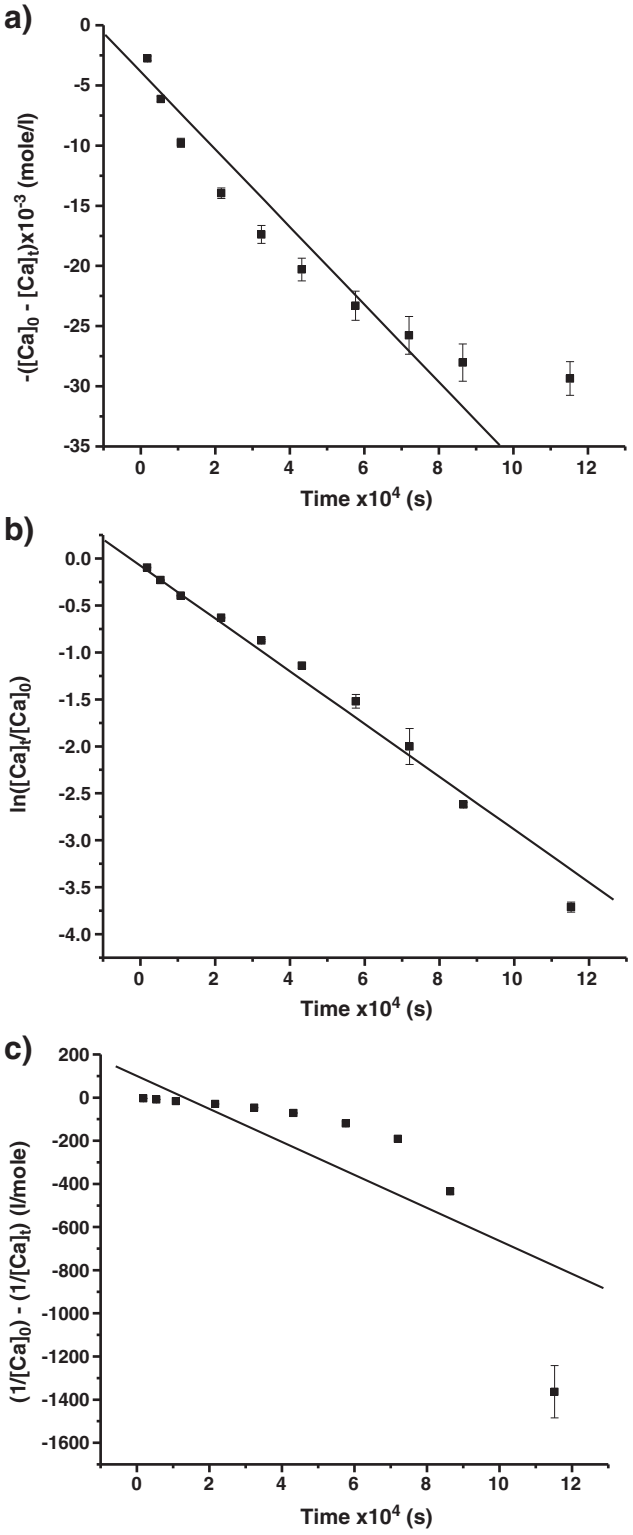

Fig. 3. Plots of a) $-([Ca]_0-[Ca]_{t^*})$ for zero-order reaction, b) $\ln([Ca]_{t^*}/[Ca]_0)$ for first-order reaction, and c) $(1/[Ca]_0)-(1/[Ca]_{t^*})$ for second-order reaction versus time for demineralization of cortical bovine femur bone, using 0.6 N HCl at 0 °C.

Table 2
Rate constant, $k_1 \times 10^{-5}$ (s^{-1}) calculated for the demineralization of bone as a function of HCl concentration. Numbers in parenthesis are the standard deviation of the average rate constants.

	$k_1 \times 10^{-5}$ (s^{-1})								
	0.1 N HCl			0.6 N HCl			1.0 N HCl		
	0 °C	20 °C	37 °C	0 °C	20 °C	37 °C	0 °C	20 °C	37 °C
Cortical bovine femur bone	N.D.	N.D.	N.D.	2.69 (0.30)[a]	2.86 (0.02)[a]	3.91 (0.49)[a]	3.58 (0.48)[a]	5.64 (0.10)[a]	9.08 (0.47)[a]
Cancellous bovine femur bone	2.41 (0.17)	2.84 (0.48)	4.07 (0.89)	4.80 (0.38)[b]	10.9 (1.80)[b]	13.8 (1.20)[b]	5.61 (1.40)[b]	11.8 (0.03)[b]	20.5 (0.27)[b]
Cortical antler bone	N.D.	N.D.	N.D.	3.72 (0.18)[c]	4.98 (0.21)[c]	7.42 (0.74)[c]	4.29 (0.12)[b]	5.67 (0.36)[a]	9.04 (1.20)[a]

Averages with different superscripts in a column are significantly different ($p<0.05$).

2.5. Calculation of activation energy

The dependence of the rate constant on temperature is expressed by the Arrhenius equation given in Ref [20–21]:

$$k = A\, exp\left(-\frac{E_a}{RT}\right), \tag{4}$$

where A is a constant that indicates how many collisions lead to products, and is known as the frequency factor. E_a is the activation energy, R is the gas constant and T is the absolute temperature at which the reaction takes place. The activation energy is calculated from the slope of the plot of ln k as a function of reciprocal temperature.

2.6. SEM imaging

Micrographs were obtained using a field emission scanning electron microscope (FE-SEM) (FEI-XL30, FEI Company, Oregon, USA). Samples were subjected to the critical point drying procedure in order to avoid excessive shrinkage. For imaging, samples were mounted on aluminum sample holders and air dried. Bone samples were sputter-coated with gold-platinum before observation. The electron beam was used with an accelerating voltage of 20 kV.

2.7. Statistical analysis of results

In order to determine the differences in mean values based on the three experimental replications, a Student's t-test was used. Significance level was determined at the 95% probability level. Microsoft Excel and Origin Pro 6.1 were employed for data processing and statistical analysis on the results as well.

3. Results

3.1. Demineralization reaction order

Plots of $-([C_a]_0-[C_a]_{t^*})$ for zero-order kinetics, $\ln([Ca]_{t^*}/[Ca]_0)$ for first-order reaction, and $(1/[Ca]_0)-(1/[Ca]_{t^*})$ for second-order reaction versus time are shown in Fig. 3. The slope of the plot is the rate constant of the reaction [20–22]. As shown, the data fitted a first-order reaction (Fig. 3(a)). Rate constant values calculated for all the demineralization treatments are presented in Table 2. In order to evaluate if there were significant differences between the cortical and cancellous bones and the cortical antler, a Student's t-test was performed on the rate constant. Rate constants were significantly different between the cortical and cancellous bones (Table 2).

Although the data plotted in Fig. 3(a) fell along straight line, there was some variability noticed mainly at the start and end of the reaction. To further investigate the rate constant, k_1 can be plotted as a function of time, using the method of Van't Hoff [22]:

$$k_1 = \frac{1}{t^*}\ln\left(\frac{[Ca]_{t^*}}{[Ca]_0}\right) \tag{5}$$

where k_1 is the rate constant for a first-order reaction, t* is the time at which the calcium concentration was evaluated. The method of Van't Hoff indicates the sensitivity of the rate constant as a function of time.

Plotting k_1 as a function of time revealed three stages for all demineralization conditions, as shown in Fig. 4:

a) First stage: the rate constant increased.
b) Second stage: demineralization occurred on a steady state. *All the kinetic parameter calculations were done based on data from the steady stage.*
c) Third stage: rate constant diminished.

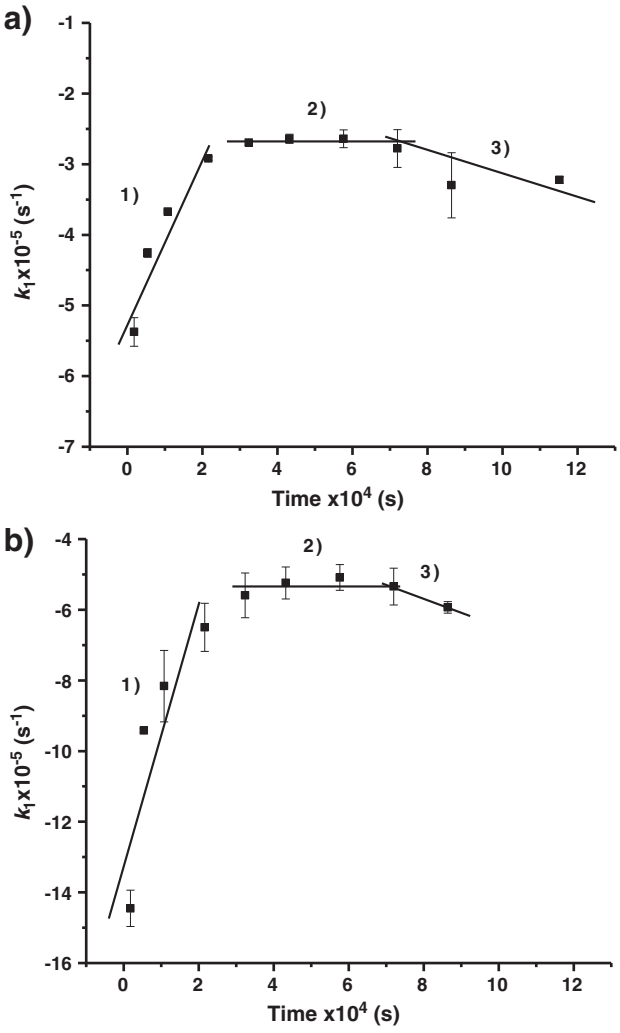

Fig. 4. The rate constant (k_1) of the first-order demineralization of a) cortical bovine femur bone and, b) cancellous bovine femur bone, using 0.6 N HCl at 0 °C. Three stages were identified: 1) rate increased as HCl advanced from the periphery of the specimen to the core, 2) demineralization is on a steady stage on the central part of the sample and, 3) rate diminished as calcium concentration on the sample also diminished. Further kinetics calculations were done from data on a steady state.

3.2. Effect of temperature on bone demineralization

Results for cortical and cancellous bovine femur bones demineralized with 1 N HCl are presented in Fig. 5. These are representative of the analysis done under the different conditions used in this work.

The rate of reaction (slope) increased as the temperature increased for both types of the bones (Table 2).

It is important to mention that the cortical antler bone and the cancellous bovine femur bone demineralized at 37 °C using 0.6 N and 1.0 N HCl, experienced a permanent deformation of its structure after completing the demineralization process, this is, samples completely shrank, reducing their volume from ~125 mm^3 to ~8 mm^3. This indicated that the combination of high temperature (37 °C) and high HCl concentration ([HCl]) (0.6 N and 1.0 N), adversely affected the architecture of the bone samples, therefore these conditions are not recommended for the compression testing followed by demineralization.

3.3. Activation energy calculation

The dependence of the rate constant on temperature is expressed by Eq. (4). In Fig. 6, k_1 was plotted as a function of 1/T for the demineralization of cortical and cancellous bovine femur bones using 1.0 N HCl. The activation energy was calculated from the slope (Table 3). The activation energy was higher for the cancellous bone compared to the cortical bone.

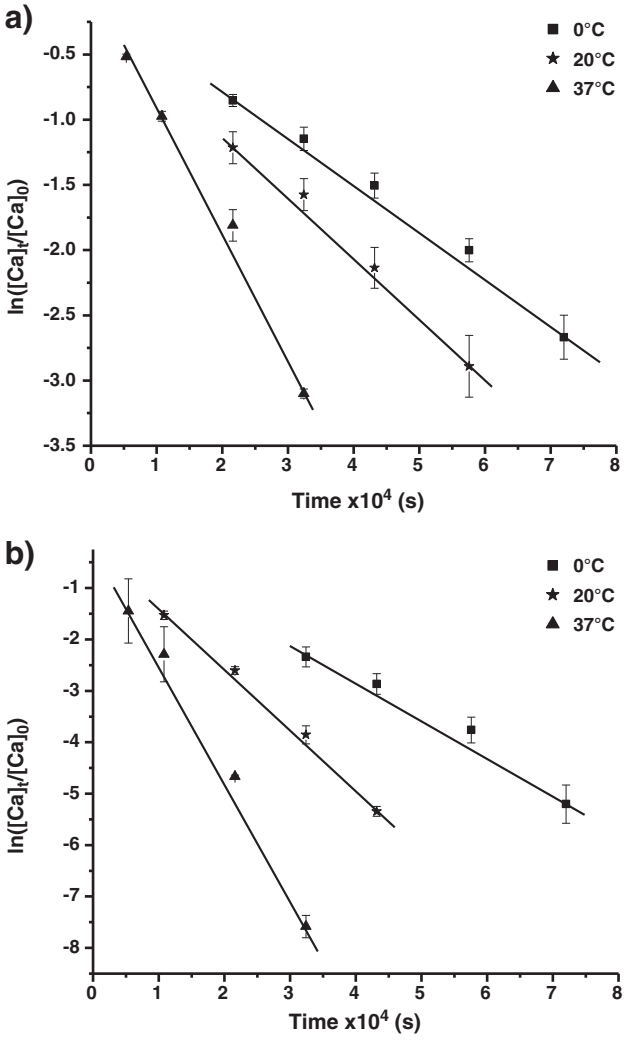

Fig. 5. Effect of temperature on demineralization of a) cortical bovine femur bone and b) cancellous bovine femur bone, using 1.0 N HCl. The data corresponds to the steady state demineralization.

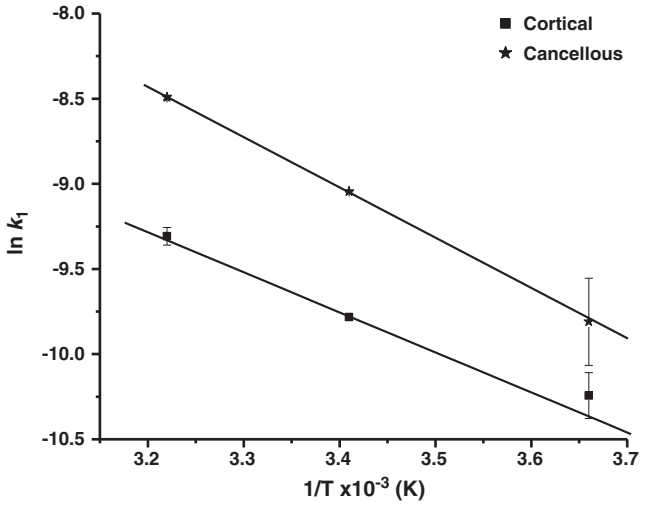

Fig. 6. The rate constant, k_1 as a function of 1/T for demineralization of cortical and cancellous bovine femur bones with 1.0 N HCl. The slope of the plot is $-E_a/R$.

3.4. Effect of HCl concentration on bone demineralization

Results of the demineralization rate of cortical bone treated in HCl at 37 °C are presented in Fig. 7. The same procedure was applied for all different conditions used in the present work. The demineralization rate constant increased as HCl concentration increased.

3.5. Fitting of demineralization data

Since data at three different HCl concentrations for cancellous bovine femur bone demineralized at 37 °C were presented in this work, we were able to plot the demineralization rate constants calculated at each HCl concentration used. Fig. 8 shows that the demineralization rate constant fitted well to a linear tendency.

3.5.1. Demineralization equation

Keeping in mind the linear tendency relationship of the rate constant as a function of [HCl], and from previous Eq. (4), we obtain a rate equation that incorporates [HCl]:

$$k_1 = A'[\mathrm{HCl}]\ exp\left(-\frac{E_a}{RT}\right) \tag{6}$$

Assuming that the steady state rate constant can be expressed by the multiple of the acid concentration formula with the temperature dependence, an equation that incorporates calcium concentration depletion in cancellous bovine femur bone (i.e. demineralization) as a

Table 3
Activation energy calculated for the demineralization of bone as a function of HCl concentration. Numbers in parenthesis are the standard deviation of the average activation energy.

	Activation energy (kJ mol^{-1})		
	0.1 N HCl	0.6 N HCl	1.0 N HCl
Cortical bovine femur bone	N.D.	6.8(0.06)[a]	17.6(1.7)[a]
Cancellous bovine femur bone	9.5(3.0)	20.4(0.3)[b]	25.1(4.8)[b]
Cortical antler bone	N.D.	12.9(0.9)	13.8(1.97)

Averages with different superscripts in a column are significantly different ($p<0.05$).

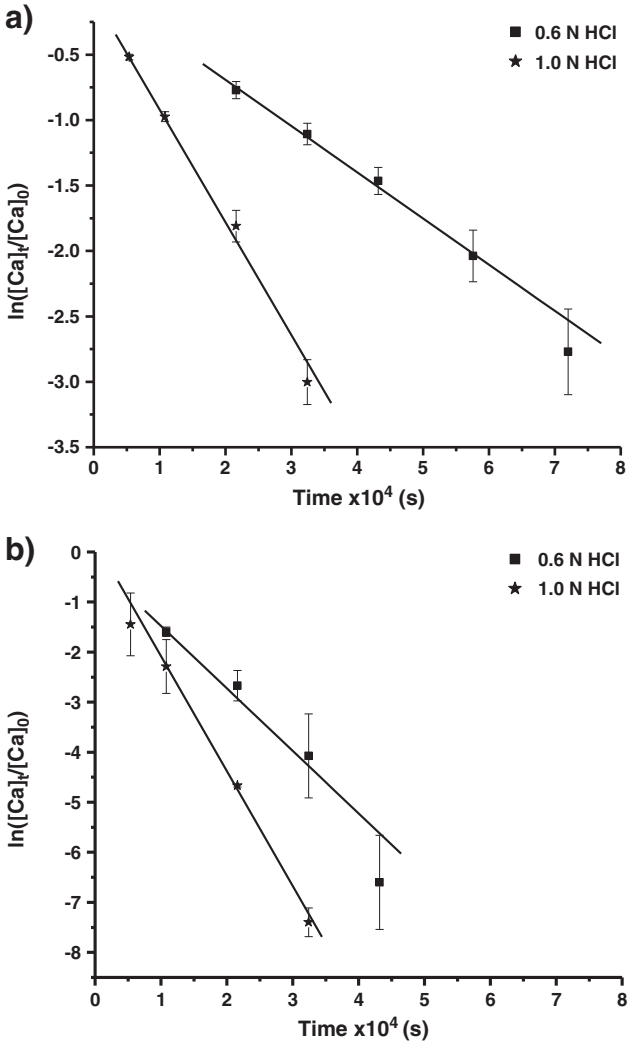

Fig. 7. Effect of HCl concentration on demineralization at 37 °C of a) cortical bovine femur bone and b) cancellous bovine femur bone. The data corresponds to steady state demineralization.

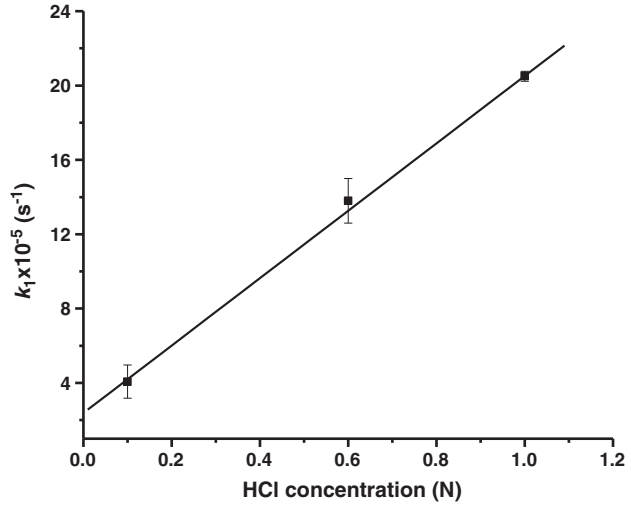

Fig. 8. Relationship of the rate constant, k_1 as a function of the HCl concentration for cancellous bovine femur bone demineralization at 37 °C. Data plotted from Table 2.

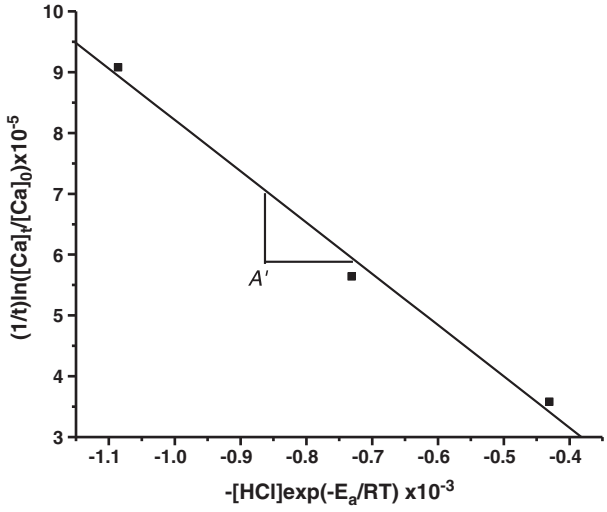

Fig. 9. Finding of A′ (collision factor) for cortical bovine femur bone demineralized with 1 N HCl. Data plotted from Table 4.

function of [HCl] and the temperature was obtained by combining Eqs. (5) and (6):

$$\frac{1}{t}\ln\left(\frac{[Ca]_t}{[Ca]_0}\right) = -A'[HCl]\,exp\left(-\frac{E_a}{RT}\right) \quad (7)$$

The slope obtained by plotting $\frac{1}{t}\ln\left(\frac{[Ca]_t}{[Ca]_0}\right)$ as a function of $-[HCl]\,exp\left(-\frac{E_a}{RT}\right)$, will give the collision factor, A'.

3.5.2. Validation of Eq. (7)

In order to prove Eq. (7), we have calculated A' for the cortical bovine femur bone demineralized with 1 N HCl (the slope in Fig. 9) and solved Eq. (7) for the three temperatures used in this work (Table 4). The variation between the numbers experimentally obtained (i.e. by plotting $\ln([Ca]_t/[Ca]_0)$ as a function of time) and the values calculated by Eq. (7) were less than 10% (Table 4), which indicated that the calculation of the calcium depletion by using Eq. (7) gives values confidentially near to those experimentally calculated.

3.6. SEM imaging

SEM micrographs of untreated cortical bovine femur bone are shown in Fig. 10a)–b), which clearly shows the mineralized collagen fibers. The protein phase alone was observed when bones where treated with 0.6 N HCl at 20 °C until complete demineralization was reached (Fig. 10c)–d)).

Table 4
Kinetics data for the demineralization with 1 N HCl of cortical bovine femur bone (data from Tables 2 and 3) for the validation of Eq. (7).

$\frac{1}{t}\ln\left(\frac{[Ca]_t}{[Ca]_0}\right) = -A'[HCl]\,exp\left(-\frac{E_a}{RT}\right)$ (7)

$-[HCl]\,exp\left(-\frac{E_a}{RT}\right)$	T(K)	Experimental $\frac{1}{t}\ln\left(\frac{[Ca]_t}{[Ca]_0}\right)$ $\times 10^{-5}$ (s^{-1})	Calculated from Eq. (7) $\frac{1}{t}\ln\left(\frac{[Ca]_t}{[Ca]_0}\right)$ $\times 10^{-5}$ (s^{-1})	Variation coefficient[a] (%)
-4.3×10^{-4}	273.15	3.58	3.62	1.78
-7.3×10^{-4}	293.15	5.64	6.14	6.00
-1.08×10^{-3}	310.15	9.08	9.12	0.31

[a] Shows the variation (%) between the depletion of calcium calculated from Eq. (7) and the value obtained experimentally from the plotting of $\ln([Ca]_t/[Ca]_0)$ versus time.

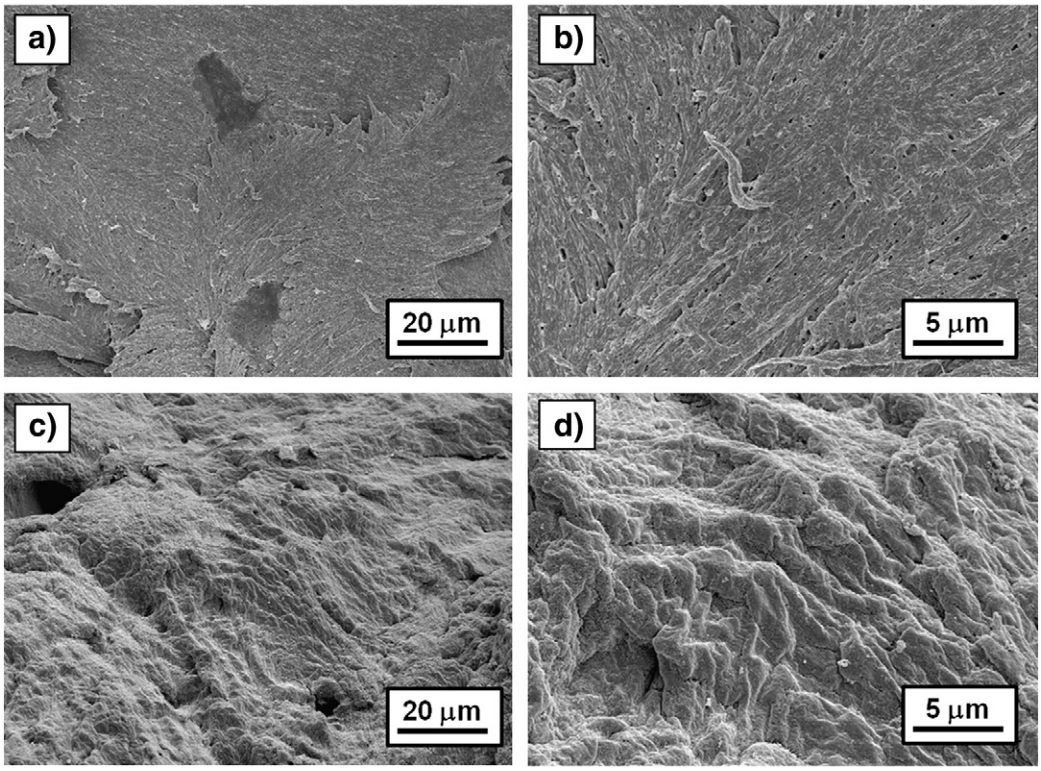

Fig. 10. Scanning electron microscopy images of a)–b) untreated, and c)–d) completely demineralized cortical bone.

4. Discussion

The establishing of the reaction order is the first step required for the calculation of the kinetic parameters of any reaction. The analysis of the demineralization kinetics of cortical antler bone corroborated the results obtained for cortical bovine femur bone.

The Student's *t*-test performed to the rate constants clearly demonstrated that demineralization occurred faster on cancellous bovine femur bone than in cortical bone. The rapid demineralization in the cancellous bone compared to the cortical could be related to the difference of diffusion of ions between both types of structures, cancellous and cortical. The complex network of connected trabeculae in cancellous bone allows easier diffusion of HCl, making calcium from mineral more accessible to chlorine from HCl, as a consequence. Therefore, the demineralization reaction advances faster in the cancellous bone than in the cortical bone, which is more densely packed. Therefore, the demineralization occurred faster in the cancellous bone than in the cortical bone.

In the first stage of bone demineralization, the rate increased as the HCl advanced from the periphery to the core of the sample. In the second stage, steady rate constant values were calculated indicating that demineralization occurred on a steady state. According to Brain [23] demineralization requires longer time to be completed in the central part than in the peripheral part. Therefore, this steady state should correspond to the central part of the bone. Finally, in the third stage, the rate constant diminished as the calcium concentration in the bone also became depleted.

The first stage of demineralization was more pronounced in the cancellous bone than in the cortical bone. This difference could be attributed to the chemical, structural and mechanical differences observed between cortical and cancellous bones [19,24,25].

The demineralization rate constants increased as temperature increased. At higher temperature, the molecules increase their energy; therefore there were more molecules with higher energy for the demineralization reaction to occur, which produced an increment in the rate constant as a consequence [20,21].

The higher activation energy value for cancellous bone was an indication of the sensitivity of this bone to the increment of temperature. This different sensitivity to temperature between cortical and cancellous bones was noted in the slopes obtained for the plots of the rate constant as a function of the inverse temperature. The slope calculated was higher for the cancellous than for the cortical bone, which indicated the reason why the activation energy was higher for the cancellous than for the cortical bone. This sensitivity could be attributed to the differences in the architecture between both types of bones. It has been reported that structural differences between cortical and cancellous bones directly affect their chemical and mechanical properties [19,24,25] and, the diffusivity in the inner matrix as a consequence. The different activation energy values for cancellous and cortical bones indicated that matrix architecture of both types of bones directly influence the rate of demineralization as a function of temperature.

The rate of demineralization increased with increasing [HCl]. This can be explained as follows: according to Eq. (8), chlorine and calcium ions react with each other:

$$Ca_{10}(PO_4)_6(OH)_2 + 20HCl \rightarrow 10CaCl_2 + 6H_3PO_4 + 2H_2O, \quad (8)$$

From the chemical kinetics theory of collisions, it is known that the rate of a reaction is directly proportional to the number of molecular collisions per second [20,21]. This relation explained the dependency of the reaction rate on the reactant concentration. As [HCl] increased, the probability to have more successful collisions between chloride and calcium ions was higher. Therefore, the reaction rate increased with increasing [HCl].

5. Conclusions

Demineralization experiments were performed on the cortical and cancellous bovine femur bones, and the cortical antler bone. Kinetic parameters of the rate equation were determined at three temperatures (0 °C, 20 °C and 37 °C), using three HCl concentrations (0.1 N,

0.6 N and 1.0 N). The following conclusions were obtained from this research:

1. As the HCl concentration or temperature increased, the rate of demineralization also increased.
2. Bone demineralization occurred in three stages:
   a. First stage: the rate constant increased as HCl solution demineralized the peripheral part of the sample.
   b. Second stage: demineralization occurred on a steady state. This steady state corresponded to the demineralization of the central part of a bone sample.
   c. Third stage: at the end of the reaction, the rate constant decreased as calcium concentration in the bone became depleted.
3. Activation energy of the steady state demineralization was calculated.
   a. Activation energy values were different for cancellous and cortical bones. This is attributed to the matrix architecture differences of both types of bones.
4. An extremely good fit to a linear equation was found for cortical bovine femur demineralized in 1 N HCl.
5. An equation that expresses demineralization as a function of [HCl] and temperature was proposed. The plotting of this equation gives the collision factor, A':

$$\frac{1}{t}\ln\left(\frac{[\mathrm{Ca}]_t}{[\mathrm{Ca}]_0}\right) = -A'[\mathrm{HCl}]\,exp\left(-\frac{E_a}{RT}\right)$$

Acknowledgements

We thank Prof. Pilar Sánchez-Saavedra (Aquaculture, CICESE) for her valuable discussion of results. Thanks to Prof. Beatriz Cordero-Esquivel (Aquaculture, CICESE) for her support for the use of laboratory facilities. Mario Vega-Aguilar (Earth Sciences, CICESE) for ICP measurements, Patricia Ascencio and Norberto Flores (Aquaculture, CICESE) are thanked for their help in the sample preparation. We acknowledge Alejandro Tiznado (CNyN-UNAM) for his valuable support in the use of laboratory facilities for sample cleaning. Aruni Suwarnasarn, Sr. Staff Research Associate (UCSD-SIO Analytical Facility) and Yen-Shan Lin, UCSD graduate student are also thanked for their help in SEM imaging. Ana Castro-Ceseña acknowledges Arturo Susarrey-Arce for his valuable insights, enthusiasm and support of this work. This research was funded by the National Science Foundation, Division of Materials Research, Biomaterials Program (Grant DMR 0510138) and by a UC-MEXUS project (2009–2010). Isabel Pérez Montfort reviewed and edited the English version of the manuscript. Partial support from DGAPA-UNAM (Grant # 114010-3) is also acknowledged.

References

[1] R. Lakes, Nature 361 (1993) 511.
[2] J.-Y. Rho, L. Kuhn-Spearing, P. Zioupos, Med. Eng. Phys. 20 (1998) 92.
[3] S. Weiner, H.D. Wagner, Annu. Rev. Mater. Sci. 28 (1998) 271.
[4] P.-Y. Chen, A.Y.M. Lin, Y.-S. Lin, Y. Seki, A.G. Stokes, J. Peyras, E.A. Olevsky, M.A. Meyers, J. McKittrick, J. Mech. Behav. Biomed. Mater. I (2008) 208.
[5] T. Audersik, G. Audersik, Biology, Life on Earth, Prentice-Hall, New Jersey, 1996.
[6] J.A. Kanis, O. Johnell, A. Oden, I. Sembo, I. Redlund-Johnell, A. Dawson, C. De Laet, B. Jonsson, Osteoporos. Int. 11 (2000) 669.
[7] WHO (World Health Organization), Report of a WHO Study Group. WHO Technical Report Series 843, WHO, Geneva, 1994.
[8] A. Bhan, A.D. Rao, D.S. Rao, Endocrinol. Metab. Clin. Am. 39 (2010) 321.
[9] D.A. Chakkalakal, B.S. Strates, K.L. Garvin, J.R. Novak, E.D. Fritz, T.J. Moliner, M.H. McGuire, Tissue Eng. 7 (2001) 161.
[10] J.R. Mauney, C. Jaquiéry, V. Volloch, M. Heberer, I. Martin, D.L. Kaplan, Biomaterial 26 (2005) 3173.
[11] X. Li, L. Jin, G. Balian, C.T. Laurencin, D.G. Anderson, Biomater 27 (2006) 2426.
[12] Z.-H. Wang, X.-J. He, Z.-Q. Yang, J.-B. Tu, Artif. Organs 34 (2010) 161.
[13] R.A. Dodds, A.M. York-Ely, R. Zhukauskas, T. Arola, J. Howell, C. Hartill, R.R. Cobb, C. Fox, J. Biomater. Appl. 25 (2010) 195.
[14] J.D. Currey, J. Biomech. 23 (1990) 837.
[15] H. Birkedal-Hansen, J. Histochem. Cytochem. 22 (1974) 428.
[16] H. Birkedal-Hansen, J. Histochem. Cytochem. 22 (1974) 434.
[17] K.-U. Lewandroski, V. Venugopalan, W.W. Tomford, K.T. Schomacker, H.J. Mankin, T.F. Deutsch, J. Biomed. Mater. Res. 31 (1996) 365.
[18] G.E. Fantner, T. Hassenkam, J.H. Kindt, J.C. Weaver, Henrikbirkedal, L. Pechenik, J.A. Cutroni, G.A.G. Cidade, G.D. Stuky, D.E. Morse, P.K. Hansma, Nat. Mater. 4 (2005) 612.
[19] P.J. Thurner, B. Erickson, P. Turner, R. Jungmann, J. Lelujian, A. Proctor, J.C. Weaver, G. Schitter, D.E. Morse, P.K. Hansma, Adv. Mater. 21 (2009) 451.
[20] T.L. Brown, H.E. LeMay, B.E. Bursten, Chemistry the Central Science, Prentice-Hall, New Jersey, 1991.
[21] R. Chang, Chemistry, McGraw-Hill, New York, 1998.
[22] R. Masel, Chemical Kinetics and Catalysis, Wiley-Interscience, New York, 2001.
[23] E. Brain, The Preparation of Decalcified Sections, Charles C. Thomas, Springfield, 1966.
[24] A. Bigi, G. Cojazzi, S. Panzavolta, A. Ripamonti, N. Roveri, M. Romanello, K. Noris Suarez, L. Moro, J. Inorg. Biochem. 68 (1997) 45.
[25] D. Chappard, E. Legrand, B. Haettich, G. Chales, B. Auvinet, J.-P. Eschard, J.-P. Hamelin, M.-F. Baslé, M. Audran, J. Pathol. 195 (2001) 515.